2nd ed

NASA CONTRACTOR
REPORT

NASA CR-129017

THREE-DIMENSIONAL LASER DOPPLER VELOCIMETER TURBULENCE MEASUREMENTS IN A PIPE FLOW

By Charles E. Fuller, III, William C. Cliff, Robert M.Huffaker
REMTECH Incorporated
2603 Artie Street, Suite 21
Huntsville, Alabama 35805

April 1973

Prepared for

NASA-GEORGE C. MARSHALL SPACE FLIGHT CENTER
Marshall Space Flight Center, Alabama 35812

TECHNICAL REPORT STANDARD TITLE PAGE

1. REPORT NO.	2. GOVERNMENT ACCESSION NO.	3. RECIPIENT'S CATALOG NO.
NASA CR-129017		

4. TITLE AND SUBTITLE	5. REPORT DATE
THREE DIMENSIONAL LASER DOPPLER VELOCIMETER TURBULENCE MEASUREMENTS IN A PIPE FLOW	April 1973
	6. PERFORMING ORGANIZATION CODE

7. AUTHOR(S)	8. PERFORMING ORGANIZATION REPORT #
Charles E. Fuller, III,* William C. Cliff,** Robert M. Huffaker**	RTR 002-2

9. PERFORMING ORGANIZATION NAME AND ADDRESS	10. WORK UNIT NO.
REMTECH Incorporated 2603 Artie Street, Suite 21 Huntsville, Al. 35805	11. CONTRACT OR GRANT NO. NAS 8-25896
	13. TYPE OF REPORT & PERIOD COVERED High Series Contractor Topical
12. SPONSORING AGENCY NAME AND ADDRESS National Aeronautics and Space Administration Washington, D. C. 20546	14. SPONSORING AGENCY CODE

15. SUPPLEMENTARY NOTES

* Vice President, REMTECK, Inc.

** Aero-Astrodynamics Laboratory, Marshall Space Flight Center, Alabama

16. ABSTRACT

The mean and turbulent u, v, and w components of a gaseous fully developed turbulent pipe flow were measured with a laser Doppler velocimeter system. Measurements of important system parameteres are presented and discussed in relation to the measurement accuracy. Simultaneous comparisons of the laser Doppler and hot wire anemometer measurements in the turbulent flow provided evidence that the two systems were responding to the same flow phenomena.

17. KEY WORDS	18. DISTRIBUTION STATEMENT
	Unclassified-unlimited L. G. Richard Acting Director Aero-Astrodynamics Laboratory

19. SECURITY CLASSIF. (of this report)	20. SECURITY CLASSIF. (of this page)	21. NO. OF PAGES	22. PRICE
Unclassified	Unclassified	93	

SUMMARY

1. An argon laser along with three focused receivers operating in the forward scatter mode were employed to obtain gas velocity measurements.

2. An analog network connected with three frequency trackers, which processed the Doppler frequencies, provided an on line capability for observing three turbulent velocity components from a gaseous fully developed pipe flow.

3. The turbulent u, v, and w velocity components measured show favorable comparison with hot wire measurements taken by the authors and measurements found in the literature.

4. Simultaneous comparisons of the laser system with a hot wire anemometer sensing a common volume show remarkable similarity.

ACKNOWLEDGEMENTS

The experimental studies described in this report were performed under the Aero-Astrodynamics Laboratory of Marshall Space Flight Center, Huntsville, Alabama.

The authors wish to gratefully acknowledge Professors V. A. Sandborn of Colorado State University, Alan R. Barbin of Auburn University, A. J. Eggenberger of the University of South Carolina, and N. S. Berman of Arizona State University who were most helpful in defining the resulting measurements.

The authors wish to express their appreciation to Mr. Arthur Hullett, Mr. Charles Albert and Mr. Terry West for assistance in performing the experimental measurements. In addition, numerous other NASA personnel furnished indirect assistance in providing equipment, establishing the test facility and analyzing the data.

TABLE OF CONTENTS

1.0 INTRODUCTION

In order to provide experimental verification of the capabilities of the LDV system for the measurement of three dimensional gas turbulence, a fully developed turbulent pipe flow test was conducted. This test incorporated the three dimensional Laser Doppler Velocimeter (LDV) System with an analog network to provide a direct readout of the three fluctuating velocity components in an orthorgonal coordinate system.

The LDV System measures the Doppler frequency shift in laser light caused as moving particles scatter the light. This frequency shift is related to the wavelength of the laser light, the geometrical direction of the scattered light, and the velocity of the particles producing the shift. Since the laser wavelength and the geometrical scattering direction for a given system are known, the detection of the Doppler frequency shift allows the calculation of the particle velocity which in turn may be related to the gas flow in which the particle is suspended.

Measurements were conducted at the exit of a 10 cm (4 inch) ID pipe. A single hot wire anemometer was used to obtain a simultaneous measurement of the axial velocity component. Comparisons of the LDV data with the author's hot wire data as well as data from the literature showed the LDV system to be operating successfully. Investigations of various LDV system parameters were made to define the accuracy of the system and the measurements.

2.0 TEST EQUIPMENT AND FACILITIES

In order to provide an understanding of the test arrangement, a discussion of the different components is presented. This discussion will consider the flow facility, which provided the means for obtaining the test conditions with sufficient submicron tracer particles; the LDV equipment which provided the means for detecting the Doppler frequency shift; and the electronic equipment which provided a means for measuring the value of the Doppler frequency shift.

2.1 FLOW FACILITY

The pipe flow facility used for these measurements was established to provide a fully turbulent pipe flow. The facility was designed to be similar to that employed by Laufer [1]. A schematic of the facility layout is shown in Fig. 1. The flow facility consisted of an air supply control panel, an aerosol generator, pipe flow sections and an exhaust duct.

The air supply was obtained from a 3400 psig supply and was regulated by two large dome loading regulators. Two air heaters with thermostat controls were used to maintain the air temperature at 70°F.

A large aerosol generator with a flow capacity of 720 SCFM, was used to provide the tracer particles needed for the LDV measurements. The generator

produced small liquid particles of silicon liquid (20 centistoke viscosity) by passing high speed air through small jets immersed in the liquid. Particles concentrations as high as 10^8 particles/cm^3 with mean particle sizes in the submicron range were obtained with the generator. The generator consisted of an upper and lower stage, each stage containing eight separately controlled nozzles for producing particles. In addition a by-pass line was provided in each stage which allowed for the introduction of clean air which could be mixed with the particle laden air from the nozzles. Thus by adjusting the nozzle flow rate and the clean air flow rate the particle concentration in the pipe flow could be adjusted to any desired level from 10^8 particles/cm^3 to no particles.

As shown in Fig. 1, the generator outlet is connected to a flow straightening section, then to a reducing section and then to the 10 cm ID pipe sections. The flow straightening section contains a 20.3 cm (8 inch) length of aluminum honeycomb material to break up any large eddies which might be produced at the aerosol generator exit. The reducing section also contains several screens which allowed for further flow field adjustment to assure a uniform flow into the pipe sections.

Two lengths of 10 cm aluminum pipe provided the sections in which the flow field was established. The inside surface of each pipe section was smoothed by a chemical etching process. After this process the inside smoothness of each pipe was measured and found to be 1.5 - 2.5 x 10^{-3} mm RMS for the long pipe section and 0.5 - 1.0 x 10^{-3} mm RMS for the short section.

Figure 2 shows a schematic of the pipe arrangement. The first section of this arrangement was 31 pipe diameters in length and contained 4 diameters of coarse sand paper at the entrance to accelerate the boundary layer growth. These lengths corresponded to those used by Laufer [1] for obtaining fully developed

turbuelnt flow.

An additional section 20 diameters in length, which served as the test section, was attached to the first section. Both sections of pipe contained many static pressure taps 1.0 mm in diameter, which were used to measure the pressure drop down the pipe. The pressure drop measurements were made using a Hooke manamometer with a micrometer which allowed for reading of pressures to 0.254 mm (.001 inch) of water.

2.2 LDV EQUIPMENT

The LDV equipment consisted of a stand, a laser and a LDV instrument. The stand contained metal supports and adjustment blocks which allowed for support and independent adjustment of the laser and LDV isntrument. Adjustments could be made in three orthorgonal directions by increments of .0254 mm (.001 inch) which allowed measurements to be made at any position in a volume 20.3 cm (8 inch) square. The stand was designed so that the laser was placed on one side of a flow field and the LDV instrument on the other. The laser beam directed through the flow field at right angles to the centerline of the flow facility and then into the center of the LDV instrument. Before passing through the flow field the laser beam was expanced and focused at a point in the flow field.

Three scatter tubes and one center tube (referred to as the local oscillator or LO tube) made up the LDV instrument. The tubes contain the optics which collect the LO and scatter beams and direct them onto a photomultiplier tube which detects the Doppler frequency resulting from the homodyning of the two beams. The LDV instrument arrangement is normally referred to as a reference forward scatter type configuration. The arrangement is such that the three

scatter tubes are located at nominal 120° intervals around the LO tube and form a scatter angle, α, with the centerline of the LO tube. The angle α for the pipe flow tests had a nominal value of 28°. A sketch of the geometrical instrument arrangement and the pipe flow field coordinate system is shown in Fig. 3. Reference 2 provides a more detailed description of the LDV instrument.

A region referred to as the scattering volume is formed by the intersection of the focal volume of the scatter light collection optics with the focal volume of the focused input laser beam. The size of this region is important because it is the probe volume from which velocity information is obtained.

The laser used during these measurements was a CRL, Model 53, CW argon gas laser. This laser was operated with an output power of approximately 1.6 watts at 5145 A. Operation at this power level did not excite any transverse laser modes. When these modes were excited, the homodyning between them resulted in signal frequencies which appeared in the spectral range in which the Doppler frequencies occured. These signals would cause a difficulty in detecting the Doppler frequency in the electronic processing system.

2.3 ELECTRONIC EQUIPMENT

A schematic diagram of the electronic network used for the pipe flow tests is shown in Fig. 4. The major components of this network are the frequency trackers and the analog network.

The frequency trackers [3] were designed to accept the Doppler frequency as input data and to electronically "lock" onto the signal and track the frequency changes. The tracker output are a DC voltage corresponding to the mean Doppler frequency or flow velocity and a fluctuating voltage level (AC) corresponding to

the Doppler FM fluctuations or flow turbulence. With the use of calibration curves, the Doppler input frequencies can be identified and used in the equations which relate the geometrical LDV instrument and LO beam arrangement to the Doppler frequency and flow velocity, to obtain the three components of mean and fluctuating velocities.

The trackers were designed to operate over two frequency ranges, these being from 5 to 50 MHz or from 50 to 200 MHz. Within those frequency ranges the tracker will follow a frequency deviation about the mean Doppler frequency of up to 30 MHz in one mode of operation and up to 10 MHz in another mode. Two of the trackers could follow frequency modulations of the Doppler frequency up to 33 KHz and the other could follow frequency modulations to 50 KHz. The input signal to noise ratio (S/N) required for accurate tracking of the Doppler signal was 15 db.

Low pass filters with a cut-off at 50 MHz were incorporated at the input to the frequency trackers. These filters would pass only the lower spectrum range in which the Doppler frequency occurred (5 to 50 MHz) and would block the longitudinal mode frequencies from the laser which occurred at 95 and 180 MHz. If these mode frequencies were allowed to enter the frequency trackers the tracker would attempt to lock onto the mode signals rather than the Doppler signals.

Several bandpass filters were also used at the AC output of the trackers. These filters allowed for the exclusion of noise which occurred outside the bandwidth over which the turbulent frequencies occurred.

One of the significant parts of the elcetronic equipment used for this test was the analog computing network which allowed for the solution of LDV equations for the turbulent velocity components in an orthogonal coordinate system. The significance of performing this operation becomes

apparent by examining the equations which define the measurements made by the LDV system. The general vector equation defining the measurements made by an LDV system is written as

$$f_D = \frac{1}{2\pi} \left(\vec{K_s} - \vec{K_i}\right) \cdot \vec{V_T} \qquad (1)$$

where $\vec{K_s}$ and $\vec{K_i}$ are reference vectors of magnitude $2\pi/\lambda$ in the direction of the scattered and incident laser light, λ is the laser wavelength, f_D is the Doppler frequency and V_T is the velocity of the particles producing the scattering.

If the scattered light is collected from three independent directions, Eq. (1) can be expanded to yield a set of three simultaneous equations defining the U, V, and W velocity components of a cartesian coordinate system. As shown in Ref. 4, three simultaneous equations can be obtained which define the fluctuating flow field velocities, u', v', and w', in terms of the fluctuating Doppler frequencies f_1' and f_2' and f_3'. These relations are expressed as

$$\begin{aligned} u' &= A_1 f_1' + A_2 f_2' + A_3 f_3' \\ v' &= B_1 f_1' + B_2 f_2' + B_3 f_3' \\ w' &\quad C_1 f_1' + C_2 f_2' + C_3 f_3' \end{aligned} \qquad (2)$$

where A_i, B_i, and C_i relate the velocity components to the respective Doppler shifts.

Since the frequency trackers provide an AC voltage output proportional to the fluctuating Doppler frequency (f_i'), Eq. 2 may be rewritten as

$$\begin{aligned} u' &= A_1 e_1' \frac{dF_1}{dE_1} + A_2 e_2' \frac{dF_2}{dE_2} + A_3 e_3' \frac{dF_3}{dE_3} \\ v' &= B_1 e_1' \frac{dF_1}{dE_1} + B_2 e_2' \frac{dF_2}{dE_2} + B_3 e_3' \frac{dF_3}{dE_3} \\ w' &= C_1 e_1' \frac{dF_1}{dE_1} + C_2 e_2' \frac{dF_2}{dE_2} + C_3 e_3' \frac{dF_3}{dE_3} \end{aligned} \qquad (3)$$

where e_i' are the fluctuating voltage outputs and dF_i/dE_i are the slopes of the voltage verses frequency calibration

Eq. 3 may also be written as

$$
\begin{aligned}
e_u' &= \frac{dE_1}{dF_1}\frac{u'}{\lambda} = A_1' e_1' + A_2' e_2' \frac{dF_2}{dE_2}\frac{dE_1}{dF_1} + A_3' e_3' \frac{dF_3}{dE_3}\frac{dE_1}{dF_1} \\
e_v' &= \frac{dE_1}{dF_1}\frac{v'}{\lambda} = B_1' e_1' + B_2' e_2' \frac{dF_2}{dE_2}\frac{dE_1}{dF_1} + B_3' e_3' \frac{dF_3}{dE_3}\frac{dE_1}{dF_1} \qquad (4) \\
e_w' &= \frac{dE_1}{dF_1}\frac{w'}{\lambda} = C_1' e_1' + C_2' e_2' \frac{dF_2}{dE_2}\frac{dE_1}{dF_1} + C_3' e_3' \frac{dF_3}{dE_3}\frac{dE_1}{dF_1}
\end{aligned}
$$

where $A_i = A_i' \lambda$, $B_i = B_i' \lambda$, and $C_i = C_i' \lambda$.

In Eq. 4 the sensitivities, dE_i/dF_i, are the slopes of the calibration curves and are taken at the mean voltage at which the mean Doppler signal was occuring. Since the slopes of the calibration curves (Fig. 18) were slightly different at different mean Doppler frequencies (i.e. the curves were not linear), adjustments to the analog network were made at each flow field measurement to account for the changes in the slope.

Figure 5 shows the analog network which was used to perform the operation given by Eq. 4. In practice the resistances which determined the constants A_i', B_i', and C_i' were set for a given instrument configuration, and the resistances which compensated for the calibration curve slopes were adjusted at each measurement, depending on the mean voltages at which the trackers were operating.

3.0 MEASUREMENTS AND RESULTS

In addition to the primary objective of obtaining turbulence measurements of the pipe flow, many other measurements of the different system parameters and components were made. This section details all those measurements and the

results that were obtained.

3.1 Frequency Trackers

In order to evaluate the operational characteristics of the frequency trackers, measurements were made of the tracker noise levels, the ability to follow an input signal modulated by a sine and square wave, the ability of each tracker to follow the same Doppler signal input and the stability of the calibration curves. It should be noted here that of the three trackers used in the experiment one tracker (#101) was about 2 years older than the other two (#102, and 103) and had slightly different operating features. For example, Tracker #102 and 103 contained built-in amplifiers with automatic gain control to maintain the input signal at a constant level, and a mode selector switch which allowed for the tracking of either wide or narrow band turbulent signals. Tracker #101 had neither of these features. In addition, Trackers #102 and 103 differed from 101 in the maximum FM frequency with which the Trackers were designed to follow. Tracker #101 was designed to follow FM frequencies to 50kHz while #102 and #103 were designed for frequencies to 100kHz. However, it was found that Trackers #102 and #103 would not operate satisfactorily with the FM design frequency of 100kHz so they were modified to a FM frequency of 33kHz before the LDV measurements were conducted.

3.1.1 Tracker AC and DC Accuracies

These measurements were conducted on Trackers #102 and 103. A schematic of the equipment arrangement for these measurements is shown in Fig. 6. The general objectives were to determine the minimum AC noise levels from the trackers and the minimum DC voltage which could be read at the DC voltage output.

In order to measure the AC noise output, an unmodulated signal from a signal generator was connected to the trackers along with the white noise from a photomultiplier tube. The tracker was locked onto this signal and the bandpass filter at the AC output was adjusted to different widths while the RMS noise levels were recorded. The input S/N levels for these measurements was 15-20db which was slightly higher than the minimum needed for proper tracking (15db). The results are itemized below:

(1) The two trackers had almost identical noise characteristics.

(2) In Fig. 7, it is seen that as the bandpass filter was opened to 100kHz the RMS noise level increased from about 3 mv to 9 mv and as the filter was closed from 10Hz to 200Hz on the low end the noise level decreased slightly.

(3) In order to maintain the noise level at a minimum the bandpass filter on the tracker output should only be as wide as needed for the turbulence spectrum of interest.

Measurements were also conducted at the DC voltage output of the trackers. This measurements showed that the DC voltage could be read to within $\pm$ 0.001 volts at any voltage within the range from 0.5 to 4.0 volts, corresponding to an input frequency range of 5 to 50 MHz. This means that the frequency can be detected to within a nominal value of $\pm$ 10 kHz since the tracker calibration curves have a nominal value of 10 MHz/volt.

3.1.2 Performance with a Modulated Input Signal

The objectives of these measurements were to determine the degree to which each of the trackers would follow an electronically produced input signal that was modulated by either a sine wave or a square. An electronically modulated

input signal represents a somewhat idealized signal in respect to the Doppler signal, which is composed of short bursts produced as each particle travels through the scatter volume. This means that rather than a continuous input signal which is frequency modulated, the actual Doppler signal is not continuous but occurs as a series of rapid signal bursts that are both frequency and amplitude modulated. The representation of such a signal is difficult to achieve electronically, however, it was felt that a meaningful measure of the tracker performance could be achieved by frequency modulating a input signal with both a sine and a square wave. If the trackers could not behave in an identical fashion with these input signals, then they could not be expected to perform well with the complicated Doppler signal.

Figure 8 shows a schematic of the system arrangement for the measurements made with the modulated signal inputs. In this arrangement a input signal was modulated by either a square wave or a sine wave and this square or sine wave input was compared to the demodulated output signal from each of the trackers. These comparisons were made for different modulation frequencies.

Figure 9 shows the results of the sine wave modulations. It is noted that as the modulation frequency is increased the phase difference between the input sine wave modulation and the demodulated tracker output increases from about 0° at 200 Hz to about 180° at 20,000 Hz. The demodulated output frequency for the three trackers was found to be identical out to 50,000 Hz and corresponded to the input signal modulation frequency.

The results of the square wave modulation are shown in Fig. 10 through Fig. 15. These figures show the tracker response as the modulation frequency is increased from 10Hz to 20,000 Hz. For these measurements, the input signal which the tracker followed was at 18 MHz and the square wave modulated this

signal to a deviation approximately 9 MHz wide. The square wave modulation closely approximates the bursting characteristic of the Doppler signal since the input signal takes discrete jumps according to the square wave input.

The following items were noted in the square wave modulation tests.

1. As the modulation frequency was increased from 10 Hz to 20,000 Hz the tracker response went from a fairly close representation of the square wave at 100 Hz to a sine wave response at 5000 Hz.
2. A peculiar response at the 10 Hz modulation frequency was noted and most likely due to the fact that the input square wave appeared to be a kind of saw tooth-square wave at that frequency.
3. Tracker #101 (the older of the three trackers) exhibited a more noticeable difference in response than the other two. This is seen in Figs. 13 and 14 which show a slight distortion in the hip of the sine wave response.
4. A phase difference between the three tracker outputs is seen at the 5000 Hz modulation frequency and increased as the modulation frequency was increased to 20,000 Hz.
5. The three trackers give a good representation of the frequency of modulation, even though they cannot respond to the very fast steps (0.1 msec) of the square wave. It appears that the time response associated with the transfer function of the trackers conditions discreet frequency jumps of the square wave at the higher frequencies so that a sine wave demodulated output is obtained.
6. The fact that the demodulated signal at the higher frequencies appears to be a sine wave may not be due to a lack of response in the trackers. The sine wave response may be a result of insufficient response of the signal generator which was being driven by the square wave generator.

Unfortunately, there was not means available for checking on this possibility.

3.1.3 Performance with a Doppler Signal

As an additional check to determine if each of the frequency trackers would respond in a similar manner, the same Doppler signal was input to each of the frequency trackers and comparisons of the AC outputs were made. Figure 16 shows the arrangement for these measurements. The results of these measurements indicated that the frequency trackers outputs were different for the same input Doppler signal. This is shown in Fig. 17 which presents a comparison of the AC outputs of the different trackers. While several measurements showed similar tracker outputs, it was found that the trackers would not consistently give the same output. This difficulty was investigated by a representative of the tracker manufacturer (Raythcon Company) and it was found that satisfactory tracking could be achieved after reducing the maximum design modulation frequency which trackers #102 and 103 could follow from 100 kHz to 33 kHz. This provided more stability in the tracking loop. Tracker #101 was not changed since its design modulation frequency was 50 kHz which appeared to provide satisfactory performance.

After these modifications, correlation measurements of the different tracker AC outputs for the same Doppler signal input were made. A PAR electronic correlator was used for these measurements and the correlation coefficient was found using the following relation

$$R_{ab} = \frac{\overline{e_a' \, e_b'}}{\sqrt{\overline{e_a'^2}} \sqrt{\overline{e_b'^2}}} \qquad (5)$$

The results of these measurements are given in Table I and yield an average value of R_{ab} as .846.

3.1.4 Calibration Curve Stability

As pointed out previously, the slopes of the calibration curve at the point which the frequency trackers are operating, are the sensitivities of the respective instruments and are used in the analog network to obtain on line computations of the fluctuating velocity components. For this reason it is important that this slope not only be known but be stable.

Figure 18 presents the slopes of the tracker calibration curves taken on four different days. The slopes were obtained by using a least squares curve fit of the calibration curves to define a fourth order equation, $F(E)$. The derivative, $dF(E)/dE$, of this equation was taken to provide an equation of the rate of change of the calibration curve. It is noted that the newer trackers #102 and 103 appear to be more stable on a day to day basis than tracker #101. However, it was found that the trackers were stable on any given day to $\pm$ 0.003 volts.

Figure 18 also shows the region over which the trackers were operated for the pipe turbulence measurements. These regions were 1.9 to 2.5 volts for tracker #101, 1.3 to 3.9 volts for tracker #102, 0.8 to 1.7 volts for tracker #103. The rate of change of the slopes of the calibration curves through these intervals were found to be closely approximated by a straight line and to be 0.92 (MHz/volt)/volt for tracker #101, 0.576 (MHz/volt)/volt for tracker #102, and 1.166 (MHz/volt)/volt for tracker #103.

It was found (Section 4.0) that even though it is not exact to take the slope of the calibration curve at the mean voltage of a fluctuating

signal and use it in reducing the RMS fluctuations around the mean as done in the analog network for this test; the resulting errors are insignificant.

3.2 SCATTERING VOLUME

In the LDV system the scattering volume is the region from which the velocity information is obtained. This region is formed by the intersection of the focal volume of the scatter light collection optics with the focal volume of the focused input laser beam. This region is important because it defines the dimension over which the velocity fluctuations are averaged. Ideally this region should be as small as possible.

Calculations of the size of the scattering volume have been made following the theoretical developments given in Refs. 5 and 6. These developments define the diameter and length of diffraction ellipsoids of the transmitter and receiver optics. It is noted that the ellipsoids are long and may be approximated as cylinders. For such an approximation the following relation may be used to define the scattering volume.

$$V = \pi d_r^2 \, d_t/4 \, \sin\alpha$$

where $d_t > d_r$, d_r and d_t are the receiver and transmitted focal diameters and α is the scattering angle. Expressions are also given for obtaining the transmitted and receiver focal diameters. These are

$$d = 8f\lambda/\pi D$$

where f = focal length of the lens, D = diameter of the light passing through the lens and λ = the laser wavelength. For the LDV instrument the transmission lens has a focal length of 86 cm. and a beam diameter of 12.7 mm. This yields:

$$d_t = .088 \text{ mm.}$$

Likewise, the receiver optics have a focal length of 81 cm. and a beam diameter of 1.5 cm. This yields:

$$d_r = .071 \text{ mm.}$$

Using these values of the beam diameters at the focus the scatter volume is found to be

$$V = 7.4 \times 10^{-7} \text{ cm}^3$$

for $\alpha = 28°$ which is the scattering angle used for the turbulence test.

Reference 7 provides a relation defining the length of the scattering volume formed by the intersection of two cylinders of radius r_t and r_r as

$$L = 2(r_t^2 + r_r^2 - 2\, r_t r_r \cos\alpha)^{1/2} / \sin\alpha \qquad (7)$$

Using this relation and the values determined above, the length of the scatter volume was found to be

$$L = 0.27 \text{ mm.}$$

The following sketch indicates the different dimensions of the scatter volume which were defined in the preceeding paragraphs.

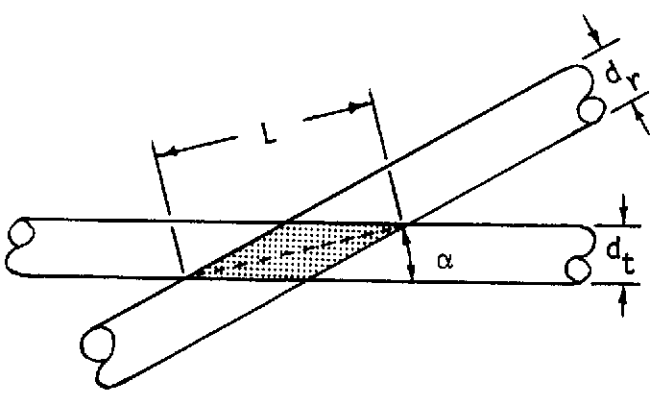

The preceeding discussion defined the size of the scattering volume based on diffraction limited optics and assuming that the scattering volume can be represented as the intersection of two cylinders. In order to define how good these considerations were, measurements of the scatter volume length and width were made using a small needle jet. The jet was moved in small increments along the length and width of the volume as the change in Doppler signal intensity was recorded. A sketch of this measurement arrangement is shown in Fig. 20. In this arrangement, a small jet (ID 0.22 mm) made from a hypodermic needle was moved along the length and width of the scatter volume. The jet was seeded with silicon particles and each of the three LDV components were aligned on the jet so that a Doppler signal was being received. As the jet was moved through the volume the change in S/N level for each LDV component was recorded. Since the total distance moved by the jet from one side of the volume to the other (i.e. from no signal on one side to no signal on the other) contained the diameter of the air jet which produced the Doppler signals a correction to the distance moved was made. This correction was defined as

$$\text{Corrected } L_i = \left(\frac{L_T - d_j}{L_T} \right) L_i \qquad (8)$$

where L_T is the total length moved by the jet from no signal on one side of the volume to no signal on the other; d_j is the inside diameter of the needle jet, and L_i is the distance moved from the no signal position to the i^{th} position at which a S/N measurement was made. These dimensions are illustrated in the following sketch.

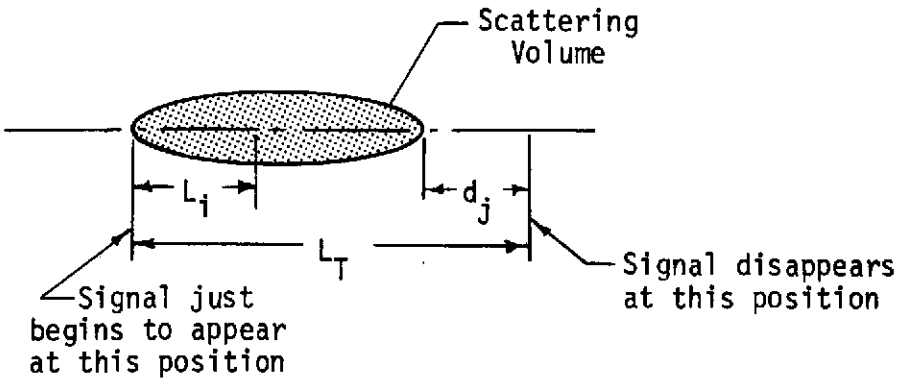

A plot of the scatter volume length and width technique are shown in Fig. 21. The lengths are plotted against the relative signal change which was determined by dividing the maximum S/N recorded for the traverse into the measured S/N at any position.

It should be noted that this measurement technique might be questioned on its accuracy because; (1) the diameter of the jet is on the order of the volume being measured and (2) the actual air jet diameter that is producing the Doppler signal is not the ID of the needle.(the air jet diameter is probably slightly larger due to the jet expansion). The problem with the jet diameter size is most evident in the measurement of the scatter volume width. It is noted that this measurement showed a relatively large region over which the signal intensity was constant as opposed to the Gaussian distribution expected. The flat region was probably due to the gross size of the needle jet in relation the width.

In order to access the accuracy of these measurements, comparisons were made with the data of Mathews and Rust (Ref. 7). Mathews reports on scatter volume measurements made on a reference-scatter and dual beam LDV system. He employed a vibrating needle, which was 0.012 mm in diameter at 0.024 mm from the tip, to obtain a Doppler signal. Using this technique he plotted equal

contour maps of the signal intensity at 20%, 40%, 60%, and 80% of the maximum value within the scatter volumes for several different LDV configurations. A comparison of Mathew's measured scatter volume sizes with that measured by the author using the needle jet for the signal intensity at 20% is given in Table II. This comparison shows that the authors data compares very closely with measurements made by Mathews.

An additional comparison is presented in Fig. 20 which shows the contour measured by Mathews in a reference - scatter system which has an optical arrangement similar to the 3-D-LDV system. The primary difference in the two systems is the scatter angles which is 28° for the 3-D-LDV system and 15° for Mathew's system. It is noted that Mathew's volume is slightly longer which would be expected due to the difference in scatter angle, and is not as wide. The contours for the 3-D-LDV system were obtained from the data of Fig. 19.

One additional point should be made concerning the scatter volume measurements. This point is that the size of the scatter volume is effectively reduced by the frequency trackers which are designed to track only those signals which have a S/N level above 15 db. This effective reduction in scatter volume length is illustrated in Fig. 23. For a maximum S/N ratio of 30 db in the scatter volume, the scatter volume length would be about 0.8 mm, however, if the trackers are used this length is only about 0.4 mm.

In a similar manner, the total scatter volume is reduced by the use of the trackers. This reduction is illustrated in Fig. 24 where the scatter volumes are assumed to be ellipsoids and are computed using the data of Fig. 19.

Using the data of Figs. 21, 22, 23, and 24 and the fact that the maximum S/N usually obtained with the LDV system is 20 - 30 db, the size of the scatter

volume when using the trackers was found to be:

Length - 0.5 mm

Width - 0.08 mm

Ellipsoid Volume - 1.0×10^{-6} cm^3

3.3 PARTICLE SIZE AND CONCENTRATION

Since the LDV system does not measure the velocity of a gas flow directly, but measures the movement of particles suspended in the flow, it is important to obtain a knowledge of the particle size and concentration in order to access the performance of an LDV system.

A casade impactor was used to obtain data from which the particle size and concentration was obtained. This device consists of five stages, each of which collects particles over a calibrated particle size range by causing the particles to flow through a jet at a known speed and to be impacted on a glass slide positioned downstream of the jet. The flow rate through the device is determined by a critical orfice and the total volume of air which passes through the device is established by recording the length of time the sample is taken.

After taking a sample, the mass of collected particles on each slide is determined and this information along with the total volume of air in the sample is used to determine the particle size and concentration.

Using this technique, two samples of the particle flow within the pipe were made. These samples were taken at the pipe centerline and 3.8 cm from the exit (location at which the LDV measurements were made), using an isokinetic sampling probe. The flow velocity at the point the samples were taken was 43.6 m/sec (143 ft/sec).

The following paragraphs document the data reduciton procedure for the particle sample taken on February 2, 1973. The particle material is silicon liquid with a density of 0.95 gm/cm^3.

Casade Impactor Slide #	Mass Collected on Slide (grams X 10^6)	Cumulative Total Wt. (gram X 10^6)	Cumulative % by Wt. larger	Mean Particle Size for Slide (microns)
1	0	0	0	4
2	0	0	0	2
3	30	30	11.5	1
4	120	150	57.6	0.5
5	60	210	80.7	0.25
6	50	260	100.0	

By using the data from the mass collected on each slide, the cumulative percent by weight larger is easily calculated as indicated in the table above. The cumulative percent by weight larger is plotted against the mean particle size for each slide (determined from the manufacturer's calibration data for the particular impactor) on log probability paper. A plot of the data in the above table along with similar data from the sample taken on January 19, 1973 is shown in Fig. 25. If the points on this plot are fitted by a straight line the particle distribution is Gaussian with the slope of the line defining the width of the Gaussian distribution. For example, one standard deviation occurs at 15.87% and 84.13% on the cumulative percent axis. In Fig. 23 the mean particle size based on mass is determined at the 50% point for the size distribution plotted and the particle sizes at one standard deviation are found at 15.87% and 84.13%.

The following calculations are then performed to obtain the mean particle size based on number (N). The primary equation of interest is

$$N = \frac{6M}{\rho\pi d^3}\ \phi \qquad (9)$$

where M = mass of particles/cm of air for the sample collected.

ϕ = mass fraction collected for each slide

ρ = density of the particle material mg/cm^3

d = mean particle diameter based on number for a given slide. This value is determined using the mass distribution on each slide and assuming a Gaussian particle distribution on the slide.

Using the above relation and the collected mass distribution the following values are determined where $A = 6/\rho\pi d^3$ and

$$M = \frac{.26\ \text{mg}}{30\ \text{sec}}\ \frac{60\ \text{sec}}{\text{min}}\ \frac{\text{min}}{1.05\ \text{liter}}\ \frac{\text{liter}}{1000\ \text{cm}^3} = .4952 \times 10^{-6}\ \text{gm/cm}^3$$

and 30 sec = Time for which a sample was taken and

1.05 leter/min = Impactor flow rate.

Slide No.	ϕ	d (microns)	A X 10^{-11}	N 10^{-6} (particles/cm^3)
1	0	5.64	0.1065	0
2	0	2.84	0.843	0
3	.115	1.41	6.83	.0388
4	.461	.707	54.0	1.232
5	.230	.353	433.0	4.920
6	.192	.1775	3410.0	32.30

Total particle Number = 38.4908 x 10^6 particles/cm^3

The cumulative percent by number larger is found in a manner similar to that for the mass distribution. These values are shown below.

Slide No.	Cumulative Number X 10^{-6} (particles)	Cumulative % by Number larger	d (microns)
1	0	0	5.64
2	0	0	2.84
3	.0388	.10	1.41
4	1.2708	3.3	.707
5	6.4908	16.86	.353
6	38.4908	100.0	.1775

The cumulative percent of particle number larger is also plotted in Fig. 23 for the sample given above and for the sample of January 13.

The results of these two samples indicate that the particle concentration is 3.8×10^7 particles/cm^3 and that the mean particle size based on mass is about 0.6 microns and the mean particle size based on number is about 0.2 microns.

It is interesting to note that about 99% of all particles were less than 1 micron in diameter. In fact neither of the two particle samples showed any measurable amount of silicon liquid on the first two impactor plates. This is a strong indication that no large particles are present in the flow.

Of practical importance when considering the particle size and concentration for an LDV measurement, is the accuracy with which the particle flows represent the fluid flows. It is immediately evident that the greater the mass of particle, the greater will be the lag between particle accelerations and the fluid

accelerations. One would like to obtain complete analytical solutions to the equations defining the particle fluid interactions, but unfortunately the expressions do not lend themselves to direct solutions. Many authors (8, 9, 10) have approached this problem, however, no complete solution has been found.

The work presented by Karchnev provides one of the better approaches to the problem. Karchnev gives a solution to the equations defining the ratio of the RMS particle velocity to the RMS fluid velocity for different sizes of Al_2O_3 particles (SG-3.5) which are subjected to a turbulent spectrum at a point in a free jet. The turbulent spectrum is very similar to that found in the pipe flow, however, the particles are 3.5 times as heavy as those used in the pipe flow experiment and Karchnev only considered the behavior of a single particle.

The following figure, taken from Karchnev's report, presents his findings.

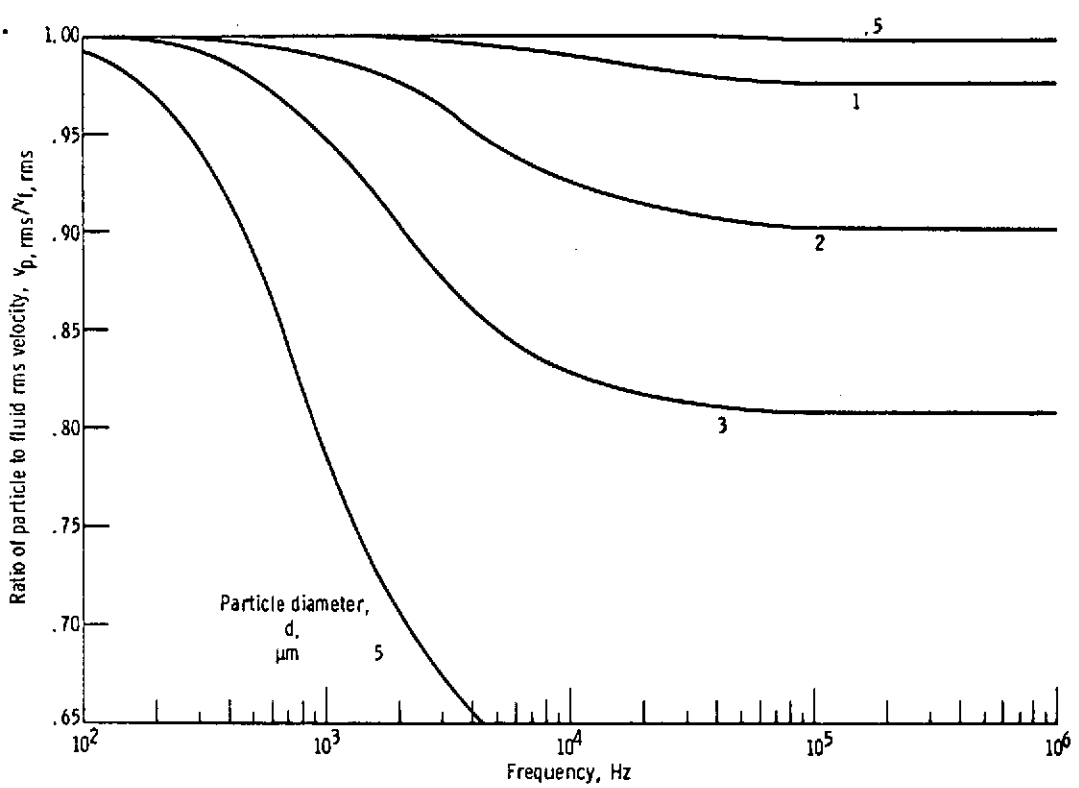

Accuracy of reproduction of rms velocity in a 8.9-centimeter diameter free jet for Al_2O_3 particles of various diameters.

Karchnev points out that this figure does not indicate that a 1 micron particle will reproduce the RMS velocity for this turbulent spectrum within 2.5 percent at 1 MHz. It does however, indicate that if the RMS particle velocity is measured for a bandwidth from 100 Hz to 1 MHz it will be within 2.5 percent of the RMS fluid velocity. Although this curve does not provide a complete or comprehensive picture of the pipe turbulence fluid-particle problem, it does indicate that particles below 1 micron exhibit very small errors (2% or less). The fact that the particles mean particle size based on number was found to be 0.2 microns would further indicate that the particles in the pipe could be expected to very closely approximate the motion of the fluid. In addition, the simultaneous comparisons between the flow fluctuations sensed by the hot wire and LDV system provided further evidence that the particles were accurately representing the flow fluctuations.

One further point should be made concerning the effect of the particle s scattering on the fluid measurement and the operation of the LDV instrument. Since the LDV system operates on the principle of light scattered from particles in the flow and it is recognized that larger particles produce stronger the Doppler signals. Then for a given particle size distribution in a fluid-flow, the actual particles size distribution which produces the measured Doppler signals will be shifted to a slightly larger size. Although, the total amount of the shift has not been determined it is known to lie between the particle distribution curves based on mass and number.

3.4 ANALOG NETWORK

As previously described, the analog network provided solution to the defining LDV equations and allowed for a direct readout of the three turbulent voltages corresponding to the turbulent velocities in the U, V, and W directions.

In order to determine the flatness of the network response through the frequency range of interest for the turbulence tests, a 0.1 volt RMS signal was fed through the network and the response was recorded as the frequency of the input signal was changed from 100 Hz to 100 kHz. The results of these measurements are presented in Fig. 26. It is noted that the system response was flat to within $\pm$ 1.0 millivolts from 100 Hz to 20 kHz which was the frequency range of interest for the pipe turbulence test. From 20 kHz to 100 kHz the response was found to be considerably less flat.

In addition, it was found that the constants in the LDV equations (Fig. 5) which were defined by the different resistor setting, could be accurately set to three significant figures.

3.5 LDV GEOMETRY

The measurements made by the three dimensional LDV system is defined by a set of simultaneous equations which relate the Doppler frequency shift, the geometrical system arrangement, the laser wavelength, and the velocity of particles producing the shift. These equations can be written as:

$$\begin{aligned} \lambda F_1 &= a_1 U + a_2 V + a_3 W \\ \lambda F_2 &= b_1 U + b_2 V + b_3 W \\ \lambda F_3 &= c_1 U + c_2 V + c_3 W \end{aligned} \qquad (10)$$

where

$$\begin{aligned} a_1 &= \cos(\theta_{12}/2)\sin\alpha_1 \\ a_2 &= -\cos(\theta_{31} - 90°)\sin\alpha_1 \\ a_3 &= -(\cos\alpha_1 - 1) \\ b_1 &= \cos(\theta_{12}/2)\sin\alpha_2 \\ b_2 &= -\cos(\theta_{23} - 90°)\sin\alpha_2 \end{aligned}$$

$$b_3 = -(\cos\alpha_2 - 1)$$

$$c_1 = \sin\alpha_3$$

$$c_2 = 0$$

$$c_3 = (\cos\alpha_3 - 1)$$

and the angles are related to the LDV system and pipe arrangement as shown in Fig. 3. In order to determine the coefficients with a high degree of accuracy it was necessary to make accurate measurements of the scattering angles, α, and the angles between the three scatter tubes, θ. Careful measurements of these angles were made using several jigs and arrangements of linear scales. Four different measurements of these angles were made. The mean values and the maximum variation about the mean are shown below:

$\alpha_1 = 28° 22' \pm 6'$ $\qquad$ $\theta_{12} = 120° 3' \pm 17'$

$\alpha_2 = 28° 37' \pm 9'$ $\qquad$ $\theta_{23} = 119° 33' \pm 17'$

$\alpha_3 = 28° 14' \pm 4'$ $\qquad$ $\theta_{31} = 120° 24' \pm 17'$

Using these values in the defining LDV equations, the following set of equations result which give the three velocity components in terms of the measured Doppler frequencies.

$$\begin{aligned} U/\lambda &= .700\ F_1 + .689\ F_2 + 1.41\ F_3 \\ V/\lambda &= 1.21\ F_1 - 1.20\ F_2 - .0036\ F_3 \\ W/\lambda &= 2.78\ F_1 + 2.74\ F_2 - 2.78\ F_3 \end{aligned} \qquad (11)$$

The constants in the above equation were the values used in obtaining the mean and turbulent velocity components for the pipe measurements.

3.6 FLOW FACILITY

Measurements on the flow facility included the pressure drop down the pipe, pitot profiles at the pipe exit, and turbulent and mean velocity measurements along the pipe centerline at the pipe exit.

As shown by Laufer [1], the following equations relate the Reynolds stresses to the mean velocity and pressure distributions in a fully developed turbulent pipe flow in a smooth pipe.

$$\overline{u'v'} = \nu \frac{dU}{dz} + \frac{z}{r} U_\tau^2 \qquad (12)$$

and

$$U_\tau^2 = \frac{r}{2\rho} \frac{dp}{dx} \qquad (13)$$

where $\overline{u'v'}$ = Reynolds shear stress, ν is the kinematic viscosity, dU/dz is the mean velocity distribution in the z direction, r is the pipe radius, U_τ is the shear velocity, ρ is the density and dp/dx is the axial pressure distribution.

It is seen from these expressions, that the absolute accuracy of the measurements of the Reynolds stresses can be obtained if the mean velocity and pressure distributions are known. For this reason measurements of the pressure distributions were made using a Hooke gauge which could read pressures to within 0.001 inch. The results of these measurements for the pipe test section are given in Fig. 27 for the pipe flow both with and without particles. For a centerline velocity of 43.6 m/s, the pressure gradient was found to be 0.146 inches H_2O/ft. and no appreciable differences were found between the seeded and unseeded flows. Using this value the shear velocity U_τ was found to be 1.58 m/sec (5.18 ft/sec).

Velocity profile measurements using a pitot tube were made at the exit

of the pipe to determine the symmetry of the pipe flow. It was necessary to make several adjustments of the screens in order to obtain an acceptable symmetry in the pipe flow.

In order to determine if the pipe flow at the exit and close to the centerline was similar both inside the pipe, measurements with a single constant temperature anenometer were made of the axial turbulent intensity and the mean velocity. These measurements are shown in Fig. 28 and it is noted that the, within the accuracy of the measurements, no discernible change was found between the measurements inside the pipe and those close to the exit. These measurements support the fact that the turbulent characteristics outside and close to the pipe exit, are very similar to those found inside the pipe. For this reason, it was felt that the relations defining the turbulent characteristics inside the pipe would also hold within the region investigated by the LDV system.

3.7 VELOCITY MEASUREMENTS

The aim of the velocity measurements that were made, was to provide turbulence data which would demonstrate the capabilities of the LDV system for making turbulence measurements in the pipe flow. It was intended that this capability would be demonstrated by making simultaneous comparisons of the LDV and hot wire signals, and making comparisons of the statistical signal parameters with data from the literature. Unfortunately time limitations did not allow for complete reduction of all the data taken and only limited comparisons were available.

The measurement effort was conducted at a position 3.8 cm from the pipe exit, with a pipe centerline velocity of 43.6 m/sec (143 ft/sec) which

provided a pipe Reynolds number of 250,000. A DISA constant temperature anenometer with a single hot wire probe was used to obtain comparison data. The hot wire probe was positioned about 1 mm downstream of the LDV scatter volume and was moved in the same increments as the scatter volume when a profile was taken. The relative size and position of the scatter volume and hot wire are indicated in Fig. 20.

Since the hot wire was operated at the same time the LDV measurements were made, the effects of the silicon particles which impacted on the wire investigated. The hot wire was platinum iridium and operated at a temperature of approximately 1000°F, the purpose being to vaporize any particles which struck the wire. A calibration curve of the hot wire was made in both seeded and unseeded flows (Fig. 29). It was found that although the shape of the curve changed, the curve appeared to be stable while operating in the seeded flows. Upon observing the hot wire output while operating in the seeded flows, it was found that relatively few particle impactions with the wire could be observed.

Simultaneous comparisons of the turbulent signals for the hot wire which was measuring the U velocity component and the U velocity component of the LDV were made in a variety of manners. Figure 30 shows a Lissajous display of the two signals as the upper cut-off frequency on the bandpass filters was increased from 5,000 to 20,000 Hz. The displays show that the correlation of the two signals decreased as the bandpass filter was opened Figure 31 shows a comparison of the correlation functions of the two signals at the same point in the pipe flow.Figure 31-A shows overlay oscilloscope traces of the two fluctuating signals. Figures 32, 33, and 34 provide an even more graphic view of the signals observed by the two systems. These traces indicate

that the signals sensed by the LDV system were almost identical to those sensed by the hot wire.

In conducting the measurements of the profile at the pipe exit, the RMS values of the turbulent output from the LDV and hot wire signals were recorded from a true RMS meter, and the signals were also recorded on magnetic tape for further analysis of the statistical quantities.

Using the RMS reading, the turbulent intensities were computed and plotted along with data from the literature. Figures 35, 36, and 37 show the turbulent intensity profile for the u', v', and w' velocity components. In addition, the three mean velocity components measured with the LDV for several sets of data is shown in Fig. 38. A comparison of the mean U velocity component profile for the LDV and hot wire with that of Laufer is shown in Fig. 39.

Further investigations of the statistical comparisons of the hot wire and LDV components were made using the data recorded on magnetic tape. These investigations employed a digital computer to obtain spectra distributions and correlation functions up to a frequency of 5000 Hz. Figures 40 and 41 show comparisons of the correlation and spectra distributions at a point in the pipe flow. Both comparisons illustrate the fact that the two systems were responding in an almost identical manner. It is also interesting to note that three discrete frequencies at approximately 2700, 3700, and 4600 Hz were picked up by both the systems. It is unlikely that these signals were of an electronic origin, since both the hot wire and LDV responded to them. These discrete frequencies are believed to be of an acoustic nature,

and were most likely related to sound harmonies within the pipe. Although it was originally intended that a more extensive analysis of the data be conducted, i.e. Reynolds stress terms, cross spectra, etc., time limitations prevented this.

4.0 ACCURACY CONSIDERATIONS

There are several characteristics of the LDV system which can produce errors. These include

(1) the ability of the particles to follow the flow field fluctuations

(2) the broadening of the Doppler signal which results from the fact that the optics collect the scattered light over a finite region of scatter angles rather than a single angle

(3) the ability of the electronic tracking systems to follow the Doppler signals

(4) the nonlinear nature of the calibration curve

4.1 PARTICLES

Although it would be desirable to arrive at some absolute method for determining how well the particles follow the flow fluctuations, it appears that the only method available is to perform analytical solutions to the equations which define the behavior of particles in the turbulent flows. At the very best, these solutions only offer some qualitative information as to the general particle size ranges that will follow given flow fields. The information is usually questionable due to the assumptions imposed on the problem in order that solutions can be obtained. For example, most solutions

only consider the behavior of a single particle of a given size and disregard any particle - particle interaction or the effect of multiple particle sizes.

As noted in the previous discussions on particle size and concentration measurements, particle sizes less than 1.0 micron in size can be expected to provide an error in the RMS velocity of less than 2% for turbulent frequencies out to 10,000 Hz. It was further noted that since the measured mean particle size was 0.2 microns it would seem logical to conclude that the particle flows in the pipe flow would represent the RMS fluid velocities to within 1 to 2%.

4.2 APPERATURE BROADENING

The LDV system used in this study has a fundamental limitation on the accuracy with which a velocity measurement can be made. This limitation is due to the fact that the Doppler shift depends upon scattering angle and the scattered light is collected over a finite range of angles. The magnitude of this limitation for the LDV system configuration used in the measurements reported here may be computed in the following manner.

For simplicity in the calculations, it is assumed that the total velocity vector $\vec{V}_T$ is in the direction sensed by one of the scatter tubes of the 3-D LDV system. This is illustrated in the following sketch.

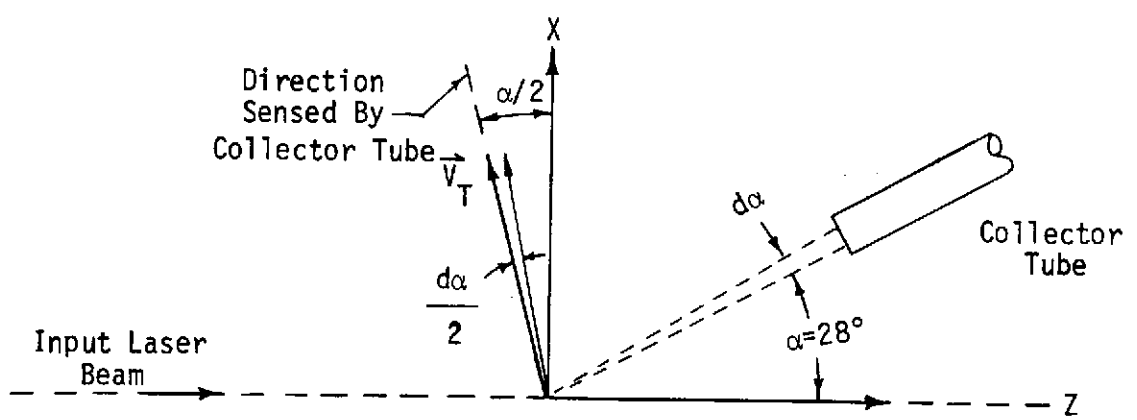

For this configuration the defining Doppler equation may be written as

$$F = 2V_T \sin(\alpha/2)/\lambda \tag{14}$$

The rate of change in Doppler frequency with scatter angle becomes

$$dF/\alpha = V_T \cos(\alpha/2)/\lambda \tag{15}$$

and substituting for Eq. 14

$$dF/d\alpha = F \cot(\alpha/2)/2 \tag{16}$$

or

$$dF/F = (\cot(\alpha/2)/2)d\alpha \tag{17}$$

which defines the variation in measured Doppler frequency with variation in scatter angles.

For the LDV conifguration used α=28° and $d\alpha$ or $\Delta\alpha$=1°, Eq. 17 yields

$$\Delta F/F = 0.035$$

Thus, it is seen that a fundamental uncertainty exists in the Doppler frequency of 3.5%. This will translate to a similar uncertainty in the measured velocities.

The above analysis assumes that the intensity of the scattered radiation is evenly distributed across the face of the collection optics. It is more likely that the scattered radiation has a Gaussian distribution across the collection optics. Such a consideration would have the effect of reducing the incremental scatter angle, $\Delta\alpha$. For example, if one assumes that the $\Delta\alpha$ of 1° represents the 3σ points, the effective value of $\Delta\alpha$ at the 1σ point will be 0.33° and the Doppler frequency uncertainty will be only.

$$\Delta F/F = 0.016$$

It should be noted that although only two dimensions were considered in the above analysis, an identical result is obtained when the scattered light is assumed to be collected over a solid angle rather than in a plane. The physical meaning of the analysis for the total velocity vector V in three dimensions being that the direction as well as the magnitude has a fundamental uncertainty.

4.3 INSTRUMENTATION

In the previous sections, fundamental measurement limitations were examined. In this section, the accuracy with which the electronic instrumentation, i.e. the frequency trackers, are able to provide a voltage readout and a subsequent velocity readout are examined. As noted in previous discussions, the equations defining the instanstaneous velocity components and the Doppler frequencies for the pipe turbulence tests may be written as:

$$
\begin{aligned}
u'/\lambda &= .700\ \frac{dF_1}{dE_1} e_1' + .689\ \frac{dF_2}{dE_2} e_2' + 1.41\ \frac{dF_3}{dE_3} e_3' \\
v'/\lambda &= 1.21\ \frac{dF_1}{dE_1} e_1' - 1.21\ \frac{dF_2}{dE_2} e_2' + .0036\ \frac{dF_3}{dE_3} e_3' \\
w'/\lambda &= 2.78\ \frac{dF_1}{dE_1} e_1' + 2.74\ \frac{dF_2}{dE_2} e_2' - 2.78\ \frac{dF_3}{dE_3} e_3'
\end{aligned}
\qquad (18)
$$

The expressions for the error in velocity in terms of the voltage error are:

$$\Delta u' = \Delta e_1(\partial u/\partial e_1) + \Delta e_2(\partial u/\partial e_2) + \Delta e_3(\partial u/\partial e_3)$$

$$\Delta v' = \Delta e_1(\partial v/\partial e_1) + \Delta e_2(\partial v/\partial e_2) + \Delta e_3(\partial v/\partial e_3)$$

$$\Delta w' = \Delta e_1(\partial w/\partial e_1) + \Delta e_2(\partial w/\partial e_2) + \Delta e_3(\partial w/\partial e_3)$$

Where from Eq. 18

$$\partial u/\partial e_1 = \lambda\ .700\ dF_1/dE_1$$

$$\partial u/\partial e_2 = \lambda\ .689\ dF_2/dE_2$$

$$\partial u/\partial e_3 = \lambda\ 1.41\ dF_3/dE_3$$

$$\partial v/\partial e_1 = \lambda\ 1.21\ dF_1/dE_1$$

$$\partial v/\partial e_2 = -\lambda\ 1.20\ dF_2/dE_2$$

$$\partial v/\partial e_3 = \lambda\ .0036\ dF_3/dE_3$$

$$\partial w/\partial e_1 = \lambda\ 2.78\ dF_1/dE_1$$

$$\partial w/\partial e_2 = \lambda\ 2.74\ dF_2/dE_2$$

$$\partial w/\partial e_3 = -\lambda\ 2.78\ dF_3/dE_3$$

Figure 18 shows the slopes of the tracker calibration curves over the ranges used during the pipe test. These ranges for the different systems are

(MHz/volt)	From (pipe ℄)	To
dF_1/dE_1	10.3	11.2
dF_2/dE_2	9.9	8.5
dF_3/dE_3	9.1	10.6

Using these ranges of values the rates of change of velocity with voltage are found to be

(ft/sec)/volt		From	To
$\partial u/\partial e_1$	=	12.17	13.23
$\partial u/\partial e_2$	=	11.51	9.88
$\partial u/\partial e_3$	=	21.65	25.22

(ft/sec)/volt		From	To
$\partial v/\partial e_1$	=	21.03	22.87
$\partial v/\partial e_2$	=	-20.05	-17.21
$\partial v/\partial e_3$	=	0.055	0.064
$\partial w/\partial e_1$	=	48.33	52.55
$\partial w/\partial e_2$	=	45.78	39.31
$\partial w/\partial e_3$	=	-42.70	-49.74

Assuming that the best accuracy with which a voltage can be measured with the trackers is $\pm$ .005 volts, the corresponding velocity errors on the different components for the ranges in which the pipe turbulence measurements were made become

(ft/sec)	$\pm \Delta u$	$\pm \Delta v$	$\pm \Delta w$
From (pipe $\mathbb{C}$)	.226	.206	.684
To (Shear region)	.241	.200	.708

Then the above errors in velocity will result from the fact that the voltages can only be measured with a certain precision. It is noted that this error is relatively constant from the pipe centerline to the flow shear region.

Since the RMS velocities had the lowest values at the pipe centerline, the voltage error will create the largest percentage error at that position. The RMS voltages measured were

$$\sqrt{\overline{u^{12}}} = 4.56 \text{ ft/sec} \quad \sqrt{\overline{v^{12}}} = 3.52 \text{ ft/sec} \quad \sqrt{\overline{w^{12}}} = 5.8 \text{ ft/sec}$$

and the percentage errors are

$$\pm\Delta u \Big/ \sqrt{\overline{u'^2}} = 4.9\% \quad \pm \Delta v \Big/ \sqrt{\overline{v'^2}} = 5.8\% \quad \pm \Delta w \Big/ \sqrt{\overline{w'^2}} = 11.8\%$$

In the shear regions of the pipe flow the RMS velocities are approximately twice as large as at the centerline. The percentage errors at the shear region will be about one half of the values shown above.

However, in the shear region an additional error begins to occur. This problem is caused by the decrease in particle concentration due to entrainment of unseeded air in the shear region. This reduction results in an intermittant Doppler signal and subsequent deterioration of the frequency tracker operation.

It is of interest to note that the errors in the w velocity component are about twice as large as those in the u and v components. This results for the geometrical arrangement of the instrument which makes the sensitivity in the w velocity direction less than in the u and v directions.

4.4 MEASUREMENT REPEATABILITY

As a check on the repeatability of the system, several profiles were made at 3.8 cm from the pipe exit. The mean values of these measurements were calculated and plotted as shown in Figs. 42, 43, and 44. In these figures the bars represent the range over which the measurements varied. It is noted that the variations became wider as the measurements progressed further into the shear region. This variation is probably a result of the decrease in particle concentration, which results in a discontinuous Doppler signal along with inaccurate frequency tracker operation.

4.5 NON-LINEAR CALIBRATION CURVE

Since the slopes of the calibration curve are not constant (Fig. 18), it is not exact to take the slope of the calibration curve at the mean voltage

of a fluctuating signal and use it reducing the RMS fluctuations around that mean. This was the procedure that was used in the reduction of the RMS data in the analog network.

The error caused by the use of this procedure was calculated for each of the trackers operating within the calibration curve intervals in which the pipe turbulence measurements were made. These calculations were performed in the following manner.

Consider that the means have been substracted from both the Doppler frequency function and the voltage function, i. e. $f(0) = e(0) = 0$. The Taylor expansion for the Doppler frequency, f, in terms of the tracker voltage, e, is

$$f(e) = e(0) + ef'(0) + \frac{e^2}{2} f''(0) + \ldots \qquad (19)$$

For a first order approximation (which was the relation used for the analog network in this test)

$$f(e) = e\, f'(0)$$

and

$$f^2(e) = e^2(f'(0))^2 \qquad (20)$$

Since the slope of the calibration curve $f'(0)$ is not constant the second order approximation will include the term defining the rate of change of $f'(0)$. This expression is

$$f(e) = ef'(0) + e^2/2\, f''(0)$$

and

$$f^2(e) = e^2(f'(0))^2 + e^3 f'(0)\, f''(0) + \frac{e^4}{4} (f''(0))^2$$

The RMS of Eq. 20 may be written as follows for the first order case

$$\overline{(f(e))}^{1/2} = (\overline{e^2})^{1/2} \; f'(0)$$

And the RMS of the second order approximation is

$$\overline{(f(e))}^{1/2} = \left[\overline{e^2}(f'(0)^2 + \overline{e^3} \; f'(0) \; f''(0) + \frac{\overline{e^4}}{4} (f''(0))^2 \right]^{1/2} \quad (21)$$

However, if e is symmetrical (which appears to be a good assumption from examinations of the data), $\overline{e^3} = 0$, and for a normal distribution of e, $\overline{e^4} = 3(\overline{e^2})^2$

Equation 21 now becomes

$$\overline{(f^2(e))}^{1/2} = \left[\overline{e^2}(f'(0))^2 + .75 \; (\overline{e^2})^2 \; (f''(0))^2 \right]^{1/2}$$

Then the percentage error in using the first order approximation rather than the second may be written as

$$\% \text{ Error} = 100 \left[\frac{\left[f'(0)^2 + .75 \; \overline{e^2} \; (f''(0)^2 \right]^{1/2}}{f'(0)} - 1 \right]$$

The following values were obtained from the pipe measurements conducted give the largest percentage error.

$f'(0) = 11.2$ MHz/volt

$\overline{e^2} = .067$ volts^2

$f''(0) = 1.16$ (MHz/volt)/volt

And the error is

% Error = .027

Thus the error from the non-linear calibration curve is negligible.

5.0 CONCLUSIONS AND RECOMMENDATIONS

The purpose of the test program was the demonstration of the capability of the 3-dimensional LDV system for the measurement of pipe turbulence. For the measurements conducted the following conclusions were drawn.

1. The flow fluctuations to which the LDV system responded were the same as that sensed by the hot wire.
2. The use of the LDV system for routinely obtaining three dimension turbulence and mean velocity measurements was established.
3. The degree of accuracy which can be achieved with the system depends on the particle trackability, apperature broadening, and instrumentation readability. For the pipe measurements the u and v components are considered accurate to within 5% and the w component to within 11%.
4. A scatter volume of $1.0 \times 10^{-6} cm^3$ with a particle concentration of 10^8 particles/cm^3 will provide a continuous Doppler signal for measurement of turbulent frequencies up to 10,000 Hz.

Based on the findings of this investigation the following recommendations are made

1. Use the system to conduct velocity measurements in flows in which conventional techniques are not adequate. For example in combustors or flames, spray nozzles, and naturally particulate laden flows such as smokes.
2. Incorporate a technique, such as an acoustic-optic modulator, for extending the usefulness of the system to lower velocities. In the present configuration the system is limited to mean velocities above about 10 ft/sec.

6.0 REFERENCES

1. Laufer, John, "The Structure of Turbulence in Fully Developed Pipe Flow," NACA Report 1174, 1954.

2. Rolfe, E. et. al., "Laser Doppler Velocity Instrument," NASA CR-1199, 1968.

3. Fridman, J. D., et. al., "Wide Band Frequency Tracker Performance," Raythcon Co. ER 70-4286, December 1970.

4. Cliff, W. C. Fuller, C. E. and Sandborn, V. A.,"Simultaneous Comparisons of Turbulent Gas Measurements by Laser Doppler and Hot Wire," AIAA Journal, May, 1973.

5. Huffaker, R. M.; Fuller, C. E.; and Lawrence, T. R.,"Application of Laser Doppler Velocity Instrumentation to the Measurement of Jet Turbulence," International Automotive Engineering Congress, Detroit, Mich., Report 690266, January 1969.

6. Morrison, L. K.,"A Study of Design Parameters for a Laser Velocity Instrument," Lockheed Missiles and Space Corp., TM 54/20-202, December, 1968.

7. Mathews, L. K. and Rust, J. H., "Laser Doppler Velocimeters - Performance in Open and Confined Flows," School of Nuclear Engineering, Georgia Institute of Technology, Atlanta, Georgia, 1972.

8. Hinze, J. O., "Turbulent Fluid and Particle Interaction," International Symposium on Two-Phase Systems, Haifa, Israel, September, 1971.

9. Berman, N. S., "Particle Fluid Interaction Corrections for Flow Measurements with a Laser Doppler Flowmeter," Arizona State Univeristy Engineering Report on NASA Contract No. NAS8-21397.

10. Karchnev, A. M., "Particle Trackability Considerations for Laser Doppler Velocimetry," NASA TM X-2628, September, 1972.

11. Patel, R. P., "Measurements of the Reynold Stresses in a Circular Pipe as a Means of Testing DISA Constant Temperature Hot Wire Anemometer," Mech. Eng. Res. Lab., McGill University, Tech. Note 63-6, 1963.

12. Sandborn, V. A., "Experimental Evaulation of Momentum Terms in Turbulent Pipe Flow," NACA TN 3266, 1955.

13. So, R.M., and Mellor, G. L., "An Experimental Investigation of Turbulent Boundary Layers Along Curved Surfaces," NASA CR-1940, April 1972.

Table I

Tracker Correlation Measurements of the AC Outputs
for the Same Doppler Signal Input

Trackers Correlated (a) - (b)	Tracker Mode (102 and 103)	$\overline{e_a e_b}$	$\sqrt{\overline{e_a^2}}$	$\sqrt{\overline{e_b^2}}$	R_{ab}
103 - 102	wide	.583	.468	.776	.962
		.559	.468	.776	.930
		.257	.197	.471	.843
		.271	.215	.497	.829
103 - 101	wide	.516	.443	.846	.845
		.525	.443	.846	.860
		.283	.550	.286	.715
		.302	.550	.286	.763
101 - 102	wide	.592	.840	.474	.940
		.588	.840	.474	.933
		.246	.165	.586	.792
		.574	.720	.515	.950
103 - 102	narrow	.555	.508	.777	.890
		.206	.403	.148	.843
		.218	.403	.148	.885
103 - 101	narrow	.575	.512	.859	.870
		.567	.512	.859	.860
		.234	.182	.569	.728
101 - 102	narrow	.583	.841	.495	.903
		.587	.841	.495	.909
		.191	.632	.111	.72
		.322	.767	.316	.654

Table II

Comparison of Scatter Volume Measurements
with Data from Mathews and Rust (Ref. 7)

			Focusing Lens				Scatter Volume*		
Data Source	LDV System	Scatter Angle (deg)	F/Number	Focal Length (mm)	Beam Dia. at Lens (mm)	Beam Dia. at Focus (mm)	Length (mm)	Width (mm)	Volume x 10^6 cm^3
Author	Ref - Scatt.	28.0	67.7	.860	12.7	.088	.584	.101	3.15
Ref. 7	Ref - Scatt.	15.0	60.9	122	2.0	.124	.711	.076	2.16
Ref. 7	Dual-Beam	20.8	52.7	37	0.701	.040	.304	.063	0.64
Ref. 7	Dual-Beam	12.5	128.3	90	0.701	.101	.914	.101	4.93
Ref. 7	Dual-Beam	11.0	256.7	180	0.701	.198	2.159	.190	40.78

* Scatter Volume dimensions defined at the points where the signal intensity is 20% of maximum

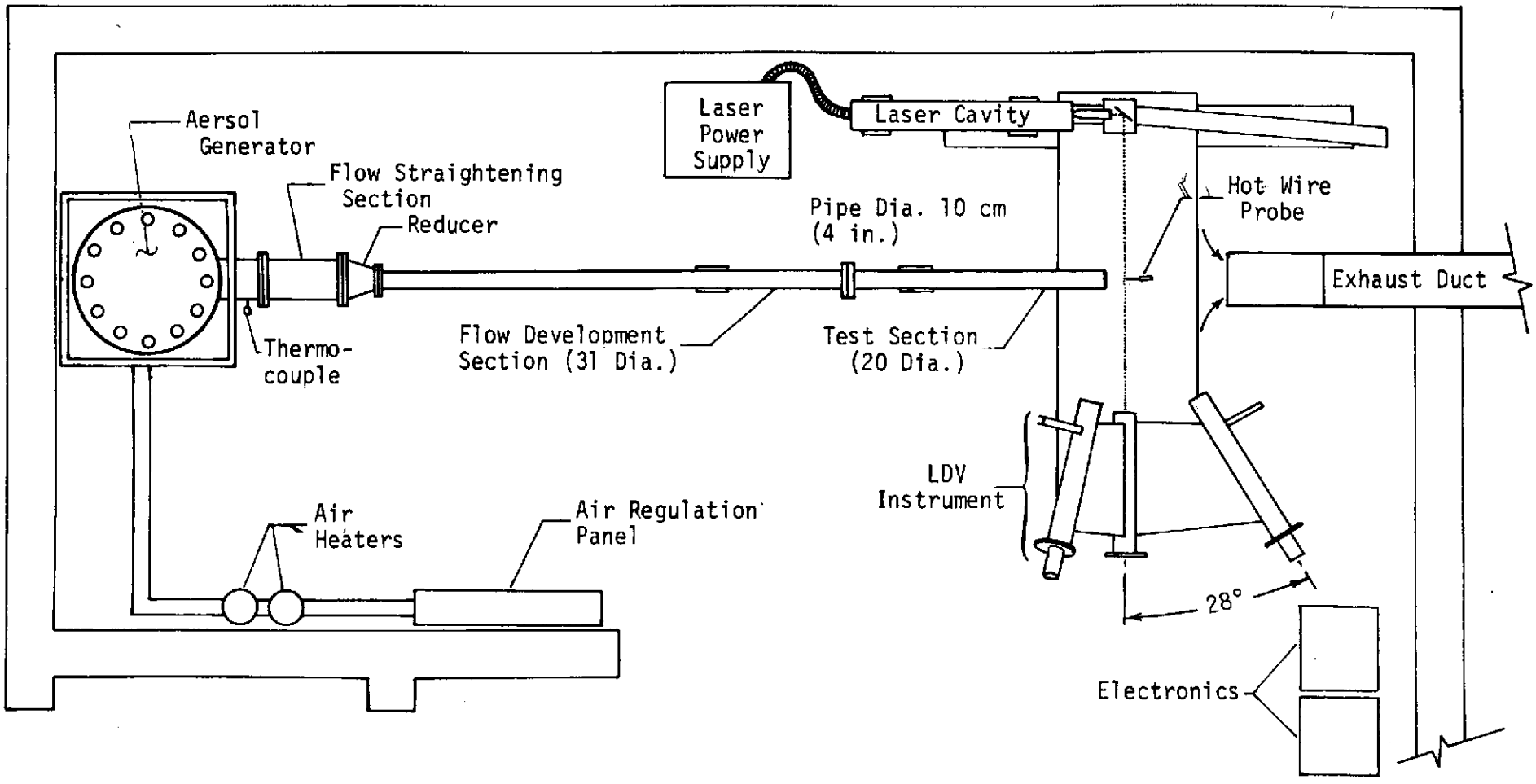

Fig. 1 LDV Pipe Turbulence Test Arrangement

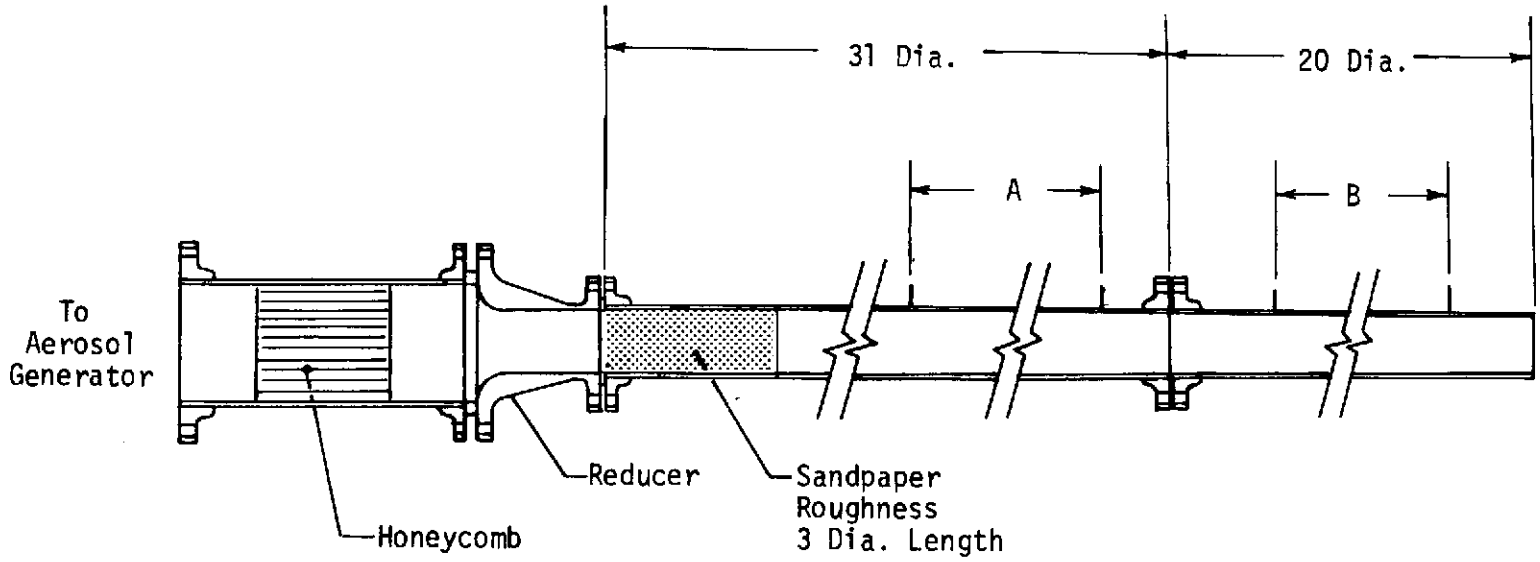

Notes:

A = 7 static pressure tapes at 12'' intervals
B = 9 static pressure tapes at 8'' intervals
Pipe diameter = 10 centimeters

Fig. 2 Pipe Flow Sections

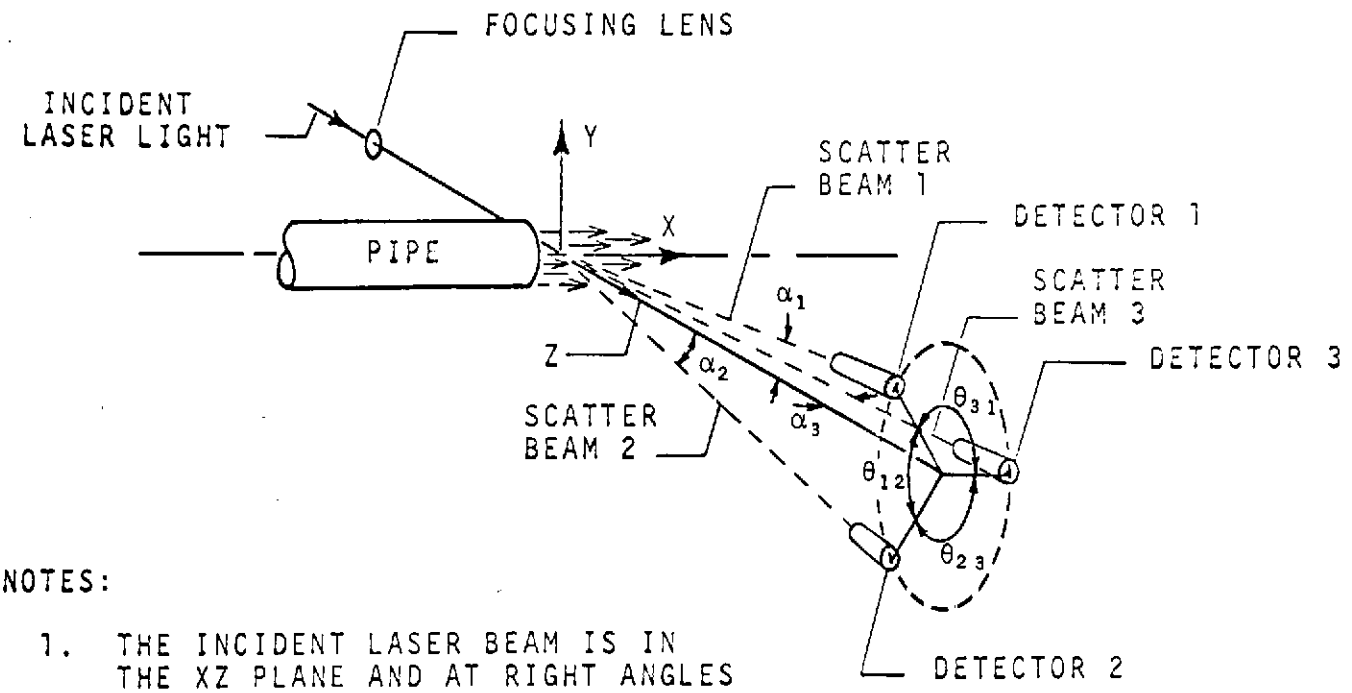

NOTES:

1. THE INCIDENT LASER BEAM IS IN THE XZ PLANE AND AT RIGHT ANGLES TO THE PIPE CENTERLINE.

2. THE VELOCITY COMPONENTS U, V, AND W ARE IN THE DIRECTIONS X, Y, AND Z RESPECTIVELY.

3. DETECTOR 3 IS IN THE X-Z PLANE.

FIG. 3 SCHEMATIC OF THE THREE DIMENSIONAL LDV AND ITS ALIGNMENT RELATIVE TO THE PIPE

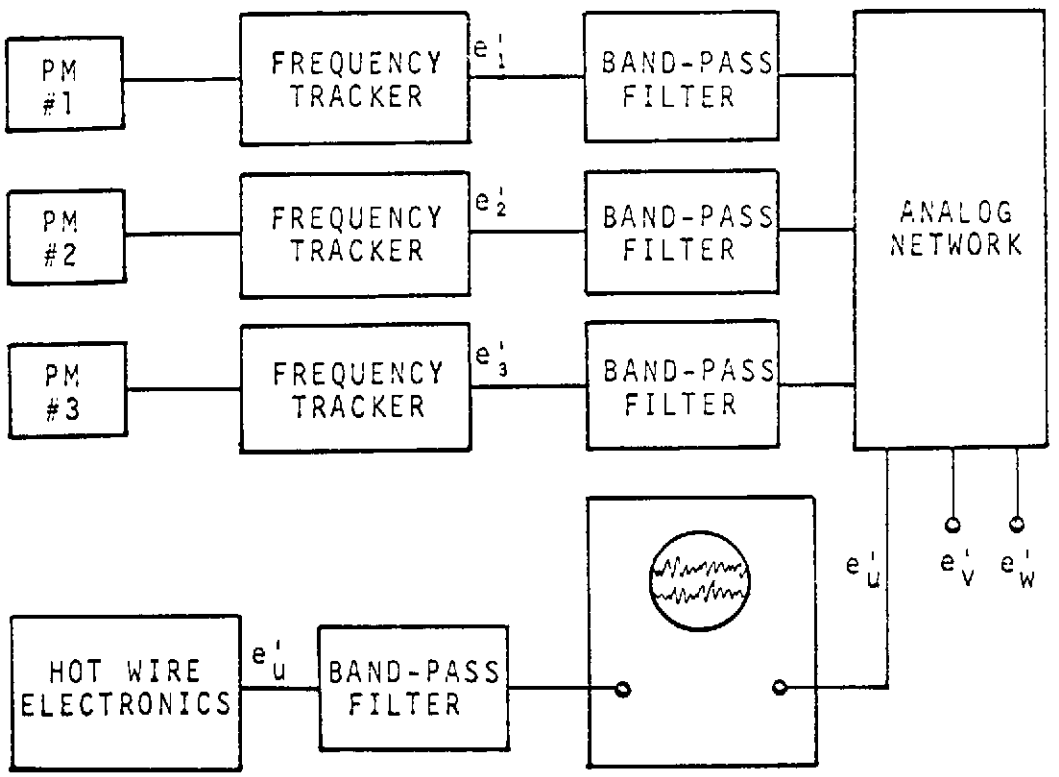

Fig. 4 Schematic of Electronic Network for LDV Turbulence Measurements

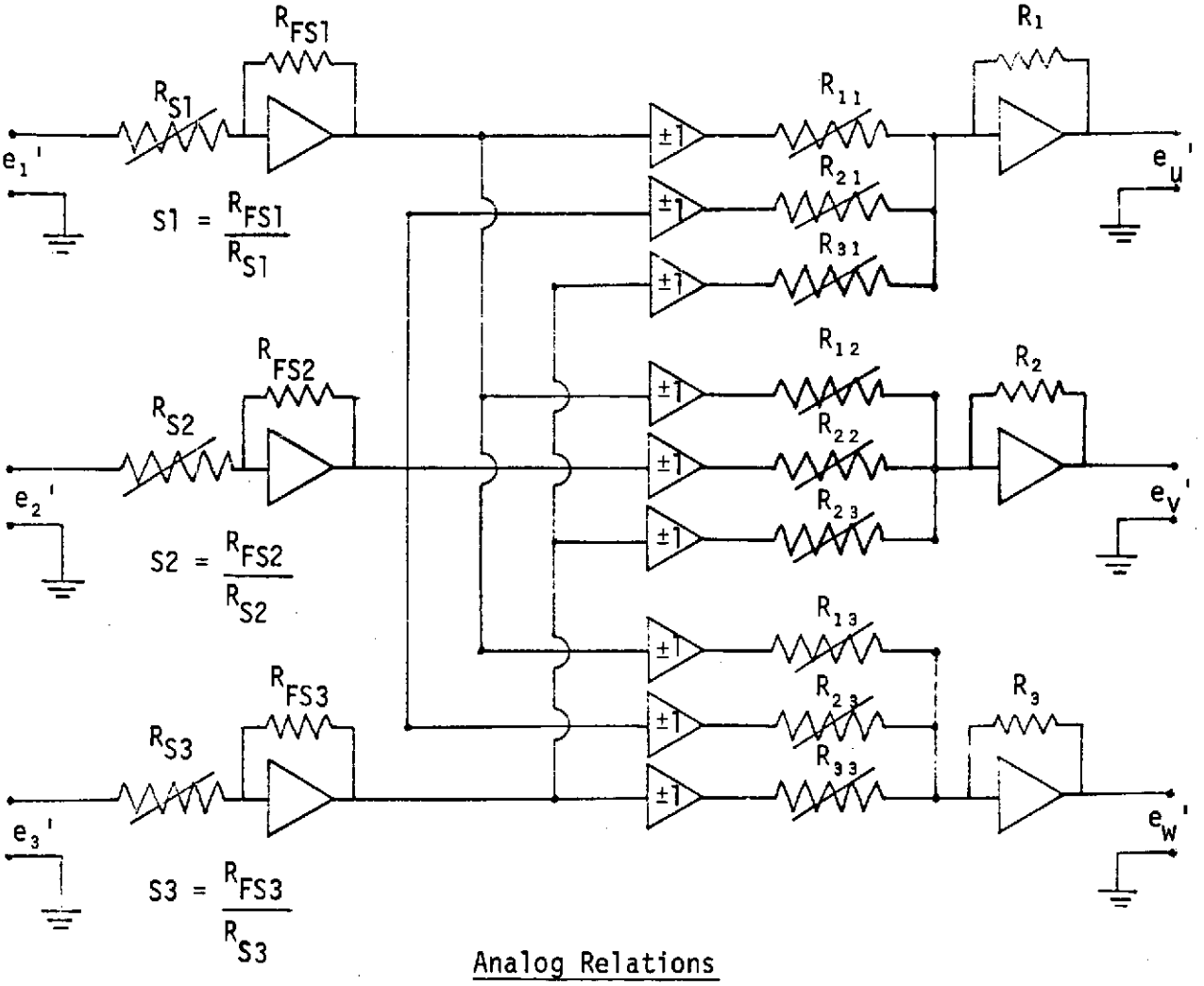

Analog Relations

$$e_u' = e_1' (S1) \frac{R_1}{R_{11}} + e_2' (S2) \frac{R_1}{R_{21}} + e_3' (S3) \frac{R_1}{R_{31}}$$

$$e_v' = e_1' (S1) \frac{R_2}{R_{12}} + e_2' (S2) \frac{R_2}{R_{22}} + e_3' (S3) \frac{R_2}{R_{32}}$$

$$e_w' = e_1' (S1) \frac{R_3}{R_{13}} + e_2' (S2) \frac{R_3}{R_{23}} + e_3' (S3) \frac{R_3}{R_{33}}$$

Corresponding LDV Relations

$$e_u' = \frac{dE_1}{dF_1} \frac{u'}{\lambda} = e_1' (1) A_1' + e_2' \left(\frac{dF_2}{dE_2} \frac{dE_1}{dF_1}\right) A_2' + e_3' \left(\frac{dF_3}{dE_3} \frac{dE_1}{dF_1}\right) A_3'$$

$$e_v' = \frac{dE_1}{dF_1} \frac{v'}{\lambda} = e_1' (1) B_1' + e_2' \left(\frac{dF_2}{dE_2} \frac{dE_1}{dF_1}\right) B_2' + e_3' \left(\frac{dF_3}{dE_3} \frac{dE_1}{dF_1}\right) B_3'$$

$$e_w' = \frac{dE_1}{dF_1} \frac{w'}{\lambda} = e_1' (1) C_1' + e_2' \left(\frac{dF_2}{dE_2} \frac{dE_1}{dF_1}\right) C_2' + e_3' \left(\frac{dF_3}{dE_3} \frac{dE_1}{dF_1}\right) C_3'$$

Fig. 5 Schematic of Analog Network for Obtaining Three Turbulent Voltage - Velocity Components

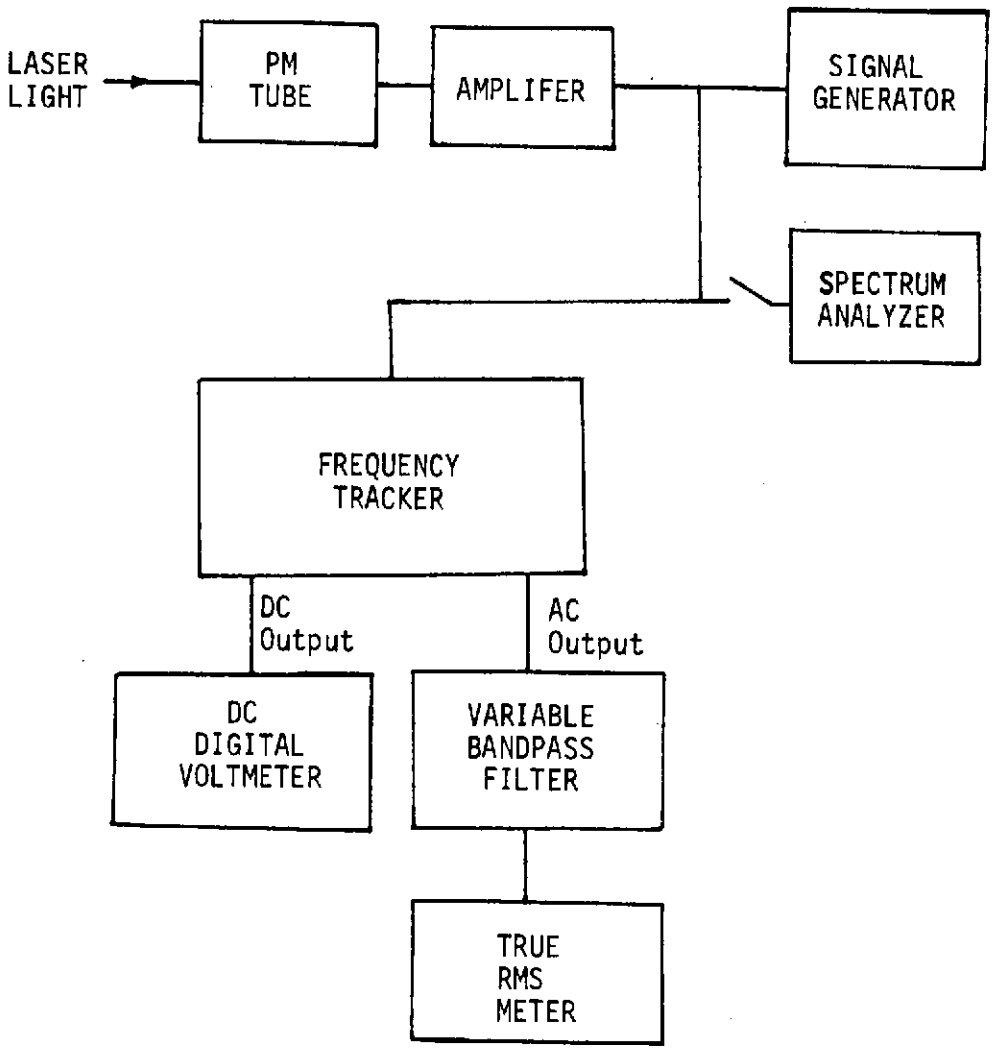

Fig. 6 SYSTEM SCHEMATIC FOR TRACKER NOISE MEASUREMENTS

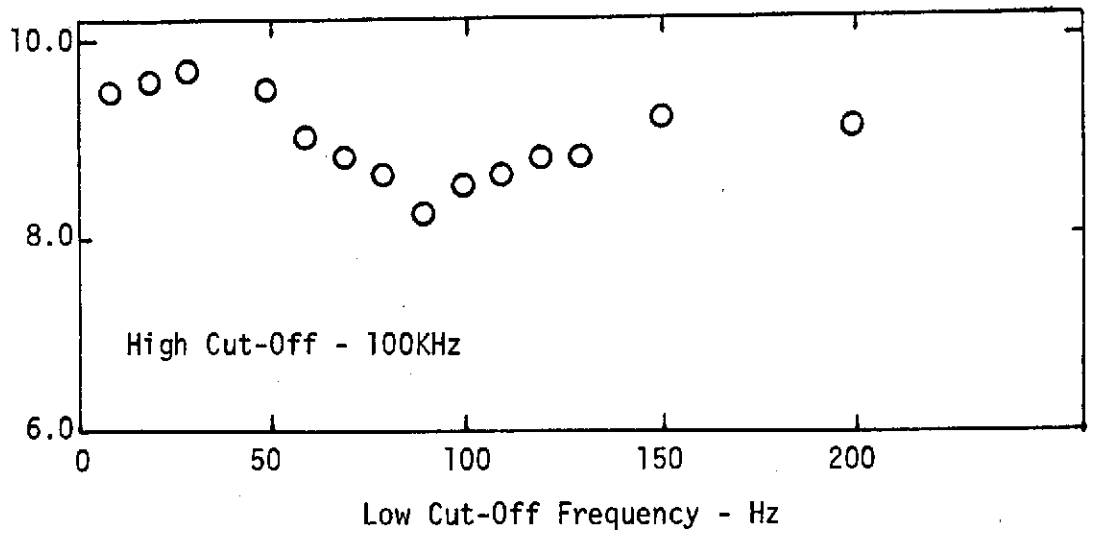

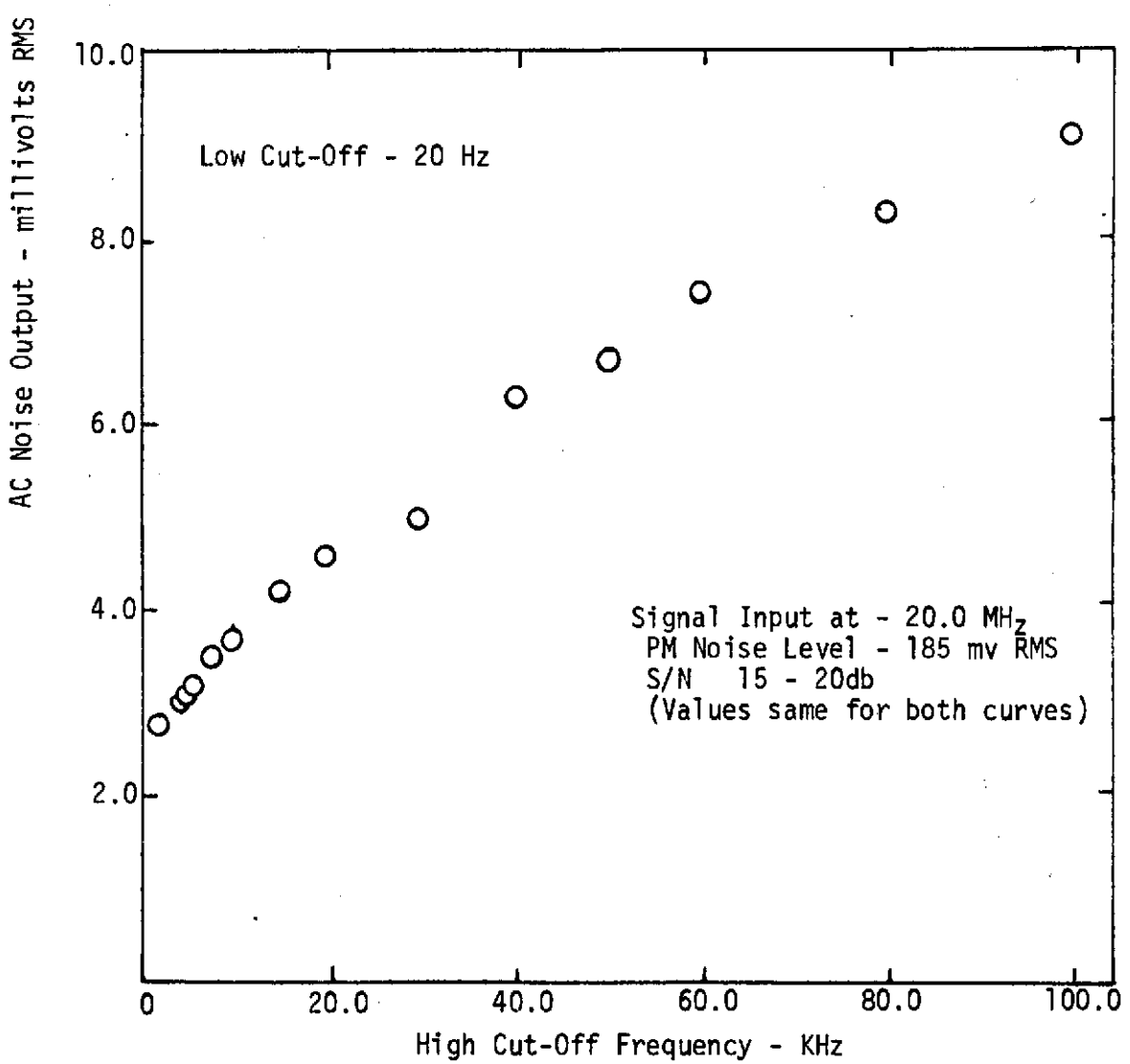

Fig. 7 Frequency Tracker Noise Levels

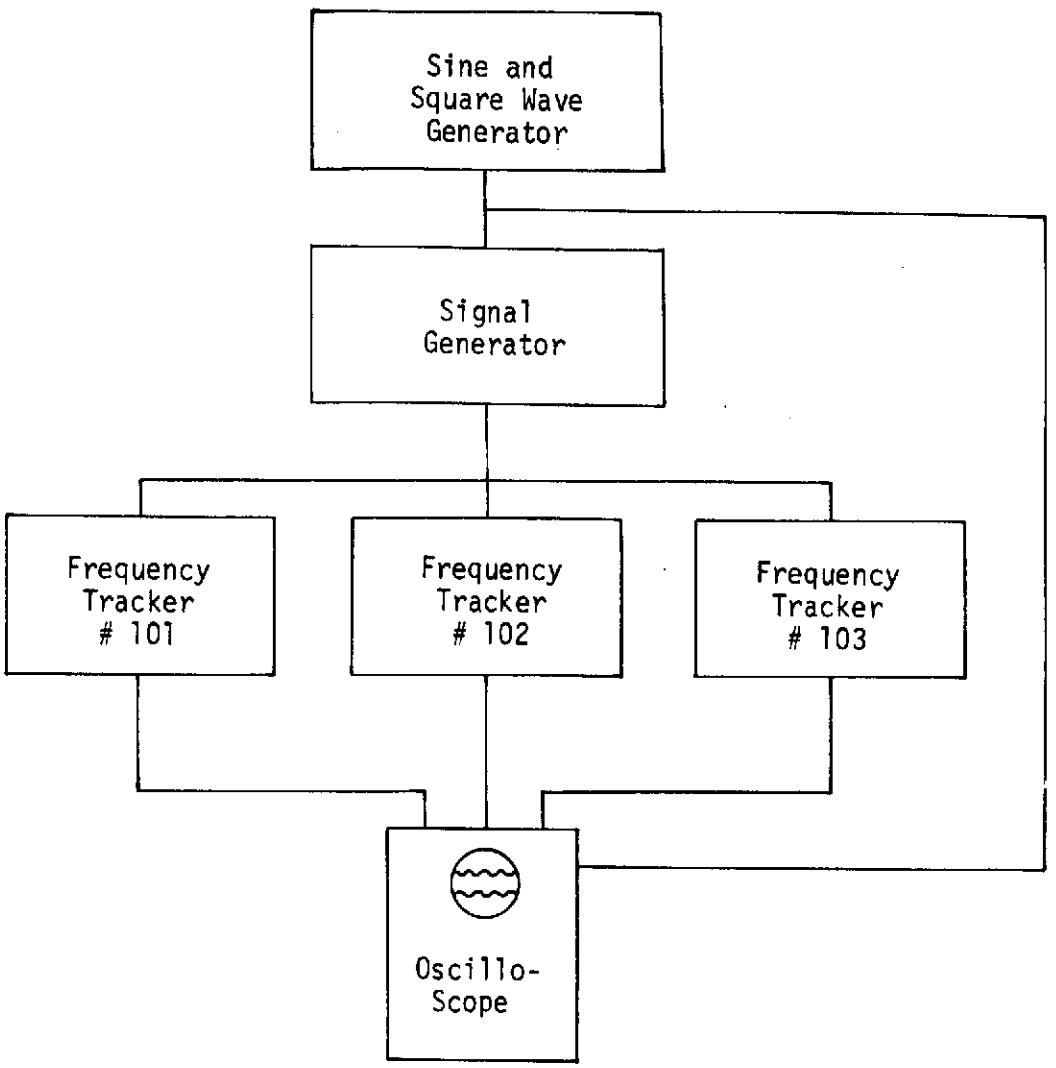

Fig. 8 System Schematic for Modulated Input Signal Comparisons

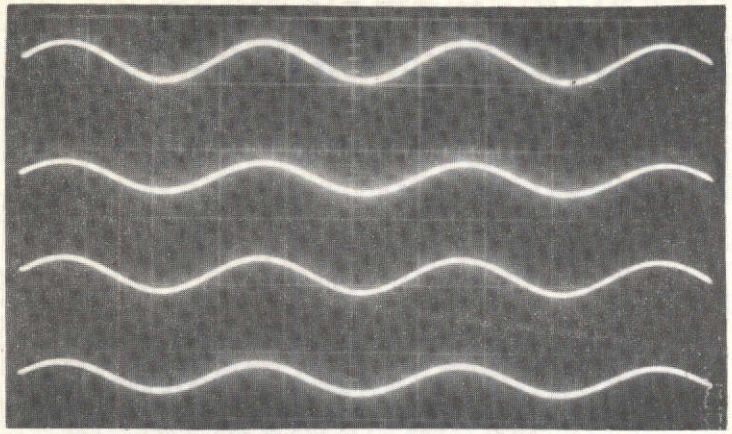

Input Signal

AC Output #1

#2

#3

Input Signal Frequency 200 Hz
Input Signal Display Amplitude 2 volt/cm
Tracker Output Display Amplitude 1 volt/cm

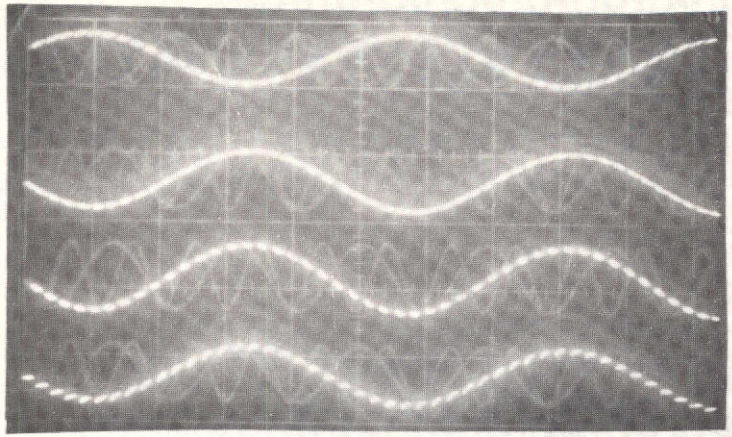

Input Signal Frequency 5000 Hz
Input Signal Display Amplitude 2 volt/cm
Tracker Output Display Amplitude 0.5 volt/cm

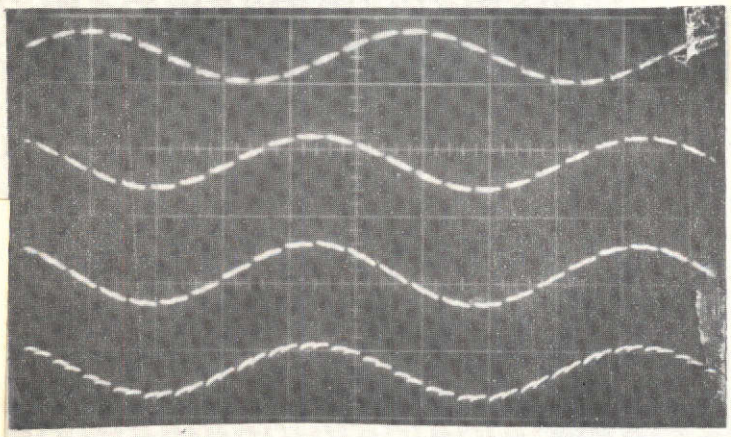

Input Signal

AC Output #1

#2

#3

Input Signal Frequency 10,000 Hz
Input Signal Display Amplitude 2 volt/cm
Tracker Output Display Amplitude 0.1 volt/cm

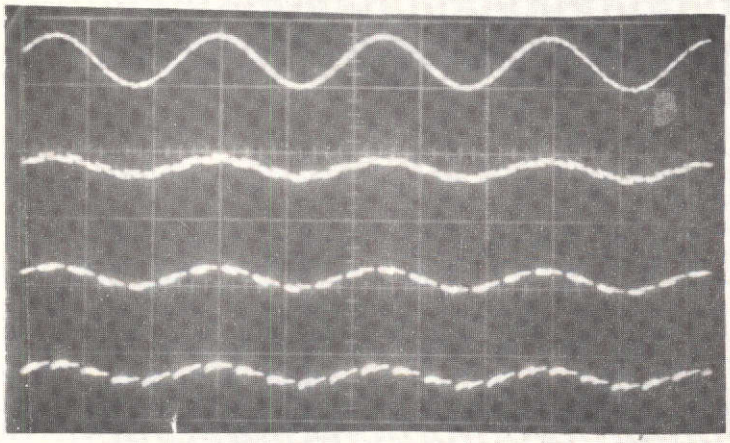

Input Signal Frequency 20,000 Hz
Input Signal Display Amplitude 2 volt/cm
Tracker Output Display Amplitude 50 m volt/cm

Simulated Doppler Carrier Frequency at 18 MHz with a Deviation of ≈ 9 MHz
and a S/N ≈ 35 db - Trackers in Narrow Mode

Figure 9 Comparison of Phase Shifts in the Frequency Trackers for an Electronically Generated FM Signal Input

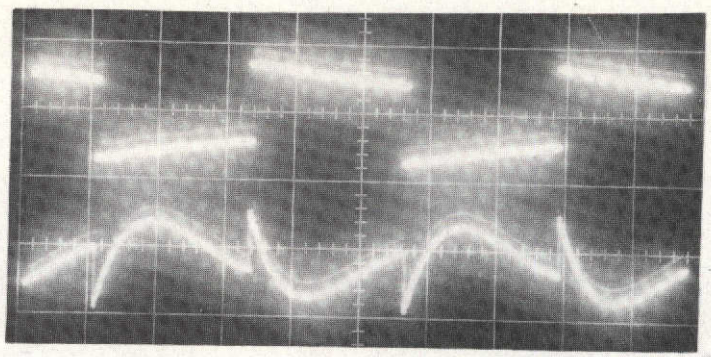

Top Trace
Frequency Modulation Square Wave
10 Hz

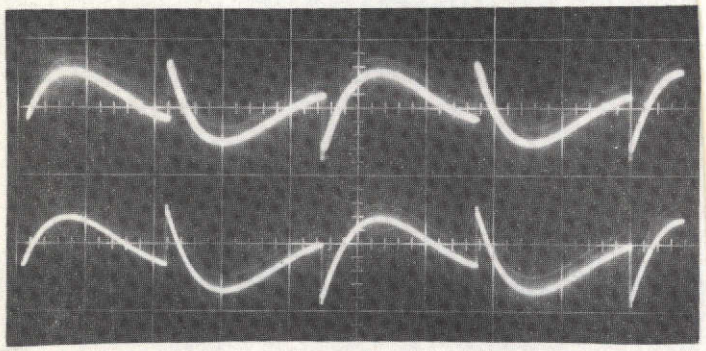

Top Trace AC #101

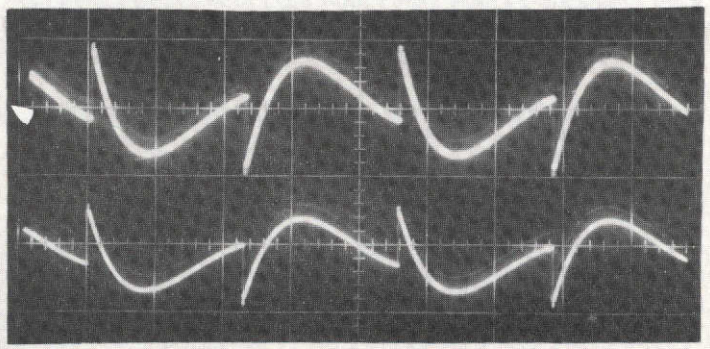

Top Trace AC #102

Bottom trace on each picture is the AC output from Tracker #103

Figure 10 - Frequency Tracker AC Output for Carrier Frequency Input Frequency Modulated With a Square Wave

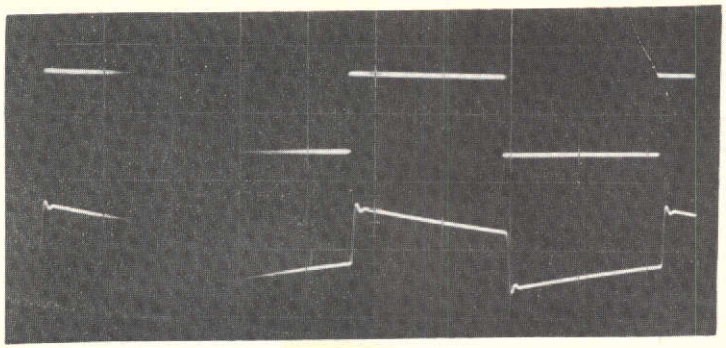

Top Trace
Frequency Modulation Square Wave
100 Hz

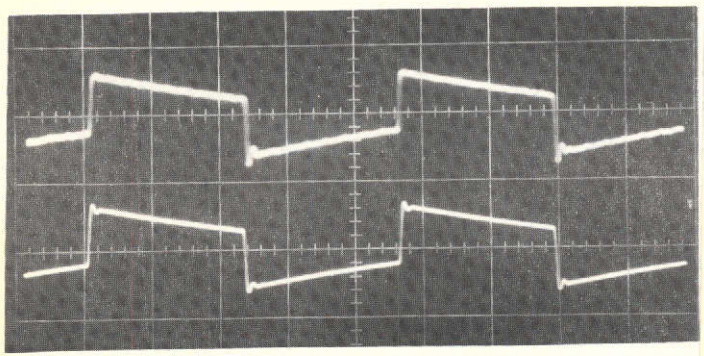

Top Trace AC #101

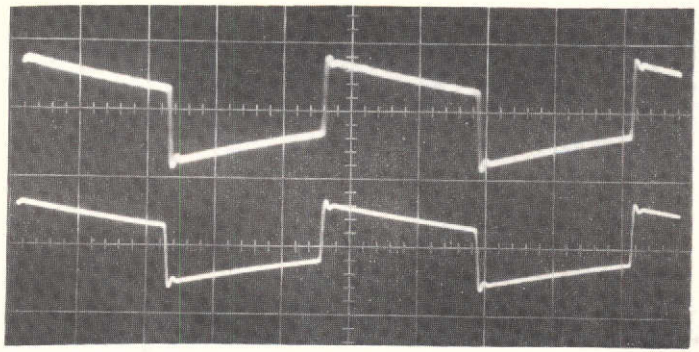

Top Trace AC #102

This page is reproduced at the back of the report by a different reproduction method to provide better detail.

Bottom trace on each picture is the AC output from Tracker #103

Figure 11- Frequency Tracker AC Output for Carrier Frequency Input Frequency Modulated With a Square Wave

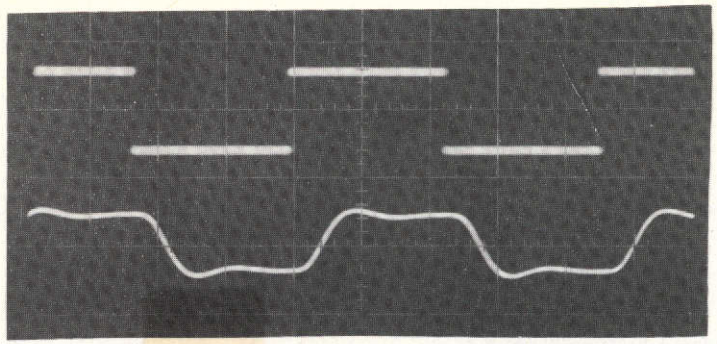

Top Trace
Frequency Modulation Square Wave
1000 Hz

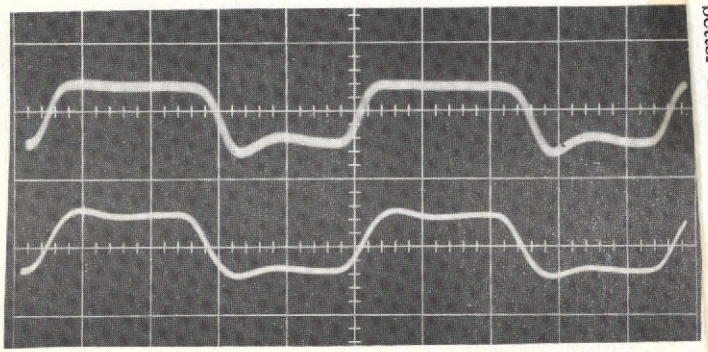

Top Trace AC #101

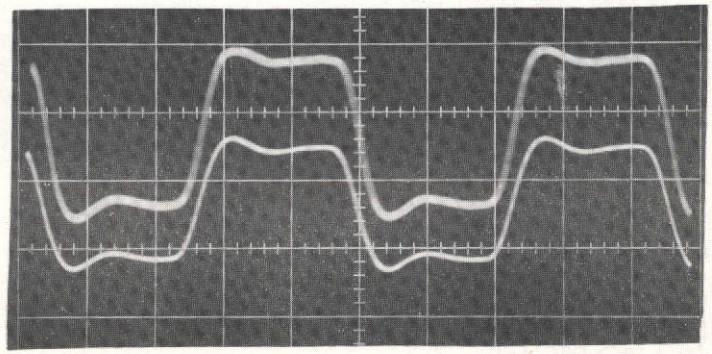

Top Trace AC #102

Bottom trace on each picture is the AC output from Tracker #103

Figure 12- Frequency Tracker AC Output for Carrier Frequency Input Frequency Modulated With a Square Wave

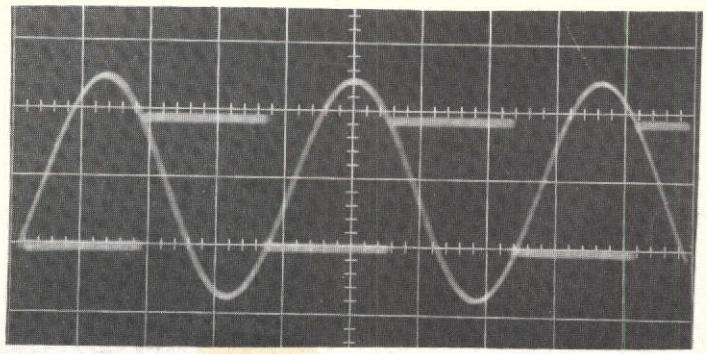

Top Trace
Frequency Modulation Square Wave
5000 Hz

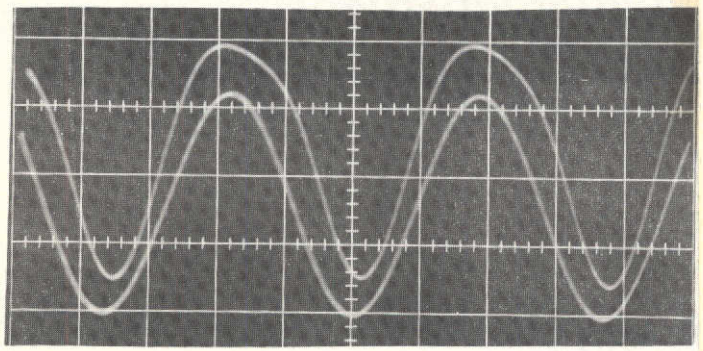

Top Trace AC #101

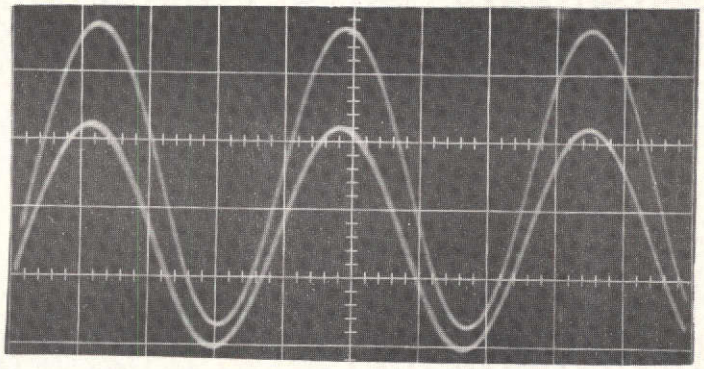

Top Trace AC #102

Bottom trace on each picture is the AC output from Tracker #103

Figure 13- Frequency Tracker AC Output for Carrier Frequency Input Frequency Modulated With a Square Wave

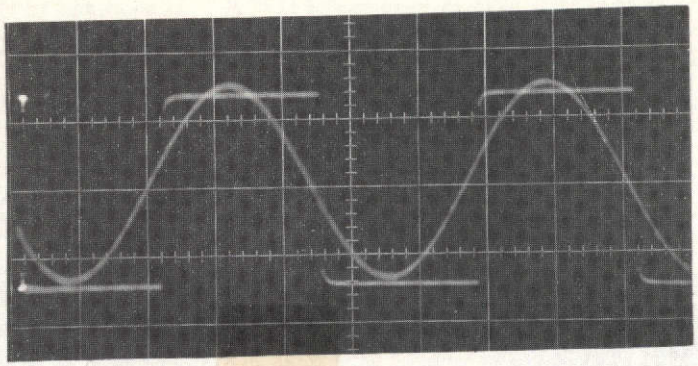

Top Trace
Frequency Modulation Square Wave
10,000 Hz

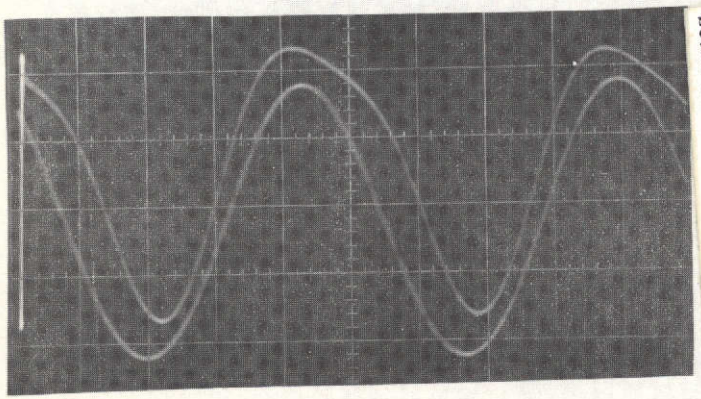

Top Trace AC #101

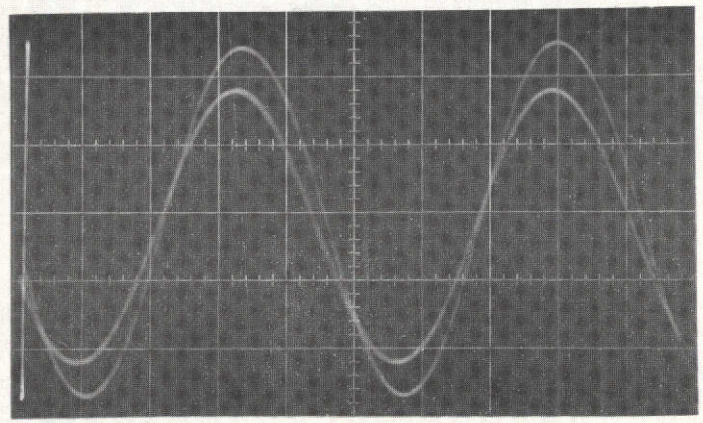

Top Trace AC #102

Bottom trace on each picture is the AC output from Tracker #103

Figure 14 - Frequency Tracker AC Output for Carrier Frequency Input Frequency Modulated With a Square Wave

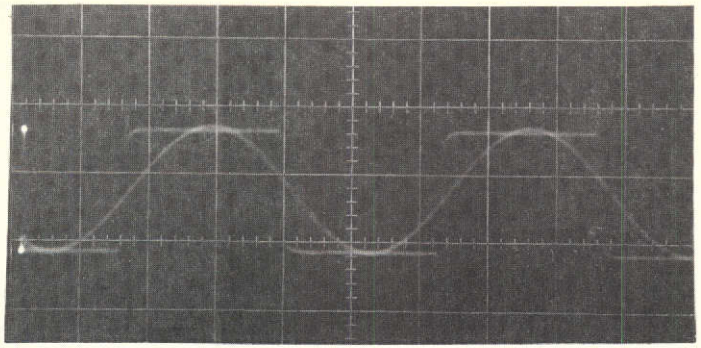

Top Trace
Frequency Modulation Square Wave
20,000 Hz

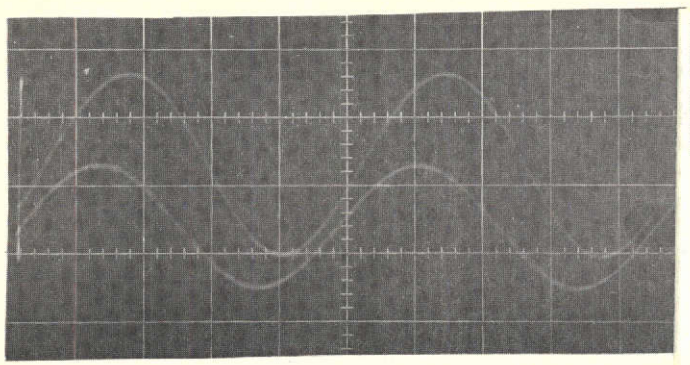

Top Trace AC #101

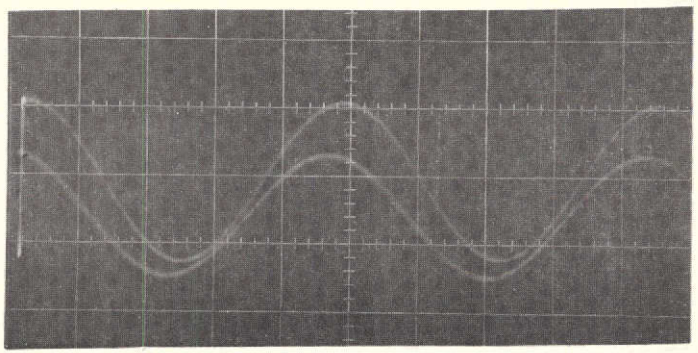

Top Trace AC #102

Bottom trace on each picture is the AC output from Tracker #103

Figure 15- Frequency Tracker AC Output for Carrier Frequency Input Frequency Modulated With a Square Wave

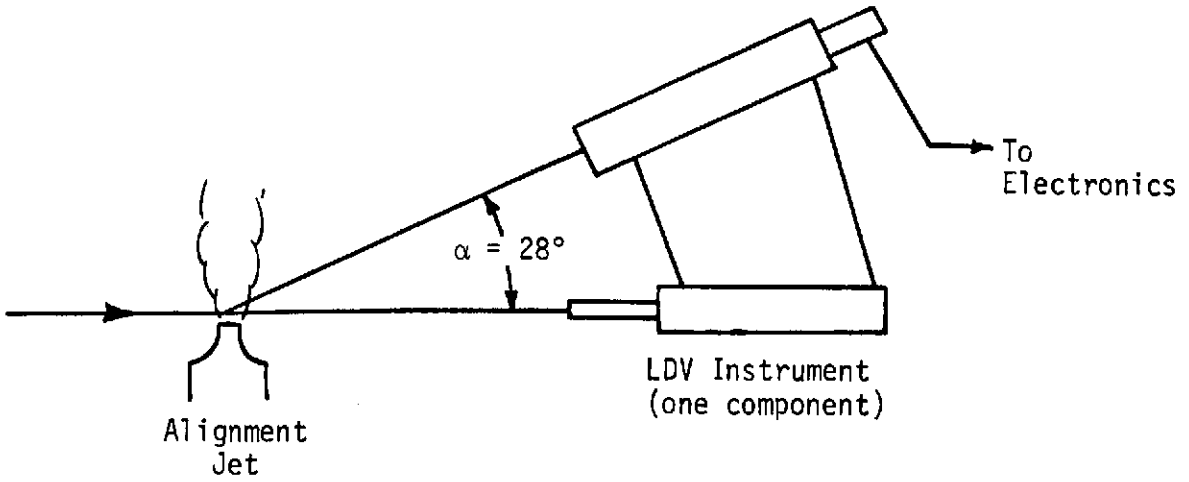

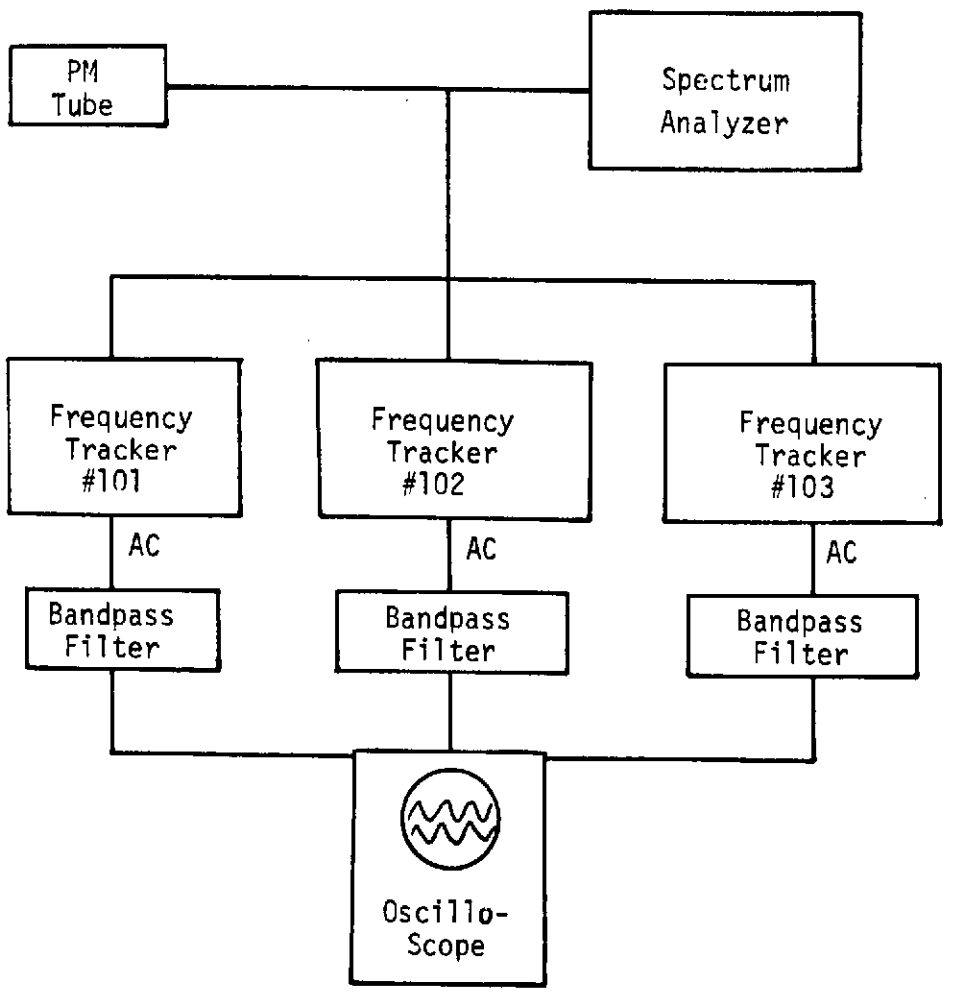

Fig. 16 System Arrangement for Tracker AC Output Comparisons with Doppler Signal Input

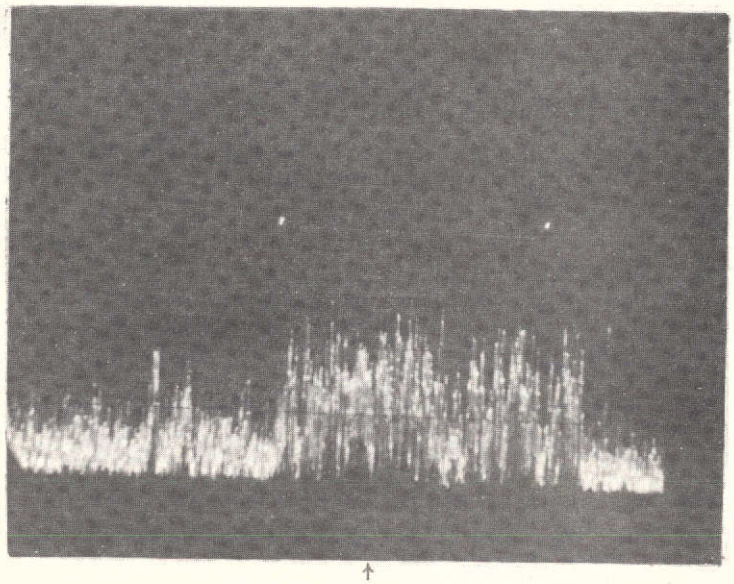

Spectrum Analyzer Display of
Doppler Signal Into Frequency Trackers

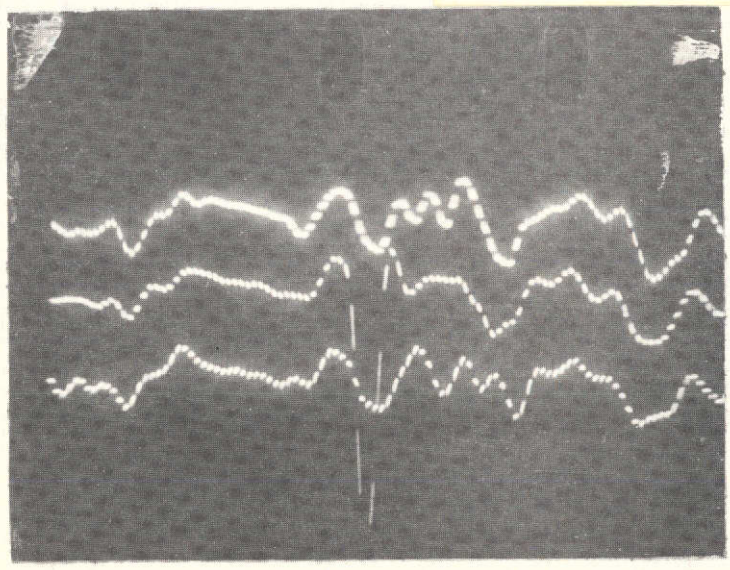

AC Frequency Tracker Output

Figure 17 - AC Output of Three-Frequency Tracking Units Showing Response and Phase Matching up to 20,000 Hz

Note: Shaded regions indicate operational range for the pipe measurements.

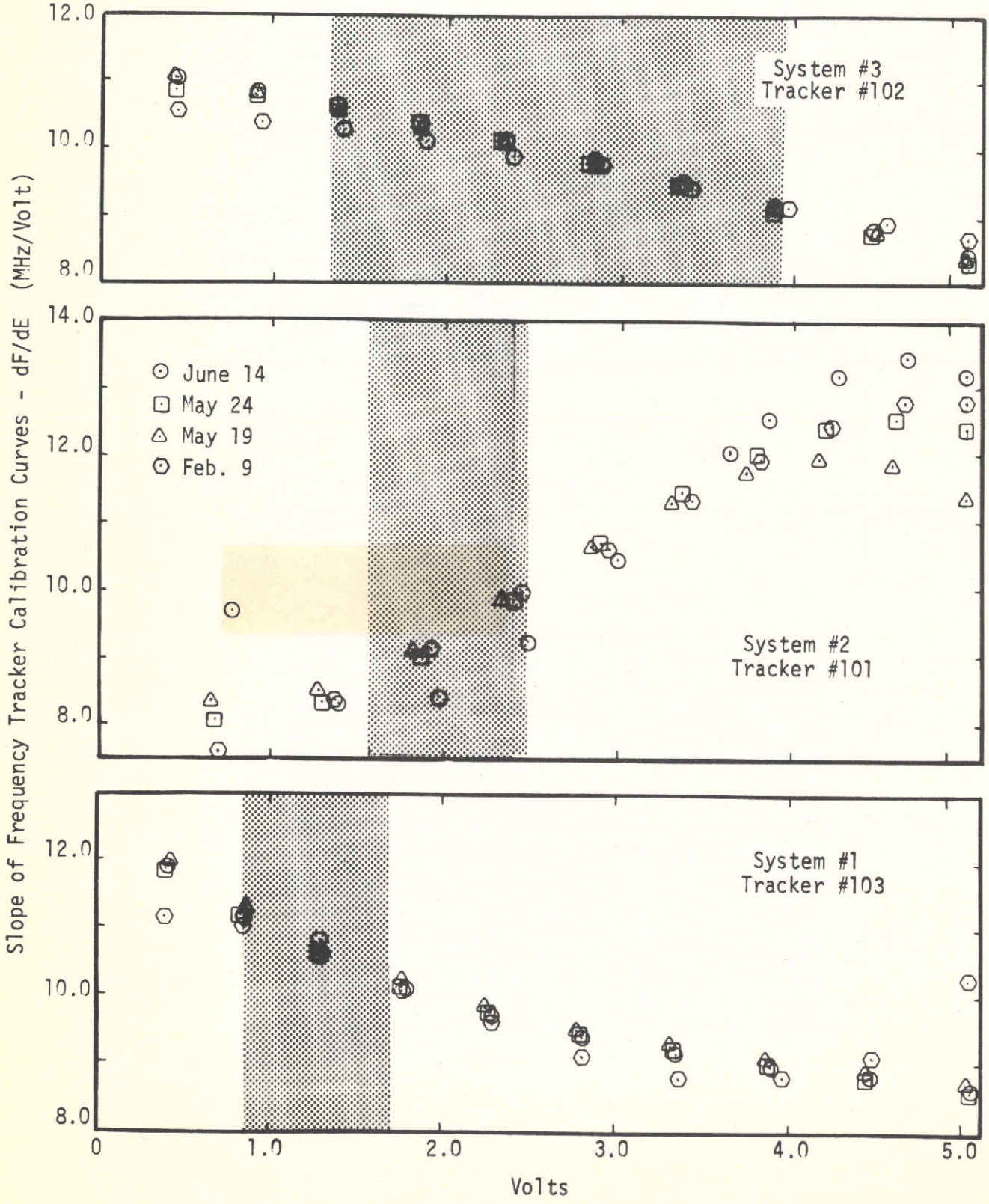

Fig. 18 Slope of Frequency Tracker Calibration Curves.

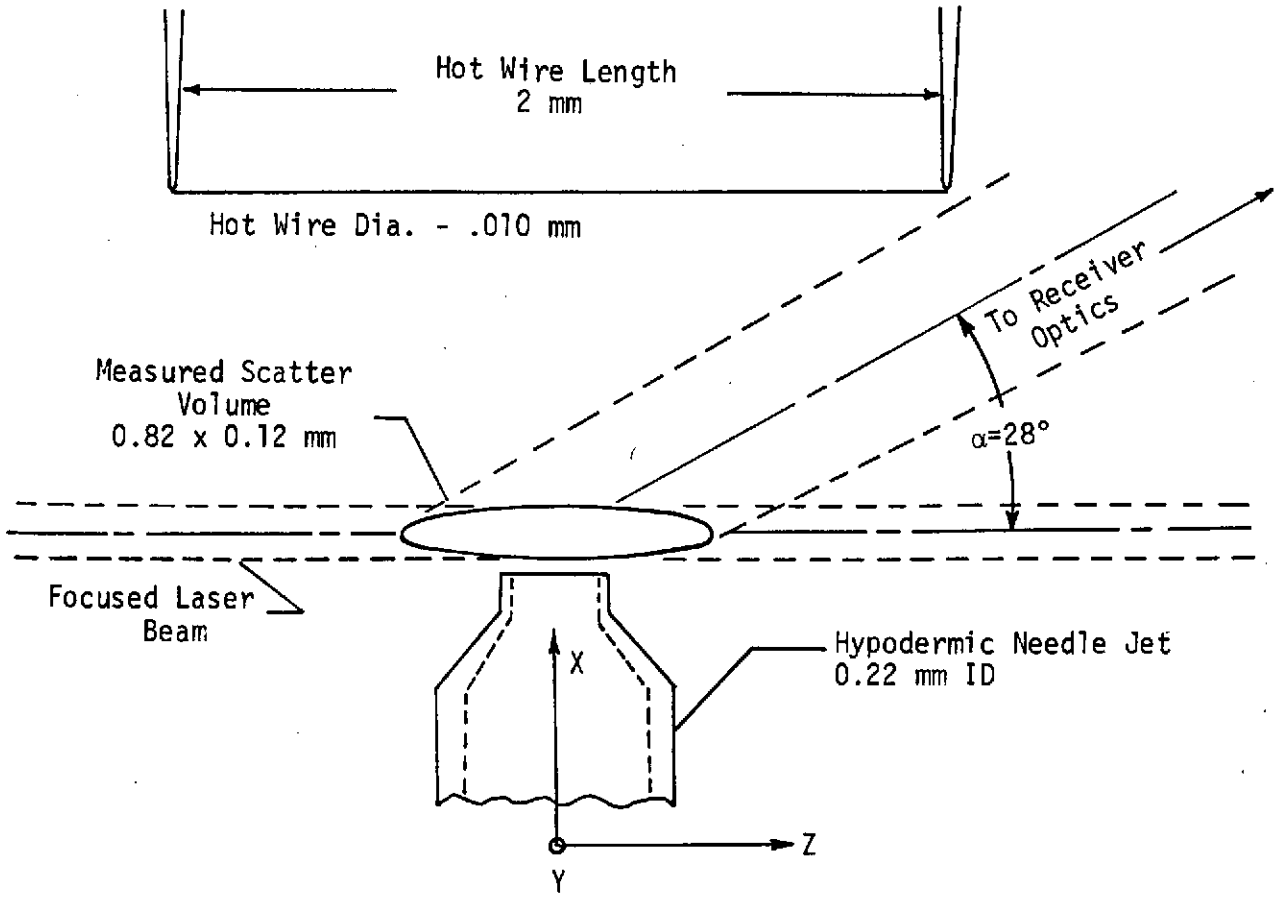

Scatter volume measurements were made by moving the needle jet along the Y and Z axis and observing the change in S/N as a function of the distance moved.

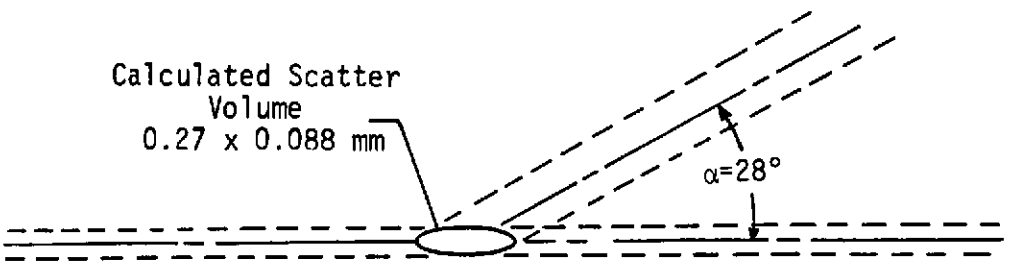

Calculated Scatter Volume

Note: All drawing to approximate scale - 5 mm = 0.1 mm

Fig. 20 Measured and Calculated Scatter Volume Arrangements

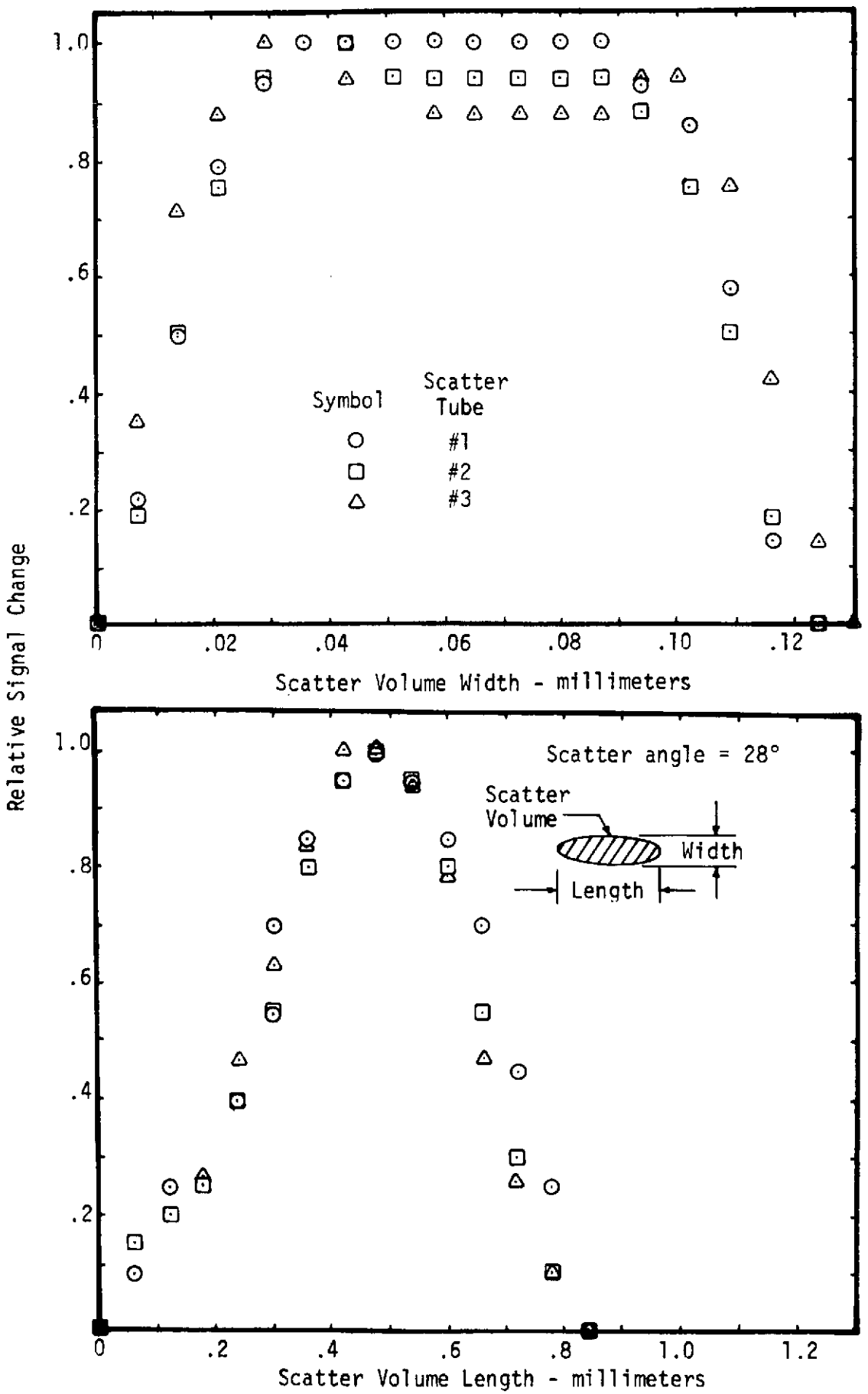

Fig. 21 Scatter Volume Measurements for 3-Dimensional LDV Instrument

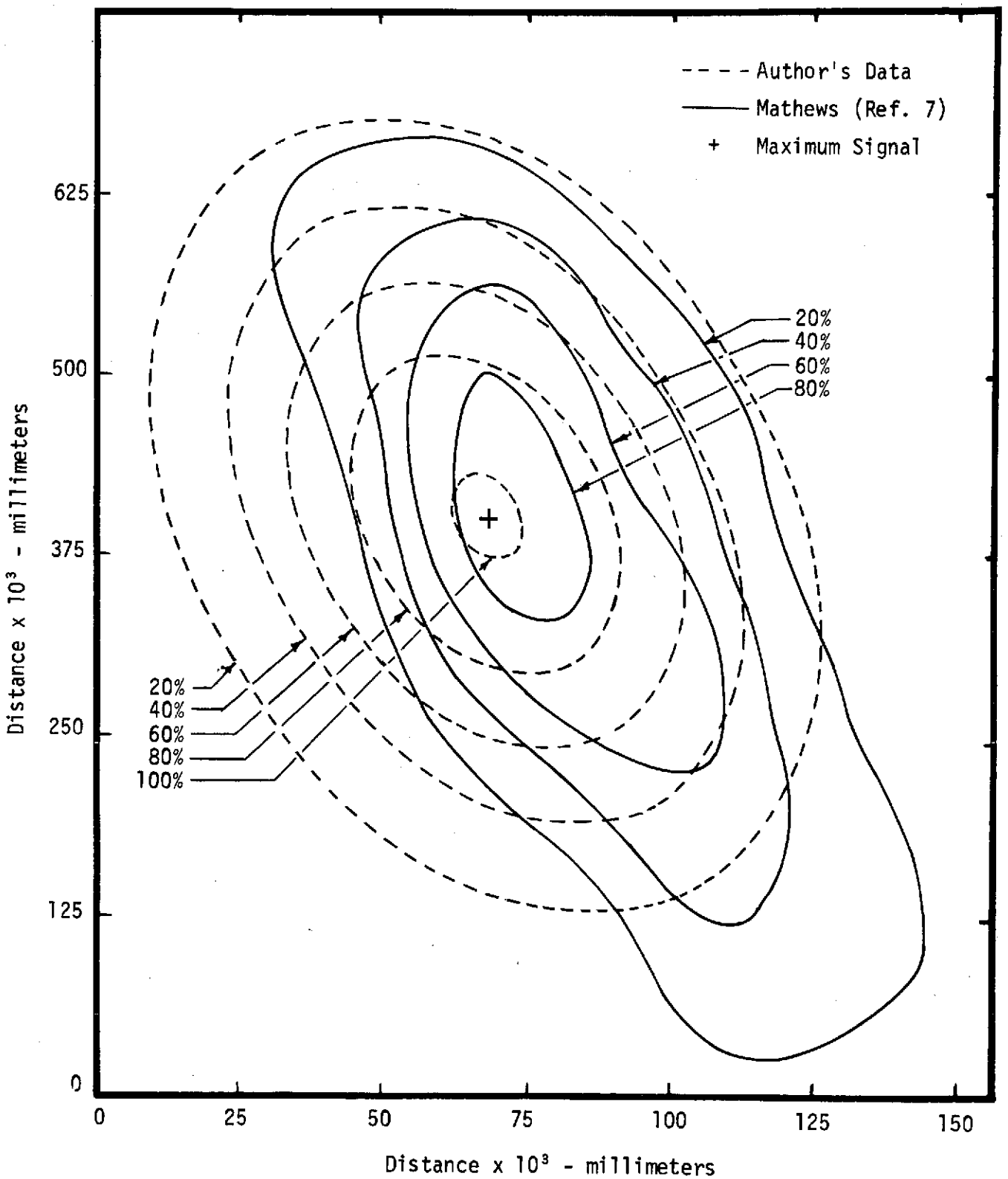

Fig. 22 Comparison of Scatter Volume Percentage of Intensity Distributions

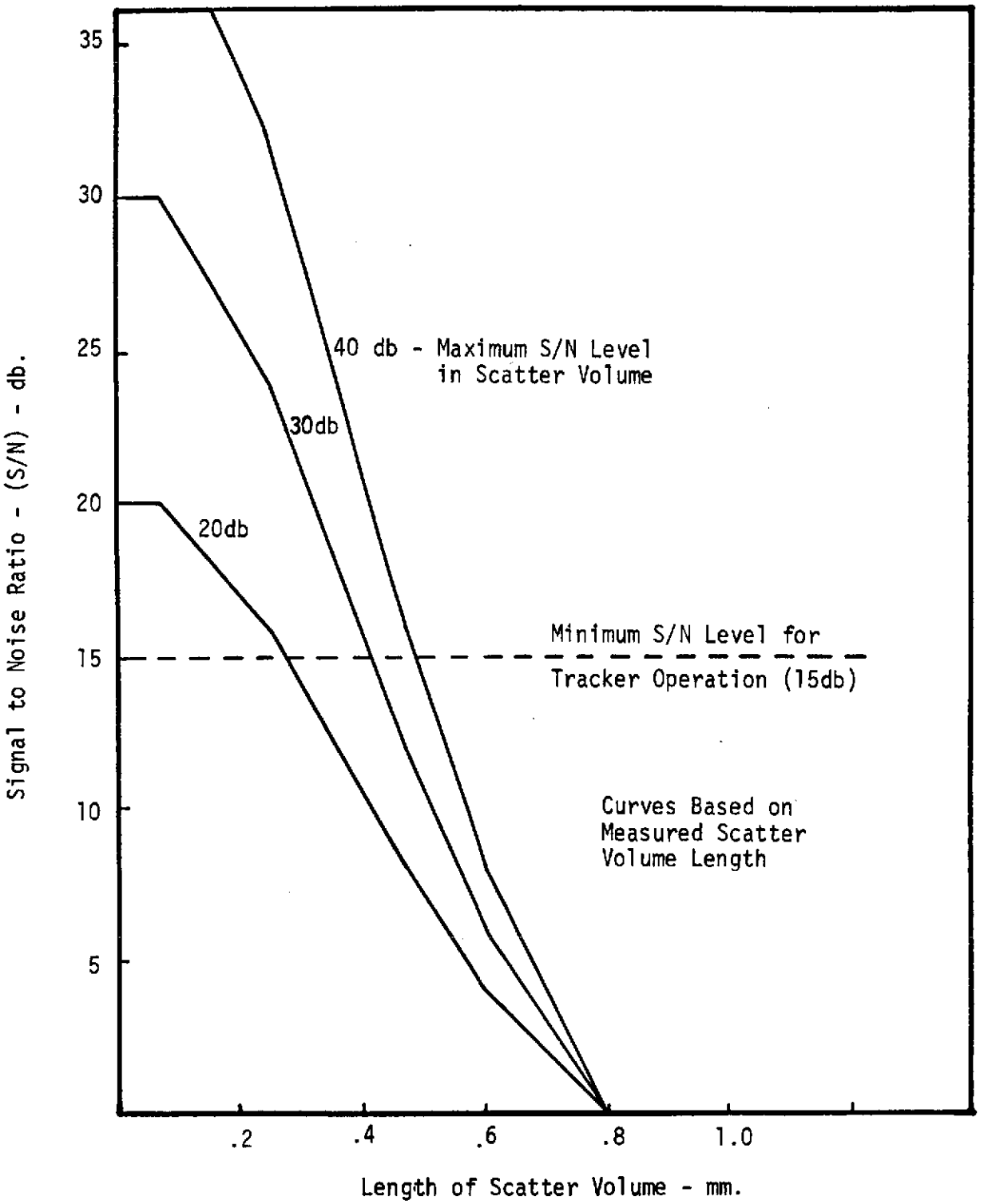

Fig. 23 Variation in Signal Strength Along the Scatter Volume Length

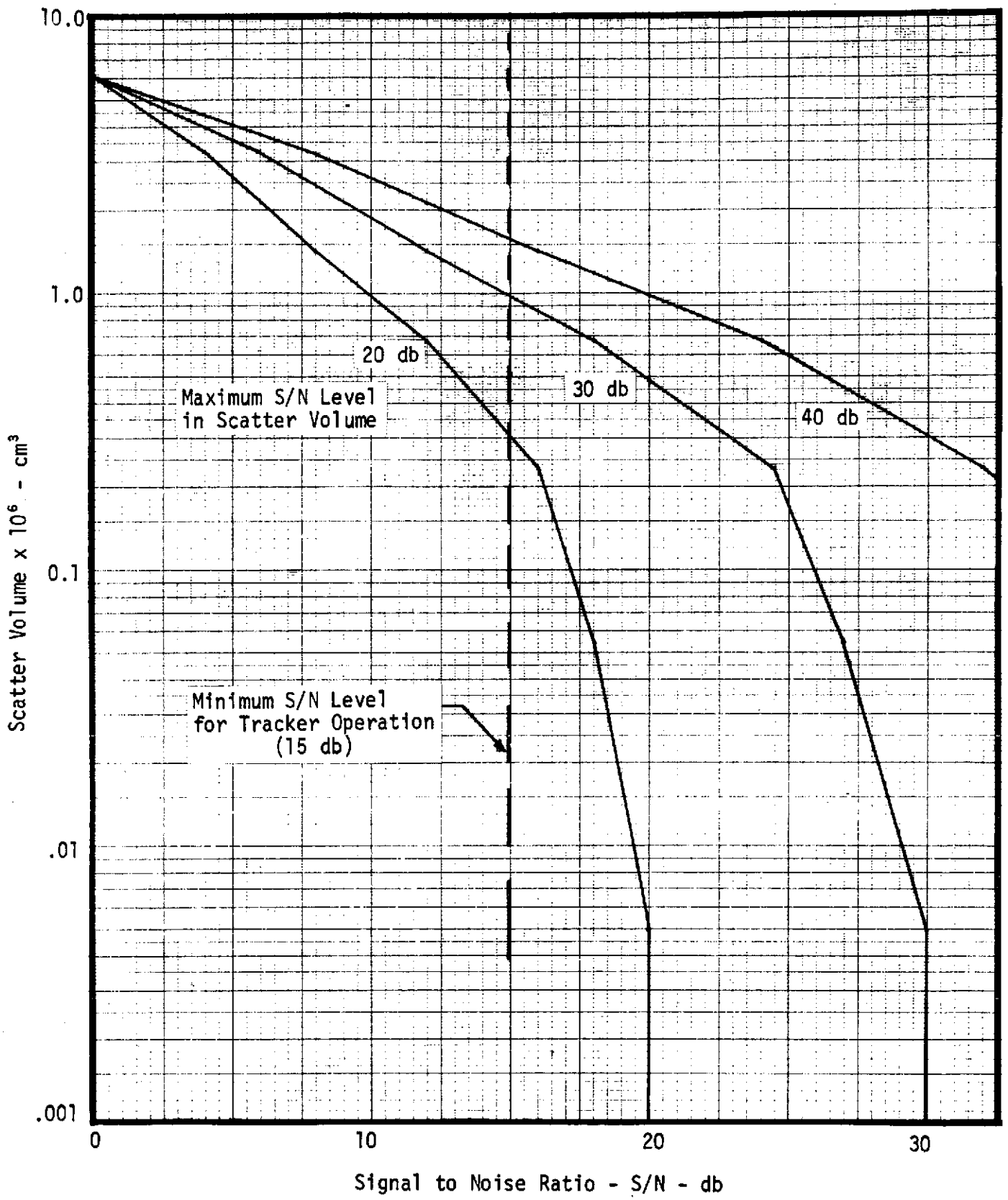

Fig. 24 Variation in Scatter Volume Size for Different Maximum S/N Levels.

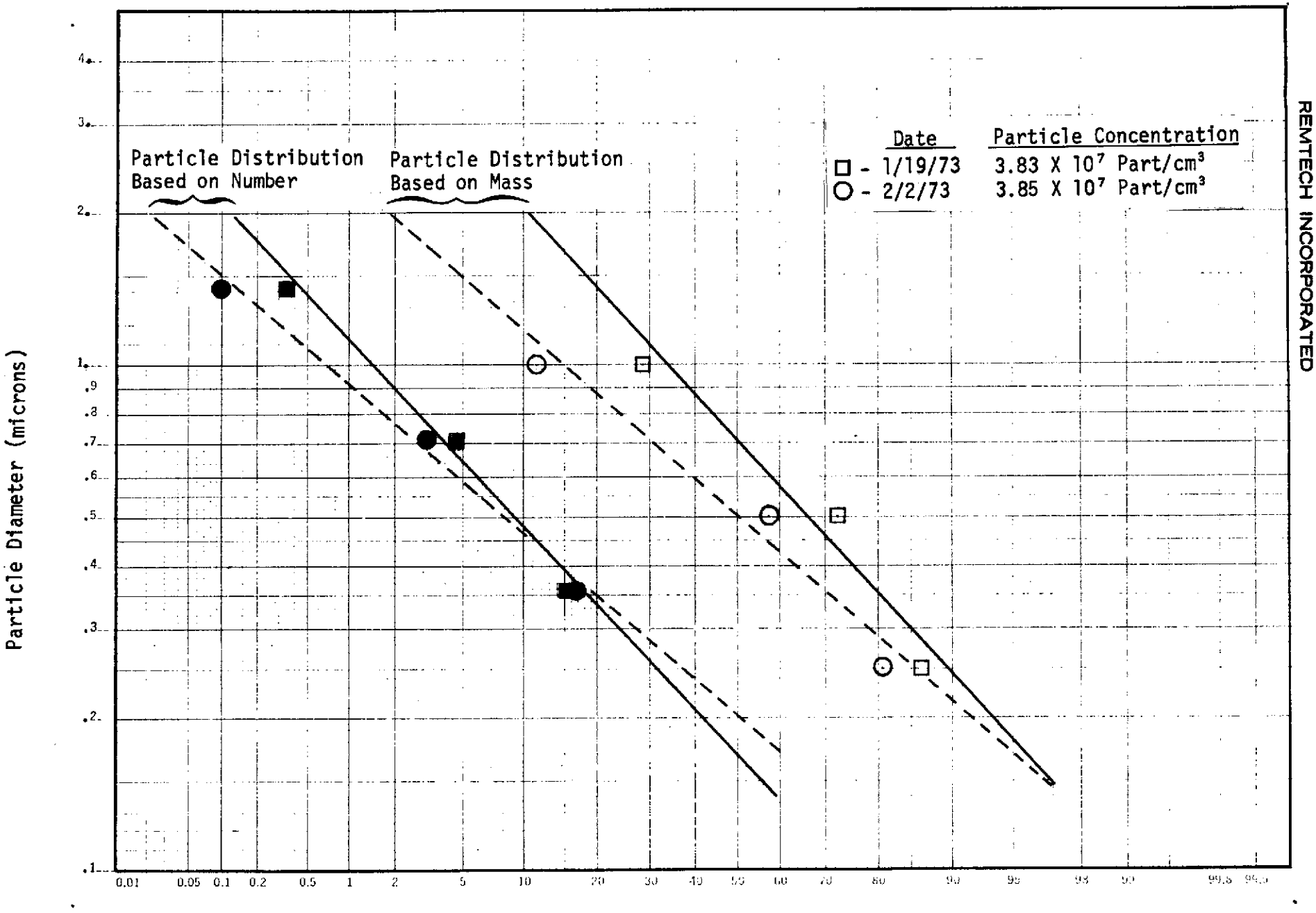

Fig. 25 Particle Size Distribution for Pipe Flow

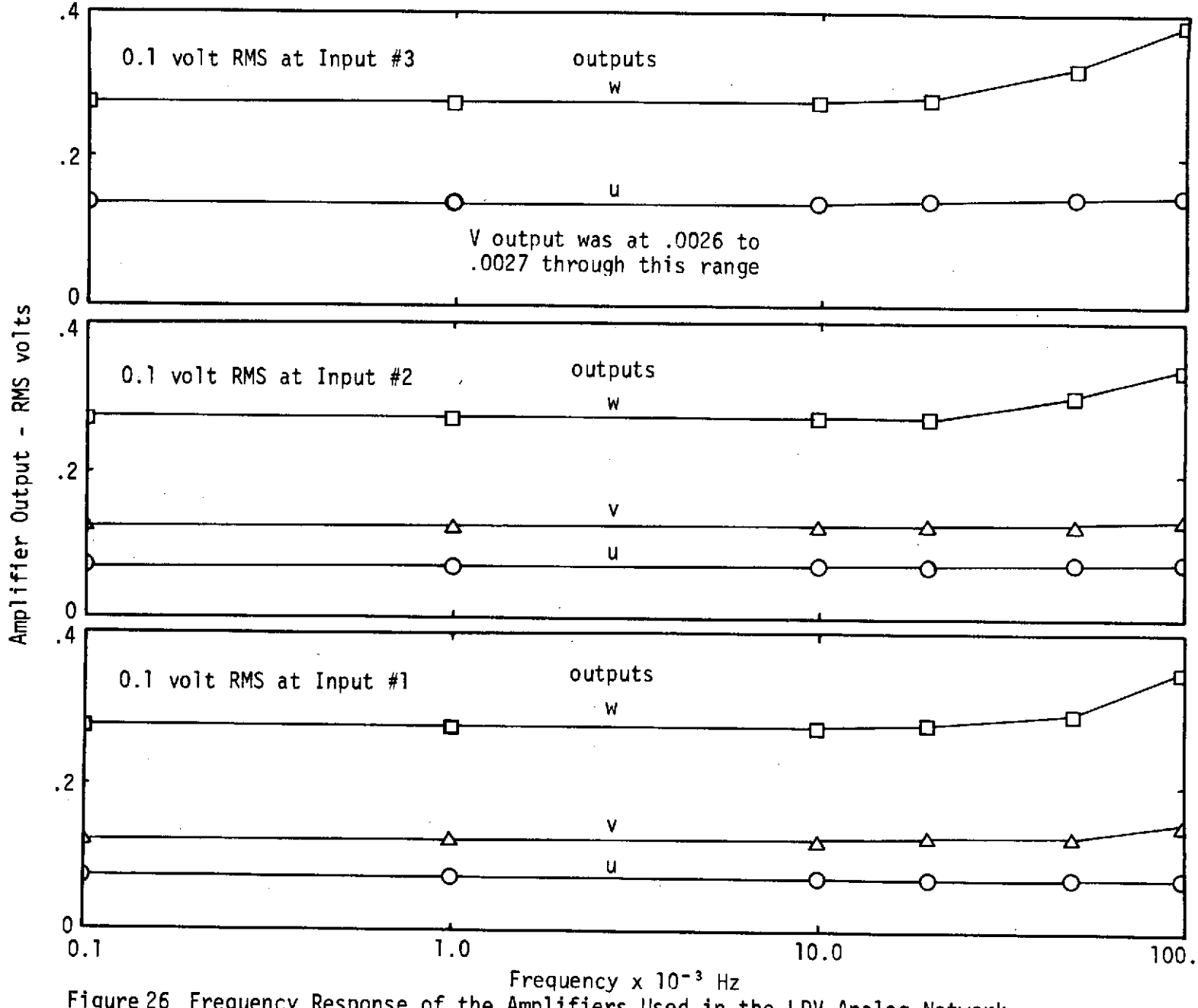

Figure 26 Frequency Response of the Amplifiers Used in the LDV Analog Network

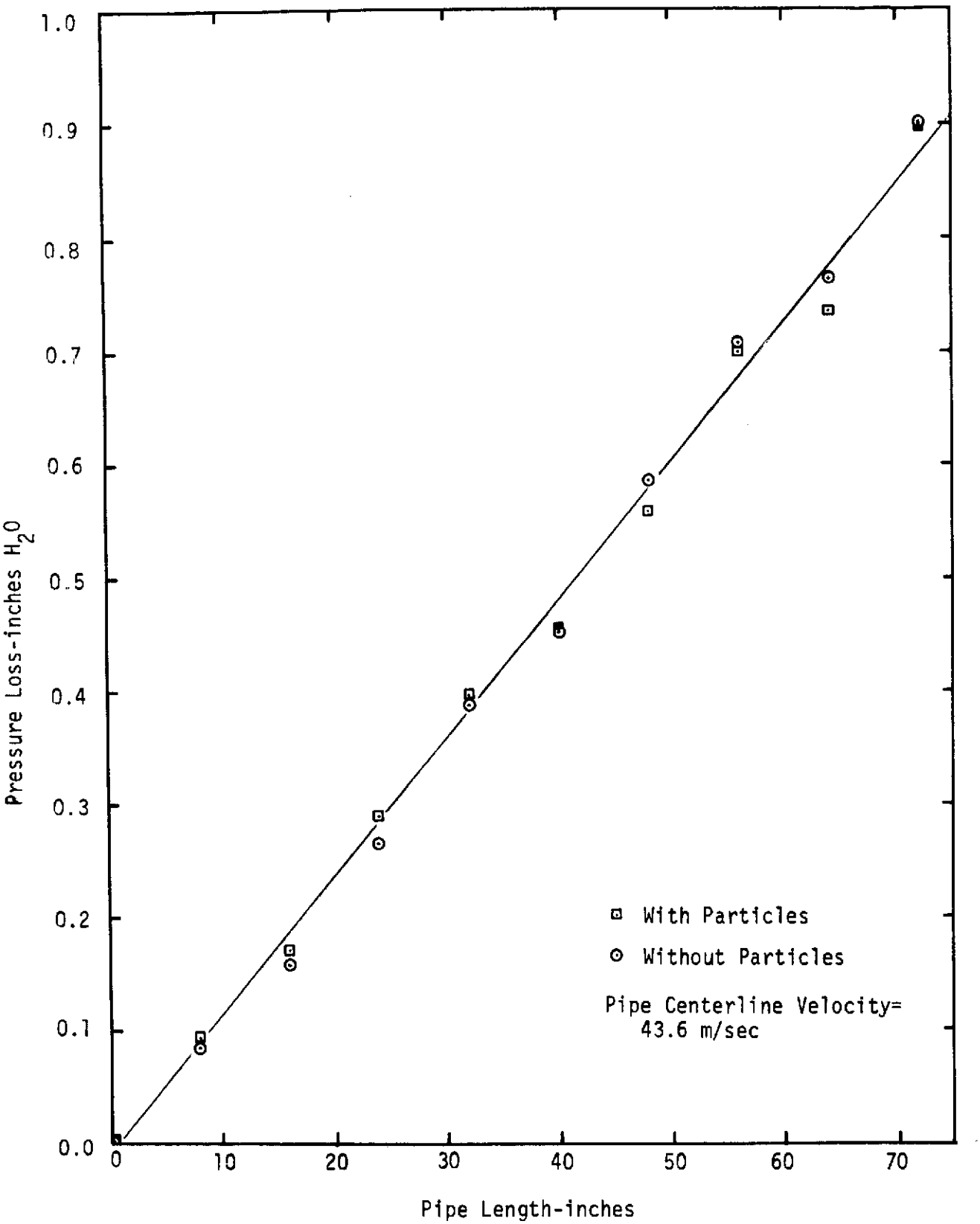

Figure 27- Pressure Loss Measurements Down the Pipe Test Section for Seeded and Unseeded Flow

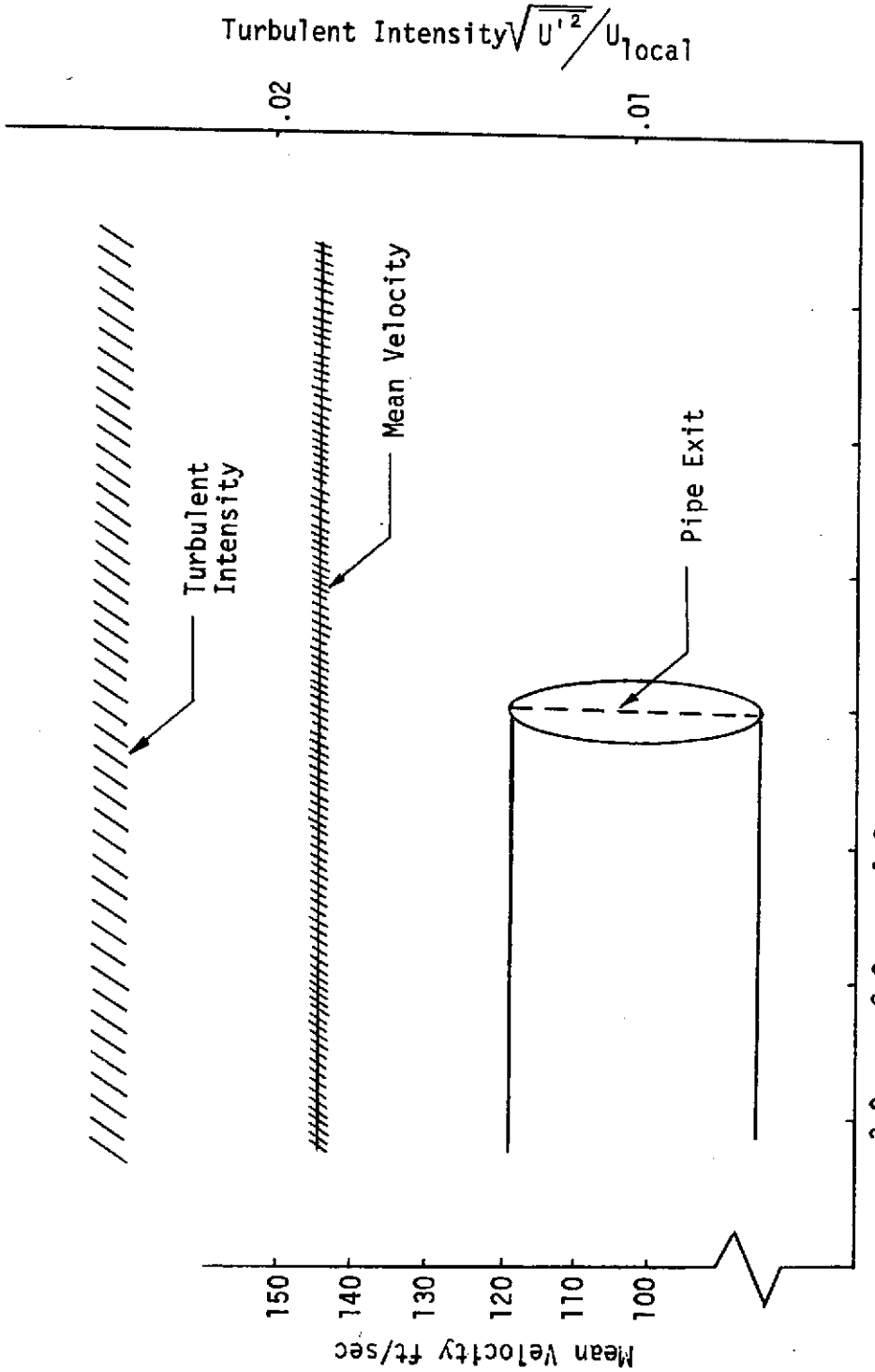

Figure 28 Pipe Centerline Mean and Turbulent Velocities

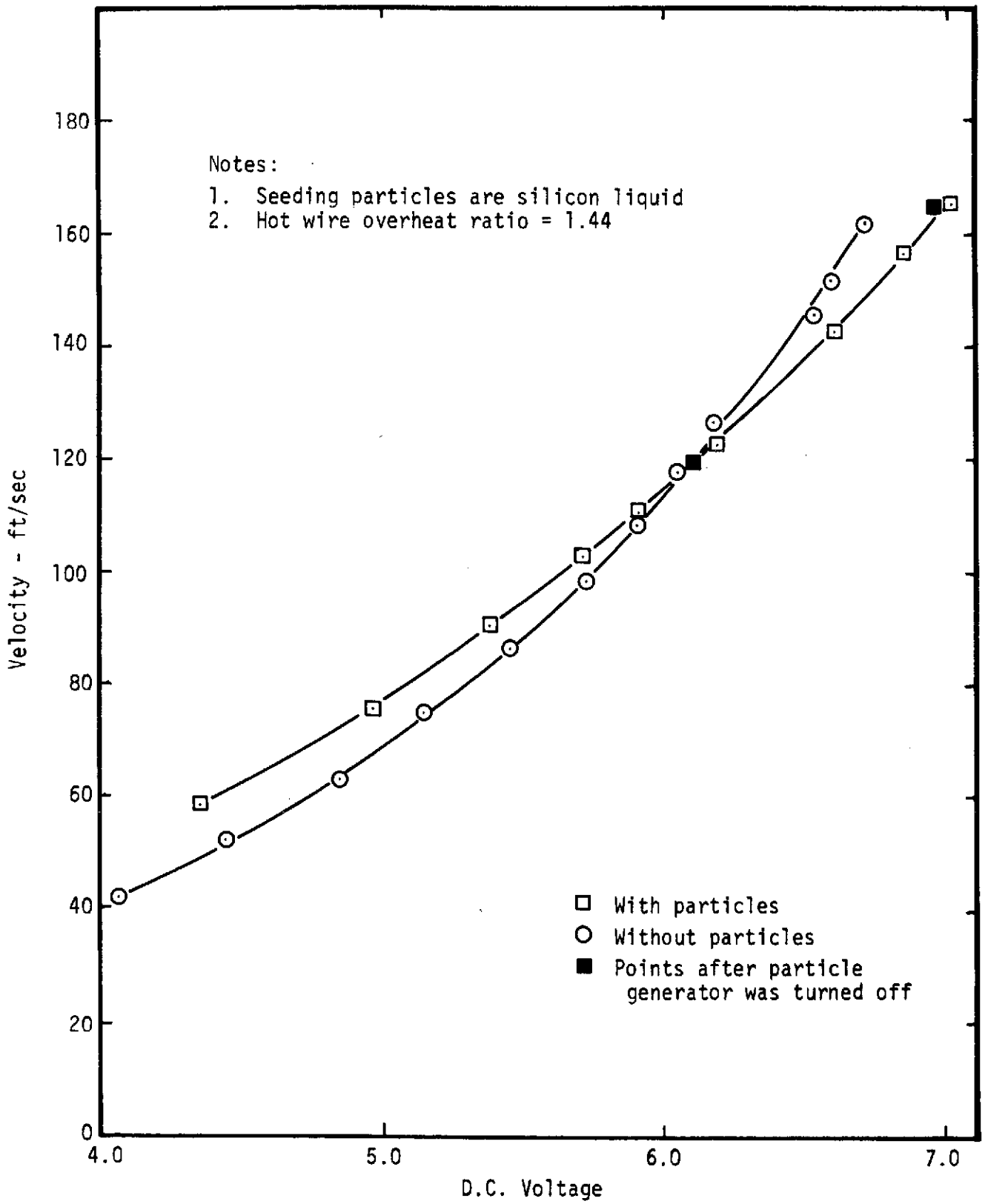

Figure 29- Comparison of Hot Wire Calibration Curves for Seeded and Unseeded Flows

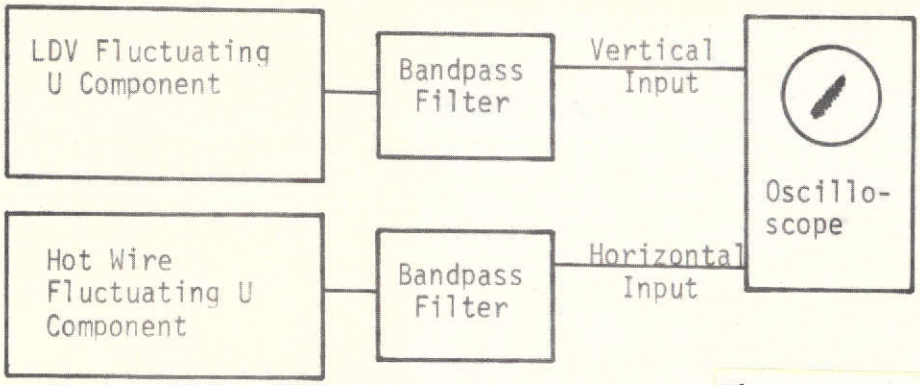

Note:
Measurement at Pipe Centerline-
Velocity-
110 ft/sec

This page is reproduced at the back of the report by a different reproduction method to provide better detail.

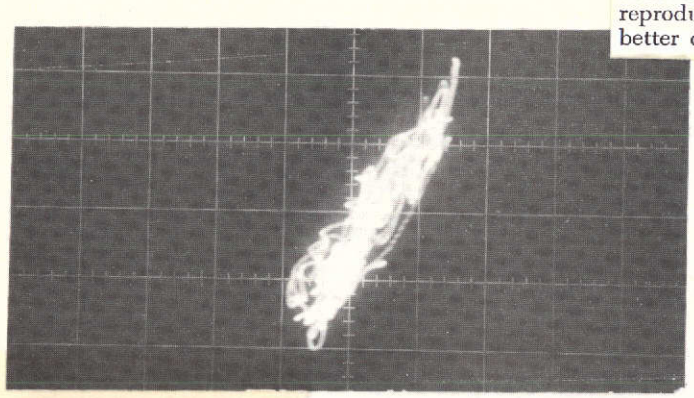

Bandpass
10 Hz- 5,000Hz

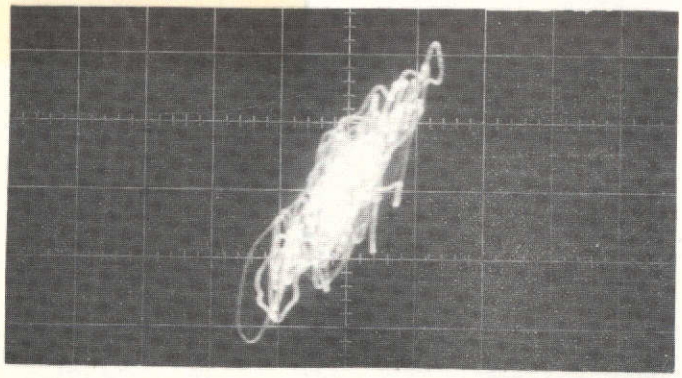

Bandpass
10 Hz-10,000Hz

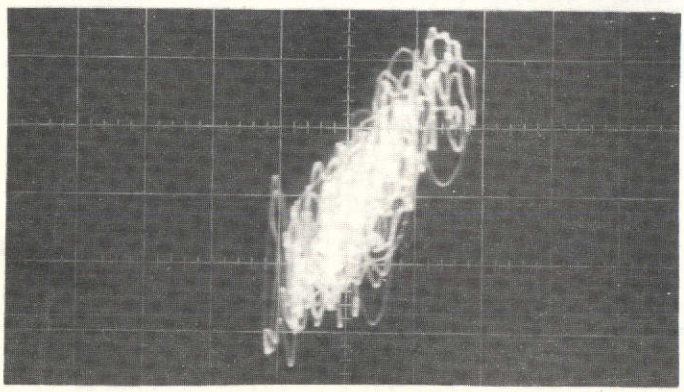

Bandpass
10Hz-20,000Hz

Figure 30 - Comparison of Lissajous Display of LDV and Hot Wire U Turbulence Components for Different Bandpass Filters

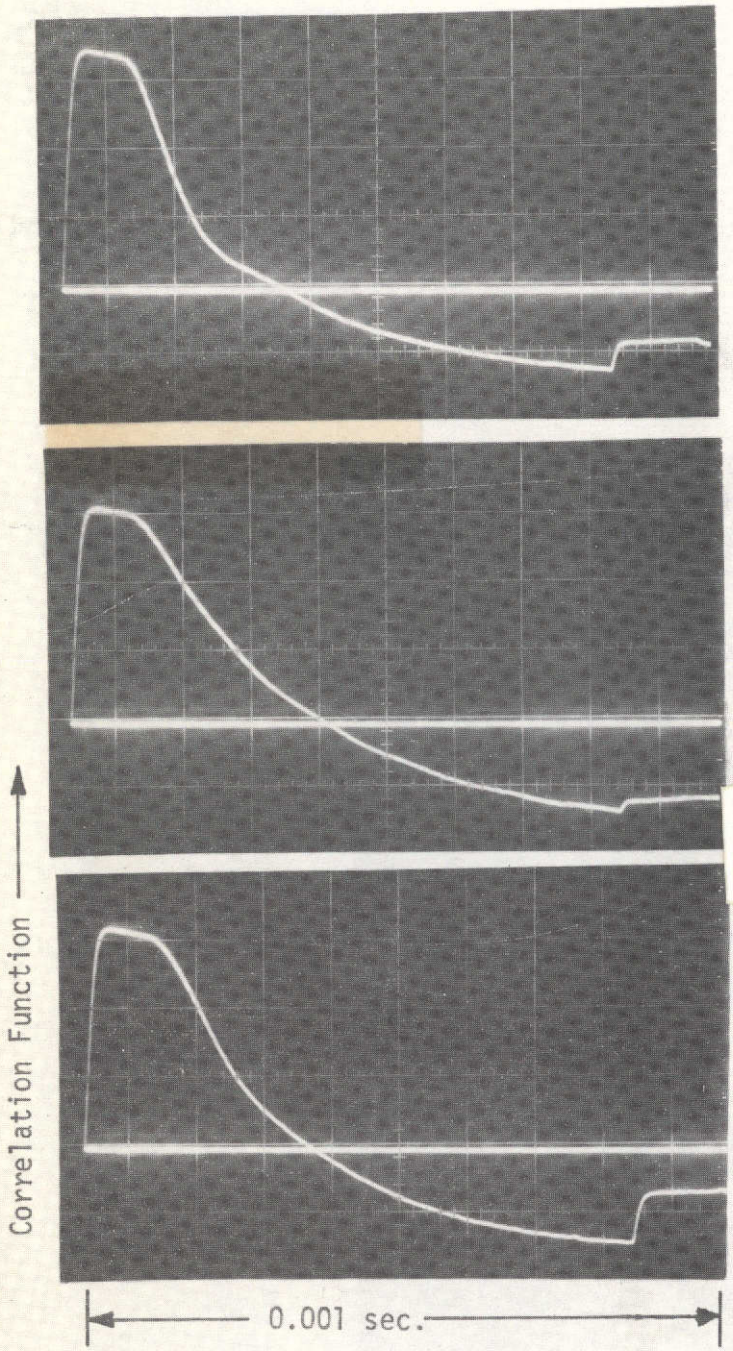

Notes:

1. Measurement at pipe centerline and 3.81 centimeters from exit - $U_{\mathcal{L}}$ = 28.34 m/s.
2. Band pass filter at 10HZ - 5000HZ.
3. Six nozzles in aerosol generator open.

Figure 31 - Comparison of Correlation Functions for U Turbulence Component for Hot Wire and LDV

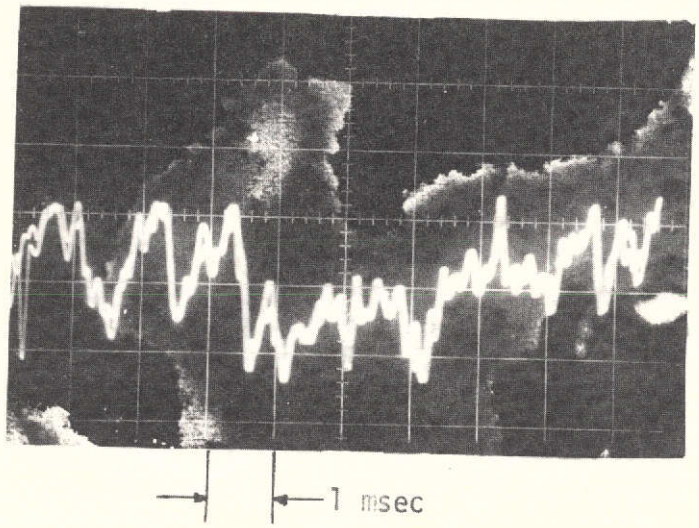

Fig. 31-A Overlay Comparison of LDV and Hot Wire Responses to Turbulent Fluctuations for Bandpass Filters at 10Hz to 5000 Hz. (From Ref. 4).

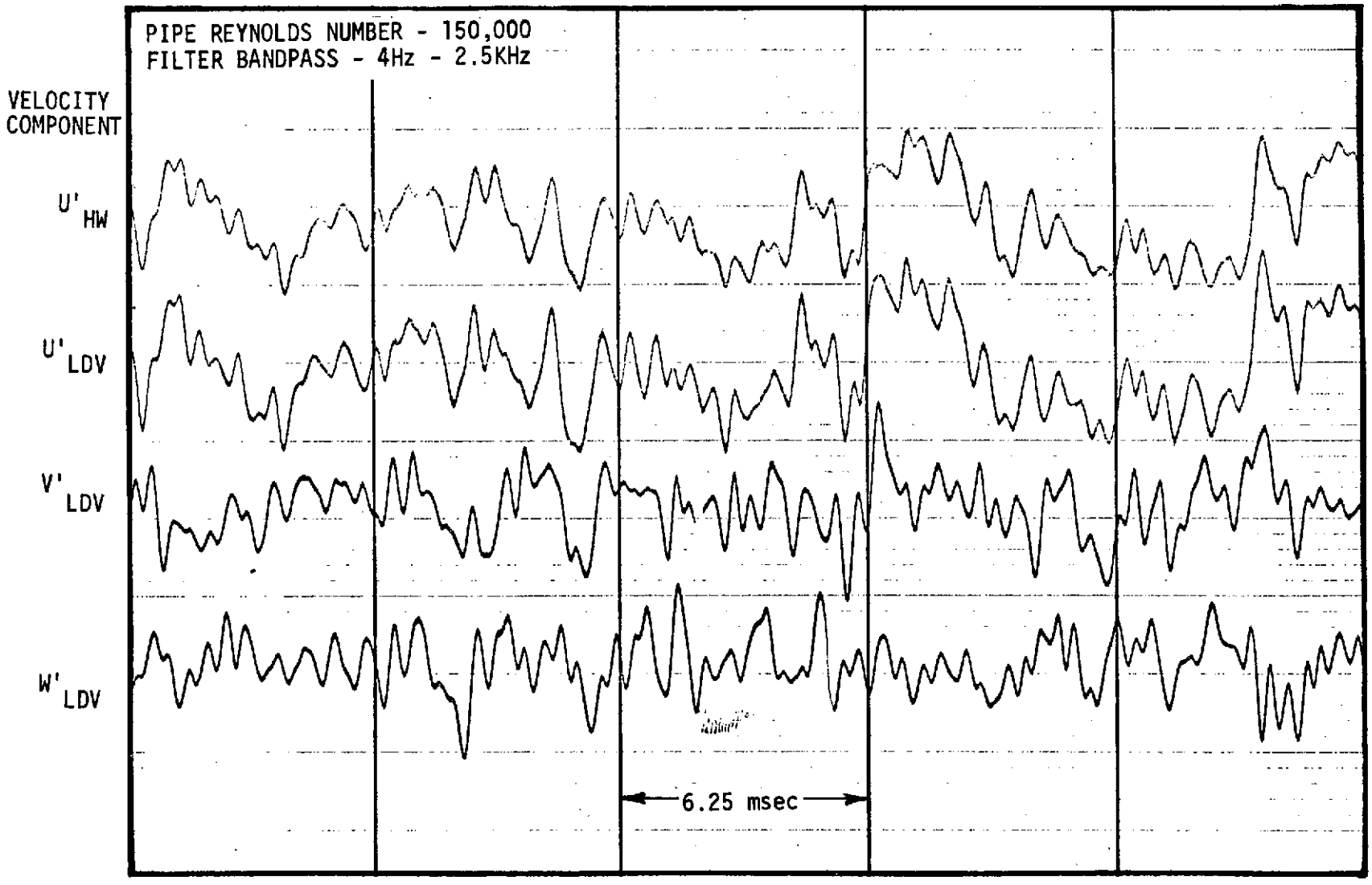

Fig. 32 SIMULTANEOUS COMPARISON OF HOT WIRE AND LDV TURBULENT FLUCTUATIONS AT THE CENTER OF A TURBULENT PIPE FLOW

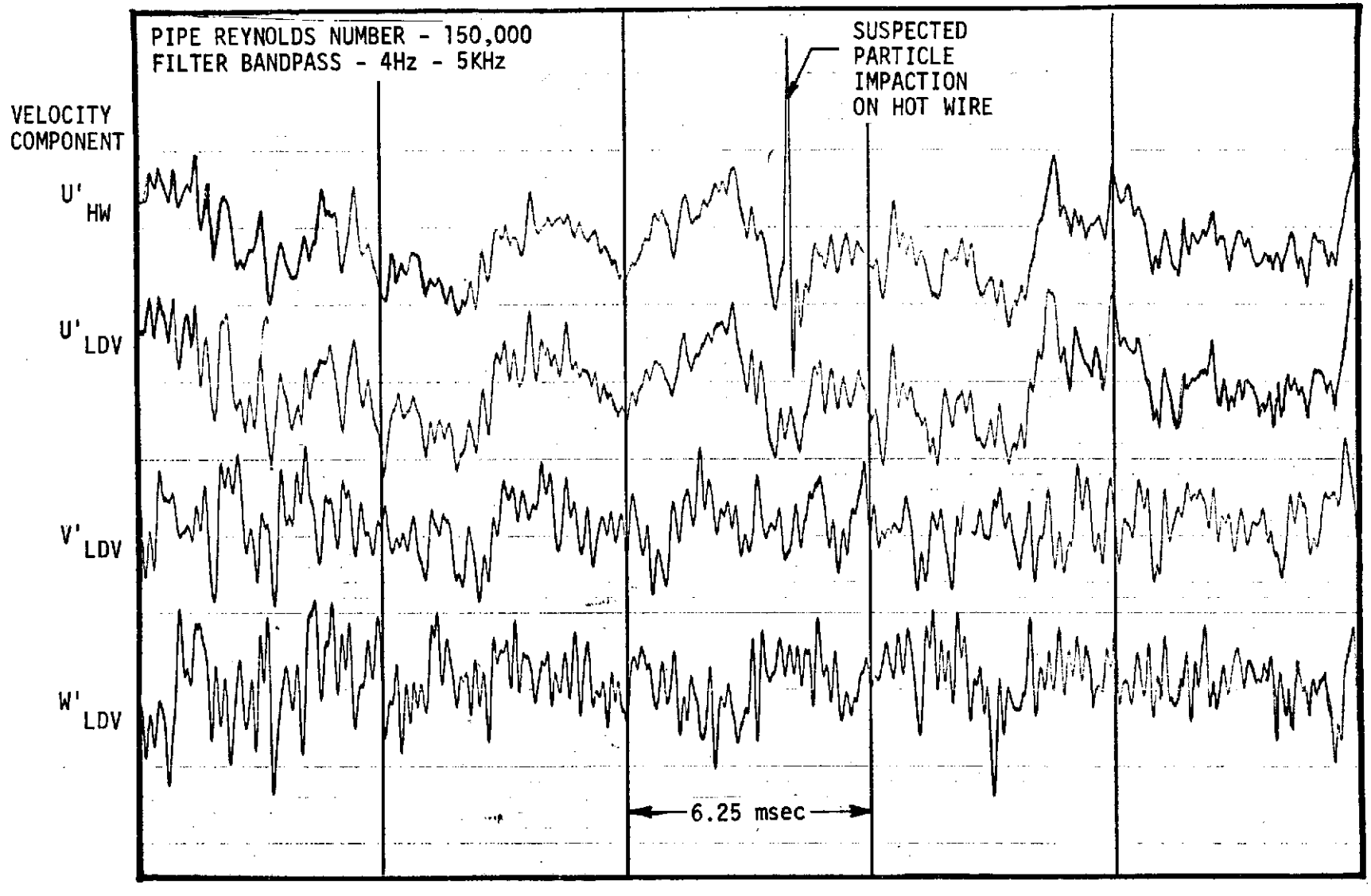

Fig. 33 SIMULTANEOUS COMPARISON OF HOT WIRE AND LDV TURBULENT FLUCTUATIONS AT THE CENTER OF A TURBULENT PIPE FLOW

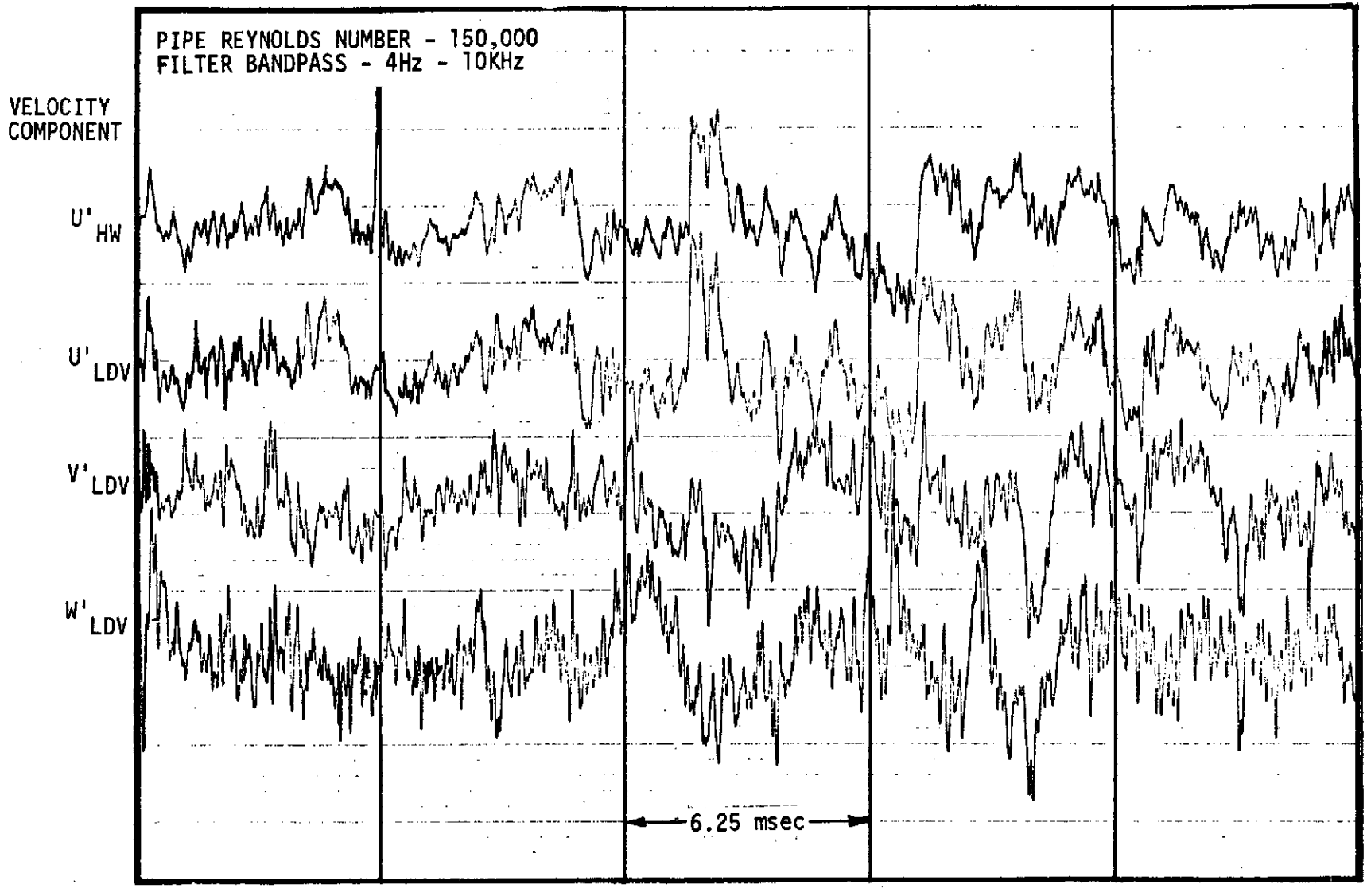

Fig. 5 SIMULTANEOUS COMPARISON OF HOT WIRE AND LDV TURBULENT FLUCTUATIONS AT THE CENTER OF A TURBULENT PIPE FLOW

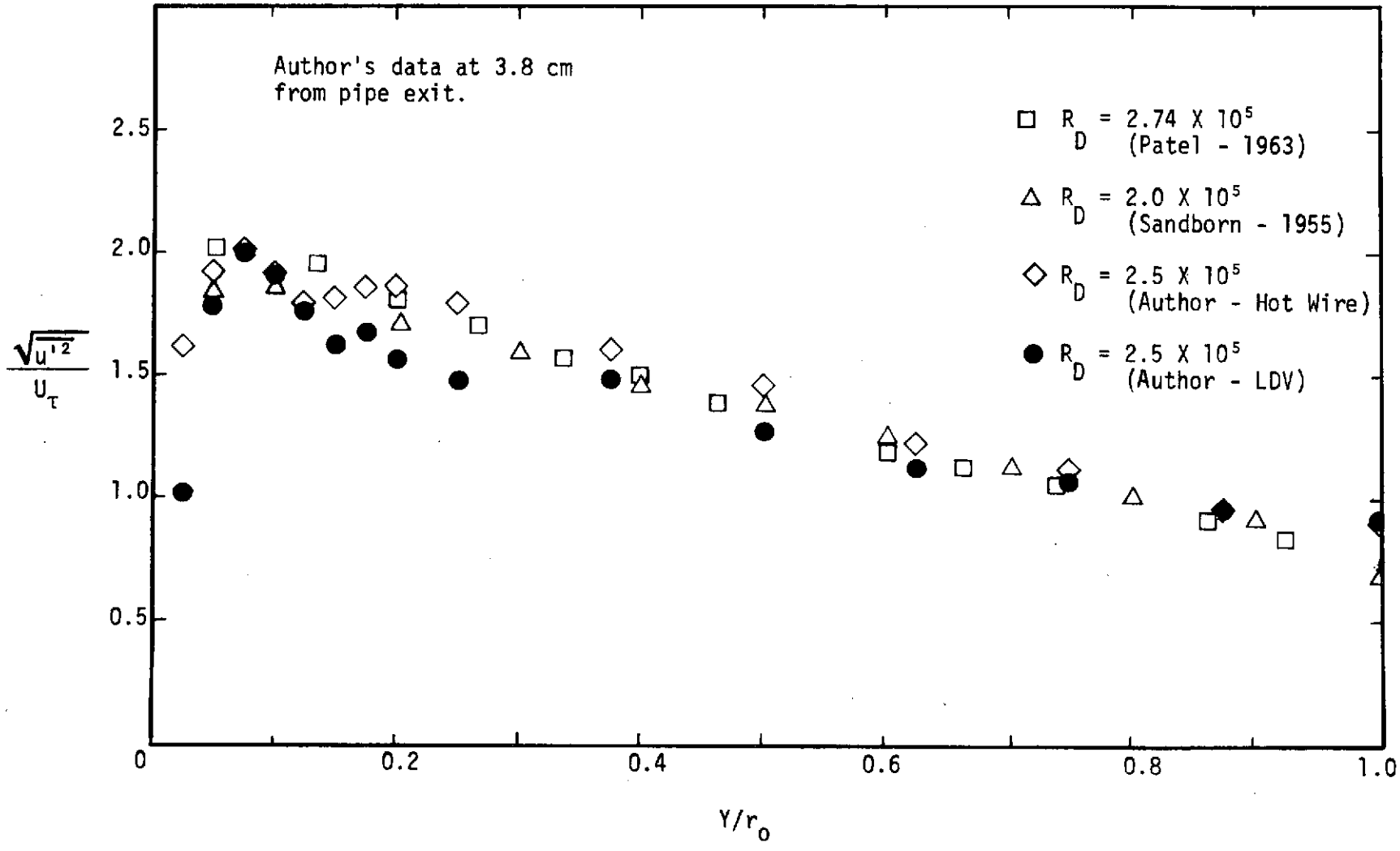

Figure 35 Comparison of $\sqrt{u'^2}$ Distribution for Pipe Flow.

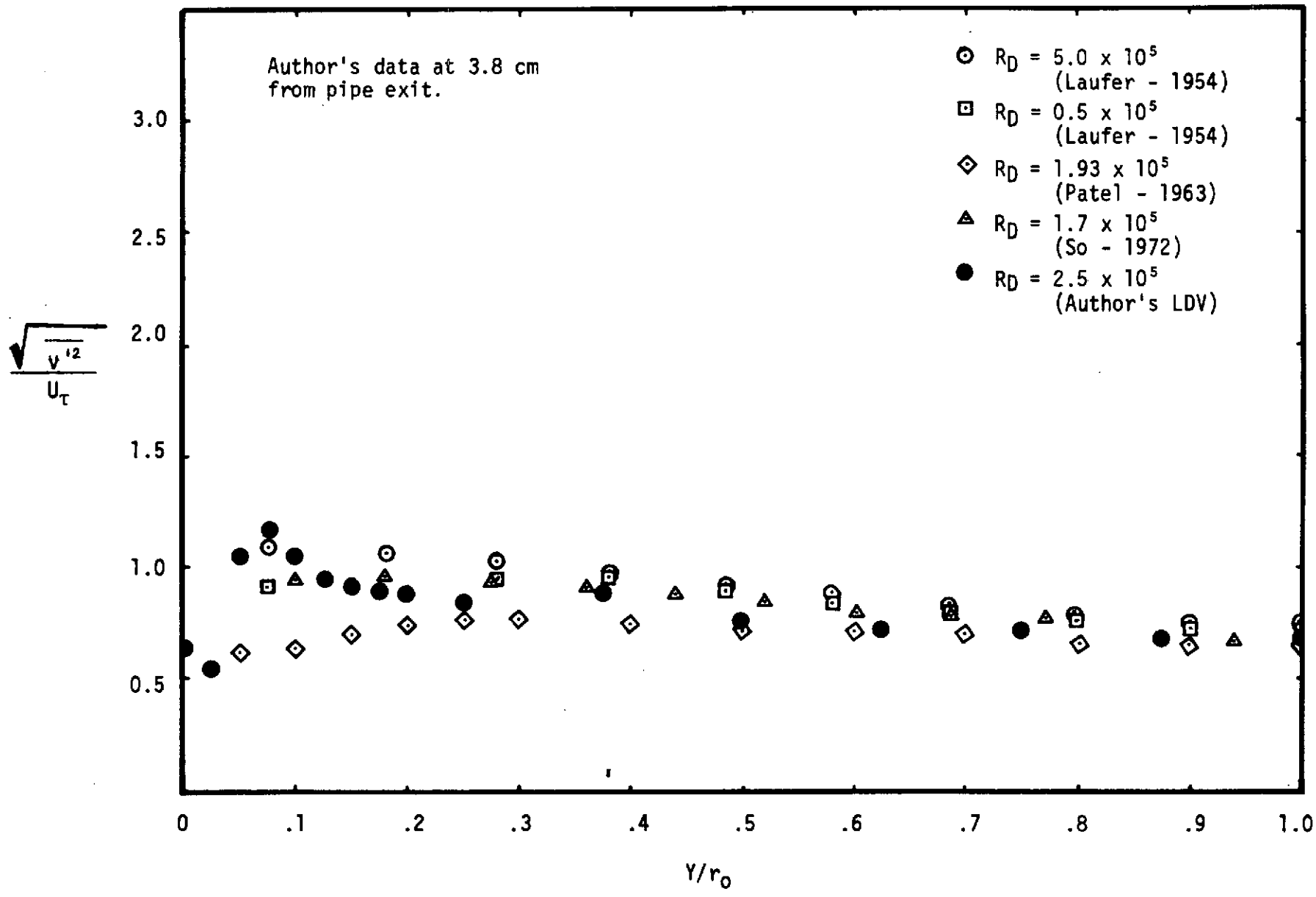

Figure 36 Comparison of $\sqrt{\overline{v'^2}}$ Distribution for Pipe Flow

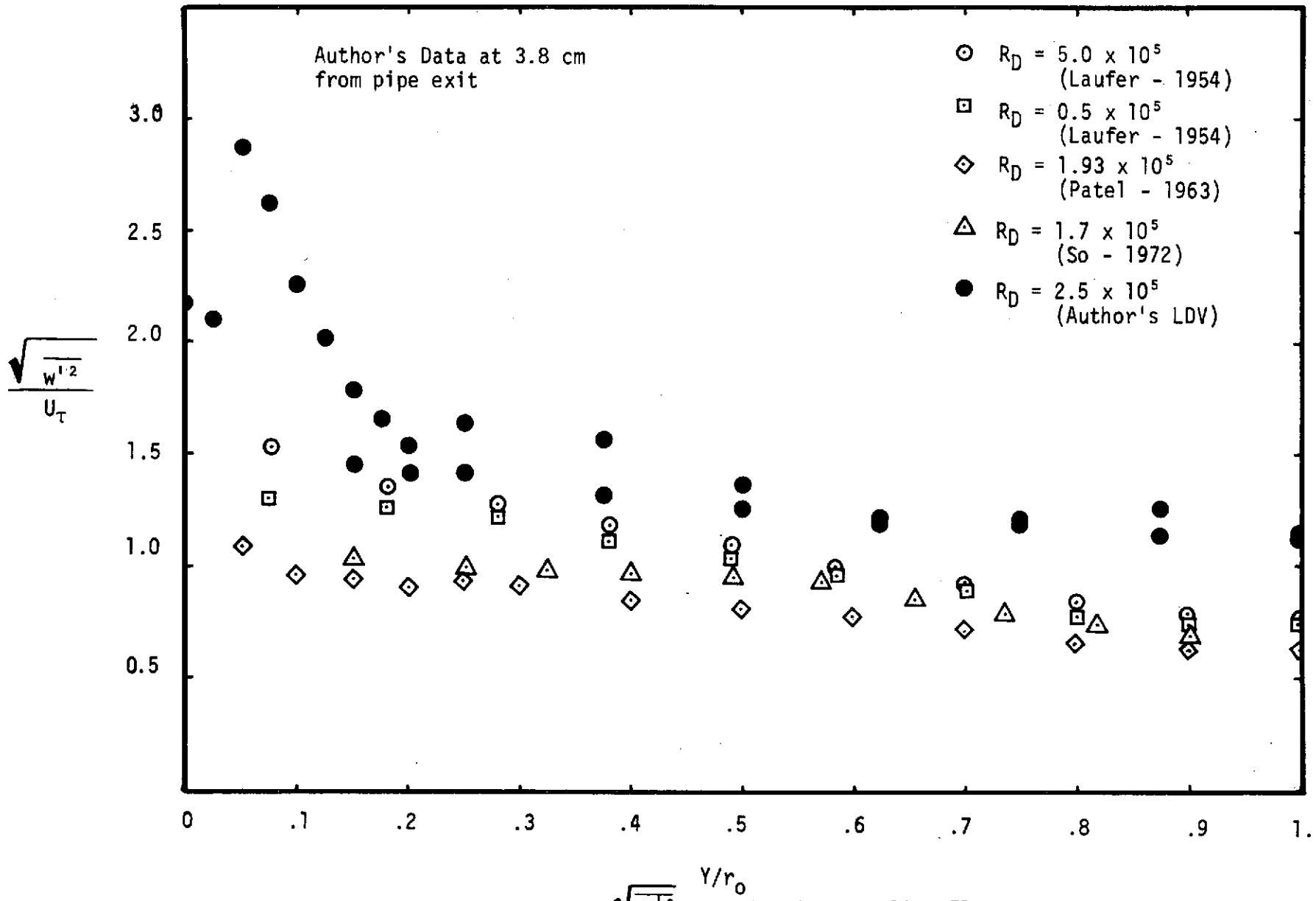

Figure 37 Comparison of $\sqrt{\overline{w'^2}}$ Distribution for Pipe Flow

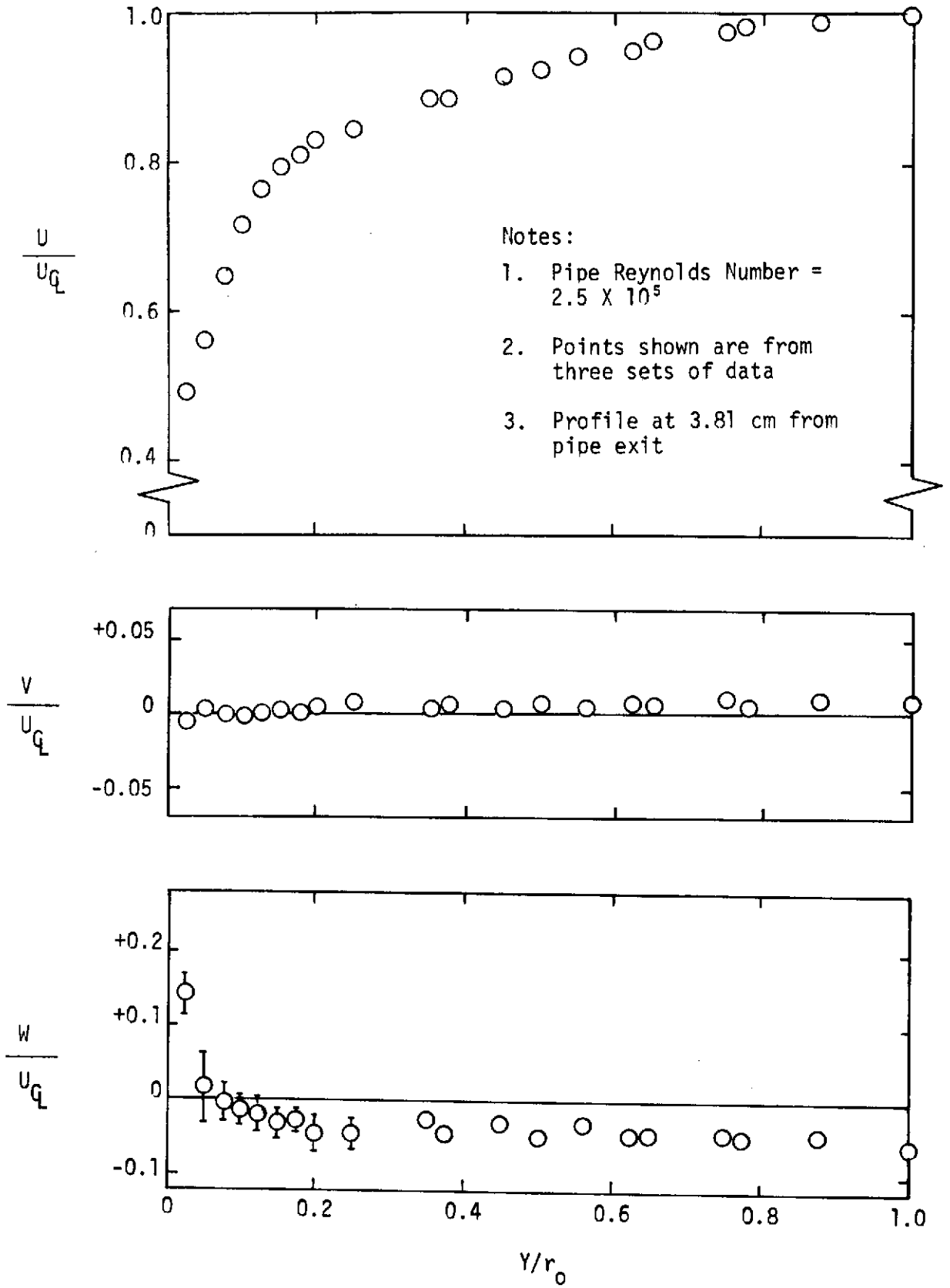

Figure 38 LDV Mean Velocity Distributions for Pipe Flow

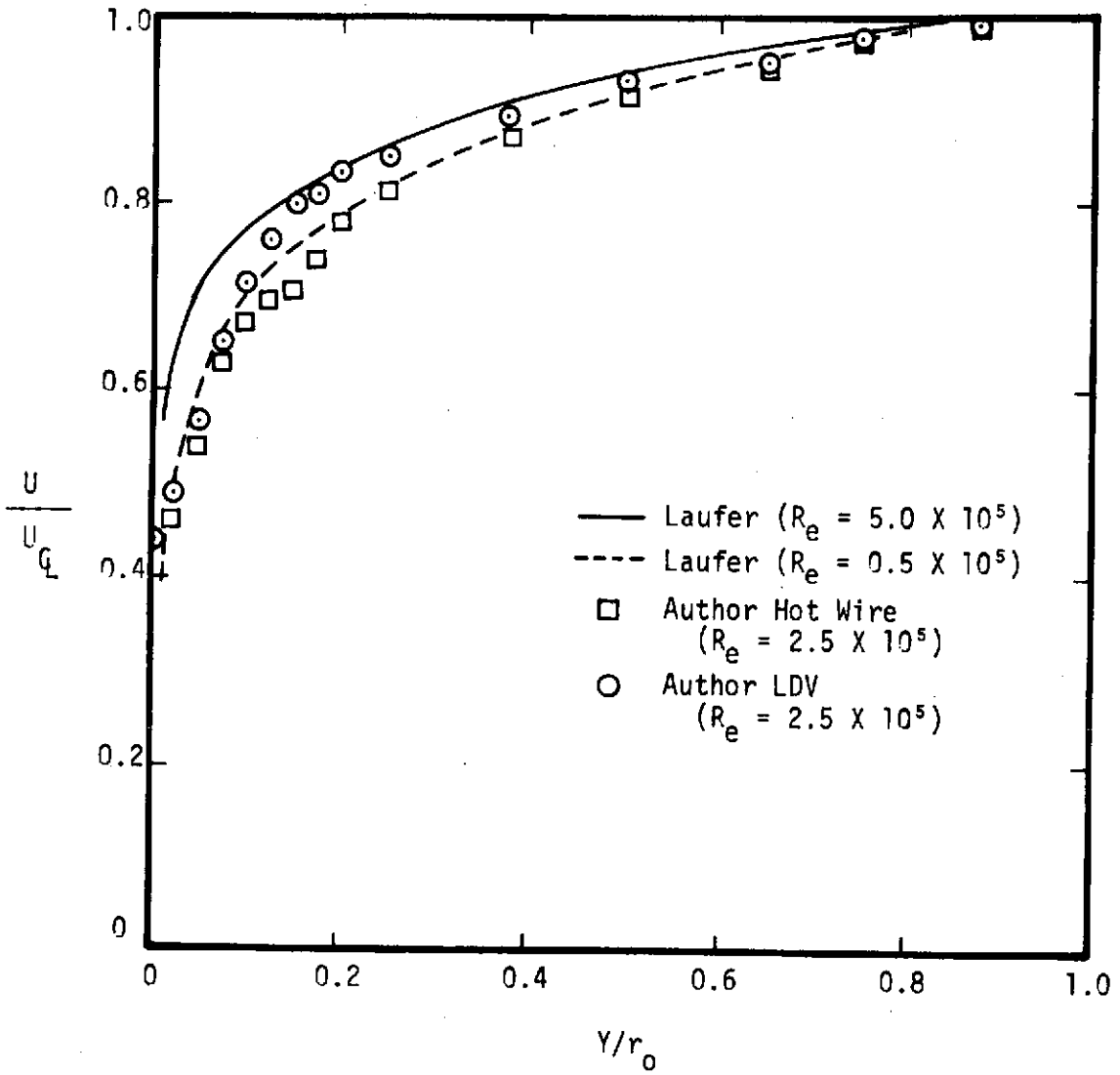

Figure 39 Comparison of Mean U Velocity Component Profile for Pipe Flow

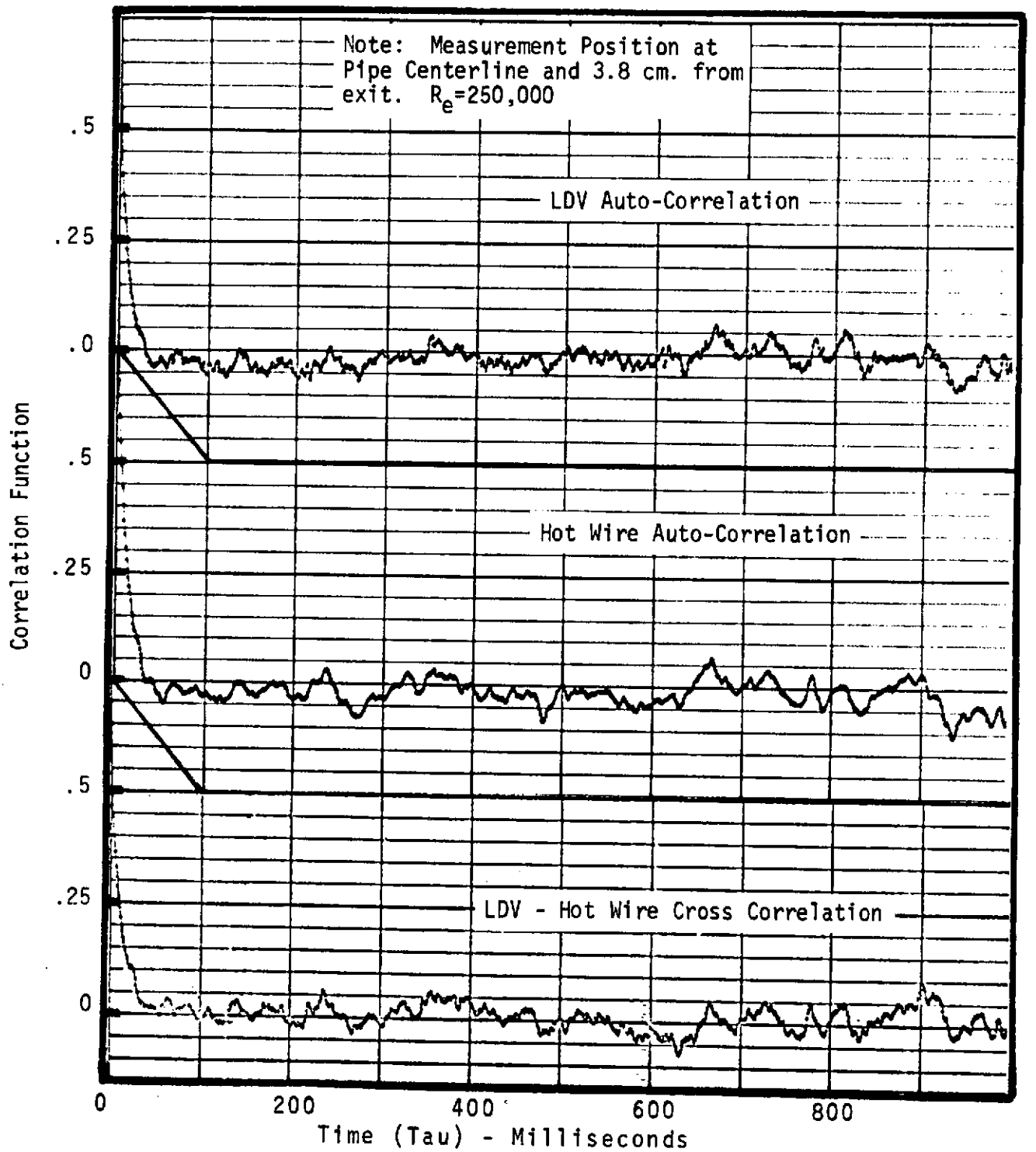

Fig. 40 Comparison of Correlation Functions for LDV and Hot Wire U' Component

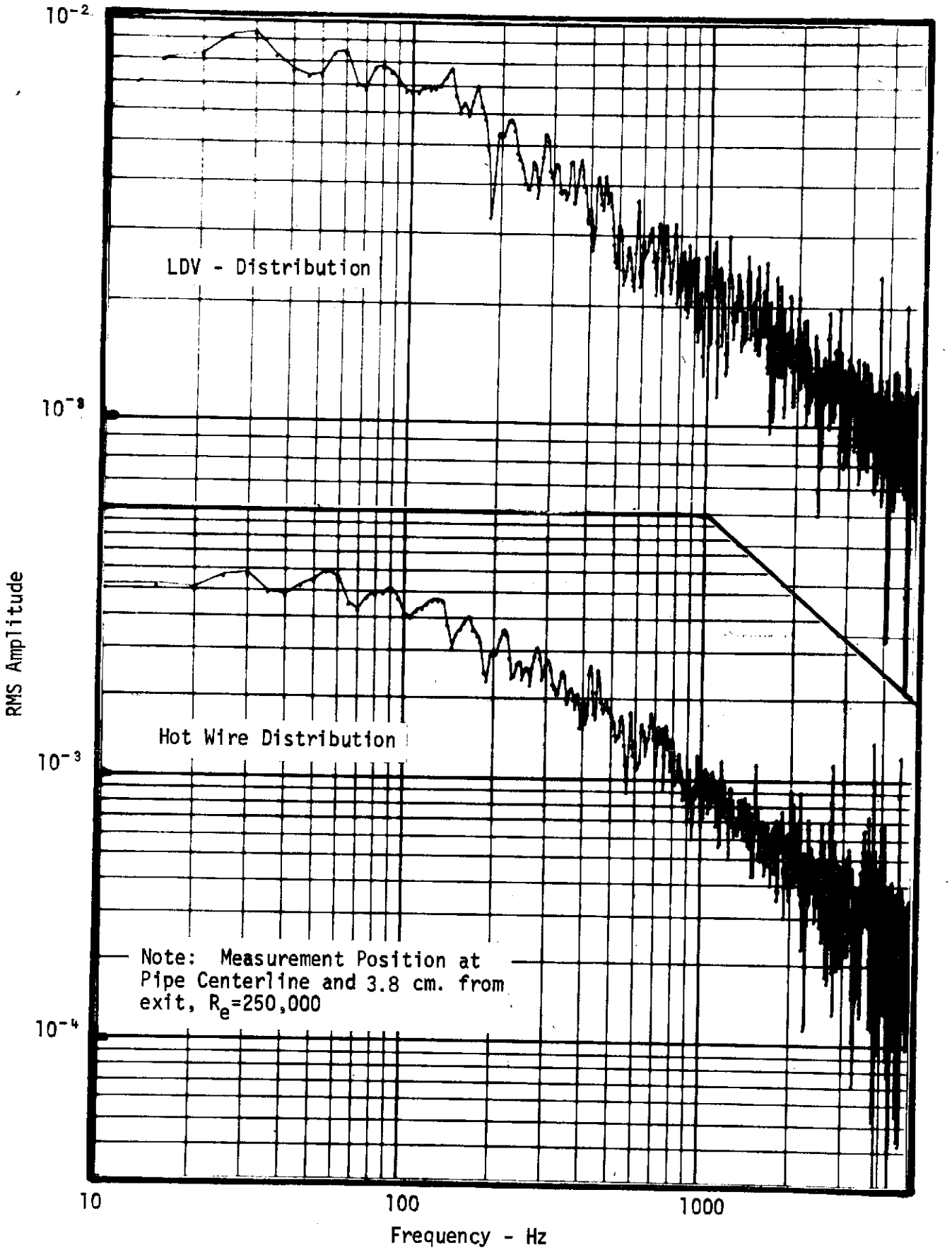

Fig. 41 Comparison of Spectra Distributions of LDV and Hot Wire U' Component

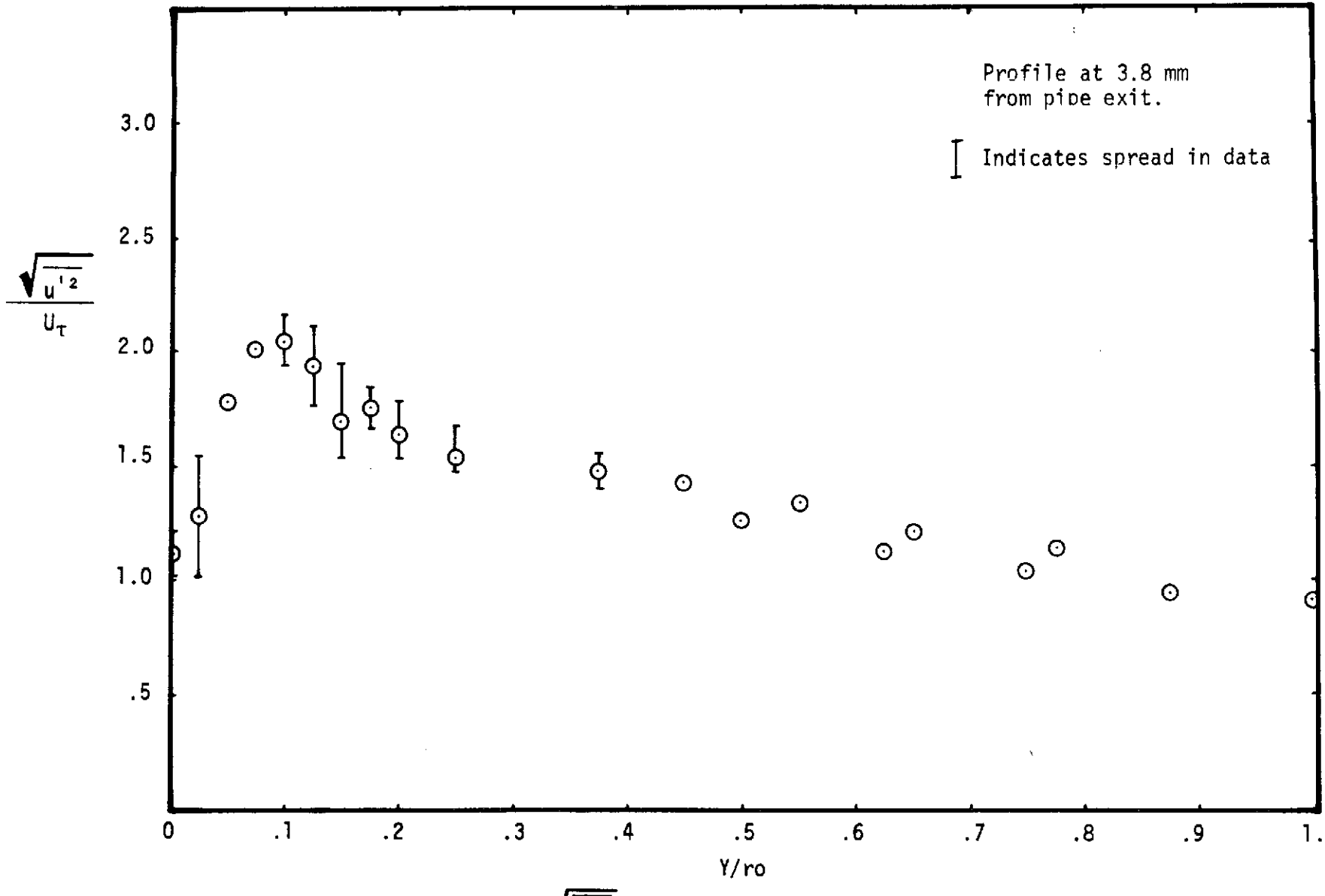

Figure 42 Average $\sqrt{\overline{u'^2}}$ Distribution for Three Sets of Data

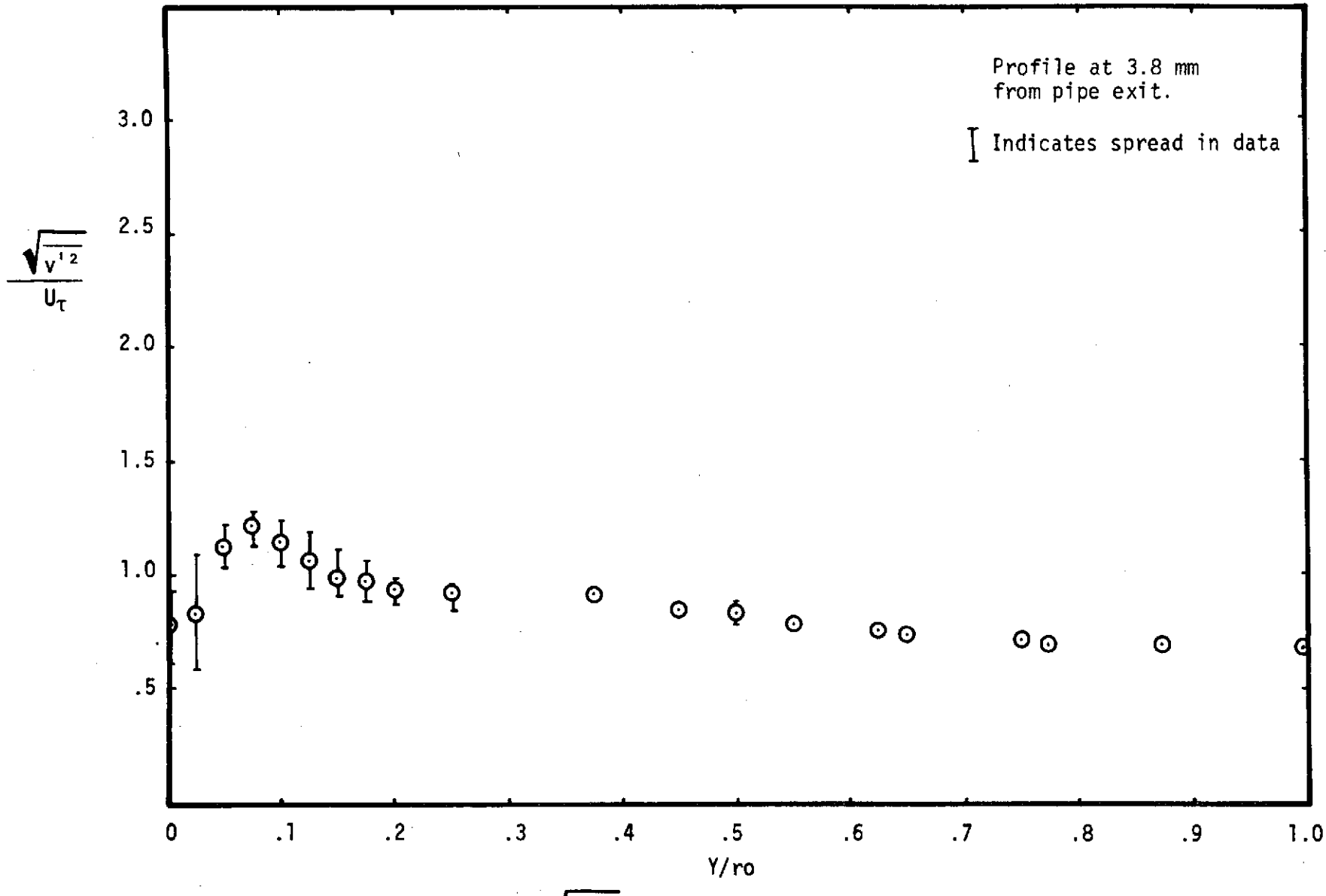

Figure 43 Average $\sqrt{\overline{v'^2}}$ Distribution for Three Sets of Data

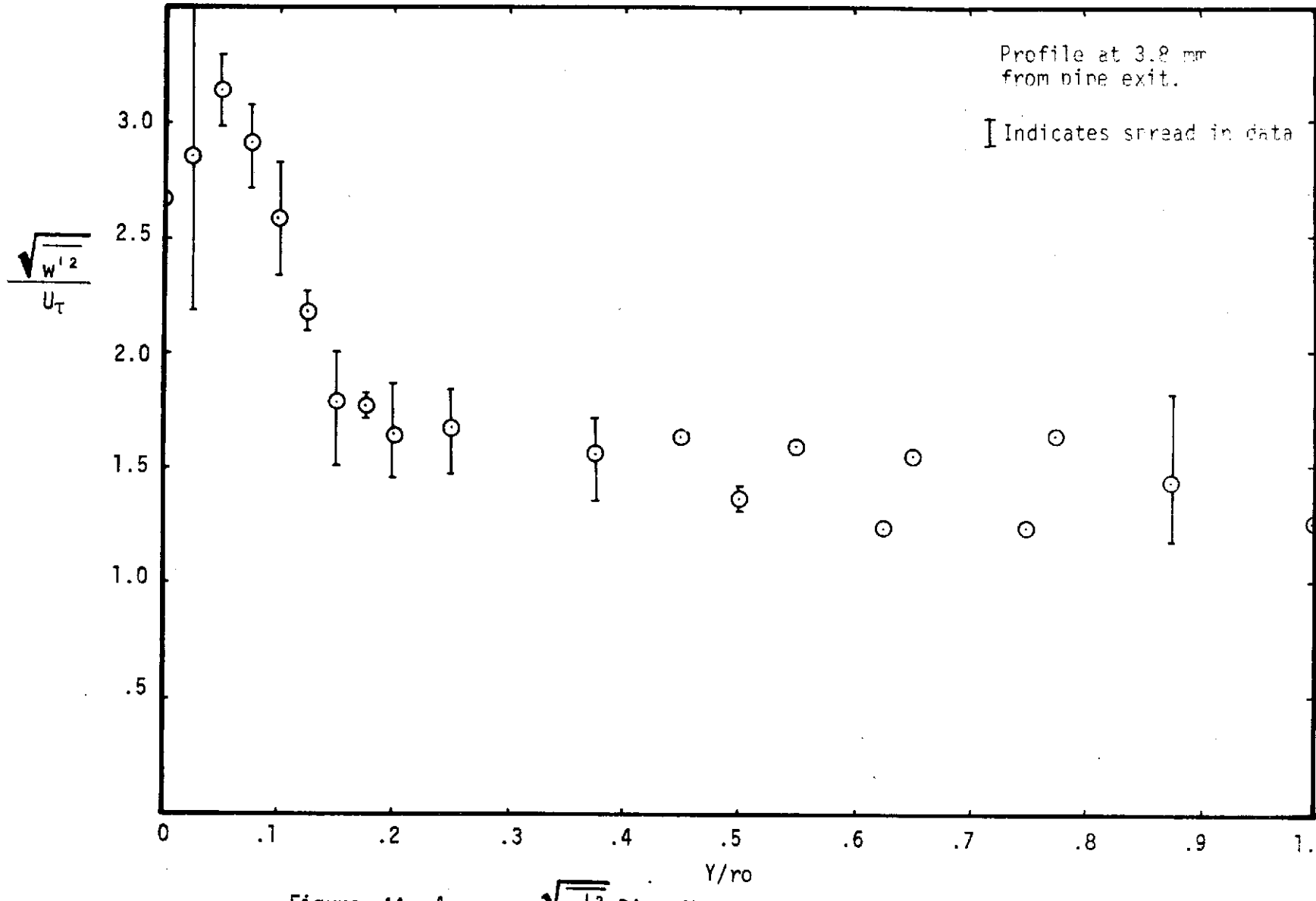

Figure 44 Average $\sqrt{\overline{w'^2}}$ Distribution for Three Sets of Data